Chem Soc Rev

REVIEW ARTICLE

View Article Online
View Journal | View Issue

Cite this: *Chem. Soc. Rev.*, 2018, **47**, 8766

New insights into the structure–performance relationships of mesoporous materials in analytical science

Jie Wang, † Qinqin Ma,† Yingqian Wang,† Zhiheng Li, Zhihao Li and Quan Yuan *

Mesoporous materials are ideal carriers for guest molecules and they have been widely used in analytical science. The unique mesoporous structure provides special properties including large specific surface area, tunable pore size, and excellent pore connectivity. The structural properties of mesoporous materials have been largely made use of to improve the performance of analytical methods. For instance, the large specific surface area of mesoporous materials can provide abundant active sites and increase the probability of contact between analytes and active sites to produce stronger signals, thus leading to the improvement of detection sensitivity. The connections between analytical performances and the structural properties of mesoporous materials have not been discussed previously. Understanding the "structure–performance relationship" is highly important for the development of analytical methods with excellent performance based on mesoporous materials. In this review, we discuss the structural properties of mesoporous materials that can be optimized to improve the analytical performance. The discussion is divided into five sections according to the analytical performances: (i) selectivity-related structural properties, (ii) sensitivity-related structural properties, (iii) response time-related structural properties, (iv) stability-related structural properties, and (v) recovery time-related structural properties.

Received 9th August 2018

DOI: 10.1039/c8cs00658j

rsc.li/chem-soc-rev

1. Introduction

Mesoporous materials refer to a special class of materials that possess pores with diameters in the range of 2 to 50 nm.[1–8] As the size of mesopores well matches the size of a great variety of compounds ranging from small biomolecules to proteins,

Key Laboratory of Analytical Chemistry for Biology and Medicine (Ministry of Education), College of Chemistry and Molecular Sciences, Wuhan University, Wuhan 430072, China. E-mail: yuanquan@whu.edu.cn

† These authors contributed equally to this work.

Jie Wang

Dr. Jie Wang got his BS degree from the School of Chemical Engineering and Pharmacy, Wuhan Institute of Technology, in 2012. Later, he joined the Prof. Quan Yuan group in the College of Chemistry and Molecular Sciences, Wuhan University. He obtained his PhD degree in 2017. Now he is a postdoctoral fellow in the College of Chemistry and Molecular Sciences, Wuhan University. His research focuses on designing functional materials for biosensing and bioimaging.

Qinqin Ma

Qinqin Ma obtained her BS degree from the College of Chemistry and Molecular Sciences, Wuhan University, in 2015. Now she is a PhD candidate under the supervision of Prof. Quan Yuan at the College of Chemistry and Molecular Sciences, Wuhan University. Her research interest includes the controlled synthesis of luminescent nanomaterials for analytical applications.

mesoporous materials can serve as excellent supports or carriers for a wide range of guest molecules.[9–15] Mesopores can provide a unique nano-confinement effect and significantly alter the local environment of guest molecules to regulate their movements or properties,[16–21] which make it possible to accomplish many reactions that cannot be replicated in the bulk phase. Since the first reports on the synthesis of mesoporous materials by Japanese researchers, and Mobil scientists, in the 1990s,[1,2] research studies on mesoporous materials have attracted burgeoning attention.[5,6,9–14,22–27] Recently, a great variety of synthesis methods have been developed and mesoporous materials with different porous structures, compositions and morphologies have been prepared.[28–34] Along with the development of synthesis strategies, mesoporous materials have also been largely applied to various areas[35] including sensing,[11,36–38] cancer therapy,[39–43] tissue engineering,[44–46] catalysis,[19,47,48] ion batteries[25,49] and solar cells.[25,50] The unique porous structures provided by mesoporous materials have revolutionized many research areas in the past decades.[51–54]

The exploration of mesoporous materials in analytical science has significantly improved the performance of many existing analytical techniques and lots of new detection methods have also been developed.[11,14,25,54–56] In particular, mesoporous materials offer attractive structural features including large specific surface area, tunable pore size or shape, tunable pore connectivity, and facile surface functionalization.[11,26,56–58] Many previous studies have demonstrated that the analytical performance could be significantly improved by rationally tailoring the structural properties of mesoporous materials.[11–14,26,50,55,59,60] For instance, the large specific surface area can provide abundant active sites to increase the contact probability between analytes and the active sites,[26,50,61] leading to the enhancement of signal intensity and improvement of detection sensitivity. Large pore volumes have shown good promise in loading a large amount of reporter molecules for signal amplification.[12,38,60,62] Large and interconnected mesopores can facilitate the diffusion of analytes, thereby increasing the accessibility of inner active sites and shortening the response time.[26,56,63] Such unique structural properties make mesoporous materials ideal candidates for analytical applications. By rationally tuning the structural properties of mesoporous materials, analytical systems with good sensitivity, high selectivity, fast response and good stability can be achieved.[11,56,57,64] Over the past decades, different kinds of mesoporous materials with fascinating

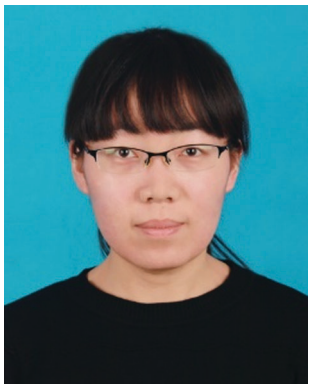

Yingqian Wang

Yingqian Wang obtained her BS degree from the College of Chemistry and Chemical Engineering, Hunan University, in 2015. She is currently a PhD candidate in the Prof. Quan Yuan group at Wuhan University. She is interested in DNA-based functional materials and their potential biomedical applications.

Zhiheng Li

Zhiheng Li earned her BS degree from the College of Chemistry and Molecular Engineering, Zhengzhou University, in 2016. Now she is a PhD candidate in the Prof. Quan Yuan group at the College of Chemistry and Molecular Sciences, Wuhan University. She is interested in the controlled synthesis of functional nanomaterials for biomedical applications.

Zhihao Li

Zhihao Li received his BS degree from the College of Chemistry and Molecular Sciences, Wuhan University, in 2016. Now he is a PhD candidate in the Prof. Quan Yuan group at Wuhan University. His current research interests include the design and applications of functional DNA nanomaterials.

Quan Yuan

Professor Quan Yuan is a full professor in the College of Chemistry and Molecular Sciences, Wuhan University. She obtained her PhD degree from the College of Chemistry and Molecular Engineering, Peking University, in 2009. Later, she continued her postdoctoral research at the University of Florida. In 2012, she joined the College of Chemistry and Molecular Sciences, Wuhan University, as a full professor. Her research focuses on the controlled synthesis of functional nanomaterials and exploring their biomedical applications.

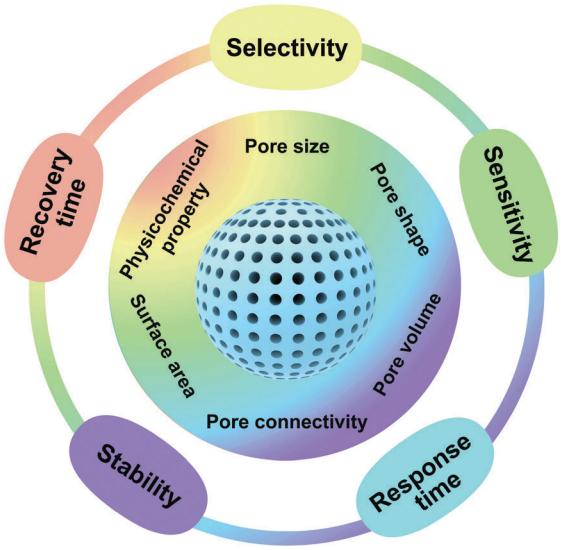

Fig. 1 Schematic illustration of the structural properties of mesoporous materials that contribute to the improvement of analytical performance.

structural properties have been developed and various kinds of analytical methods have been designed for sensing applications ranging from environmental monitoring to disease diagnosis.[11,13,25,26,55,56,65]

Many previous excellent reviews have summarized the methods for the preparation of mesoporous materials and the exploration of mesoporous materials in analytical science.[14,26,36,47,55,66,67] However, the connections between the structural properties of mesoporous materials and the analytical performance have not been discussed. Understanding the "structure–performance relationship" can contribute to developing analytical methods with excellent performance based on mesoporous materials. In this review, we provide a discussion focusing on the unique structural properties of mesoporous materials that have been used to improve the performance of analytical methods. Several important analytical performance parameters that can be improved by tailoring the structural properties of mesoporous materials are discussed (Fig. 1): (i) selectivity-related structural properties, (ii) sensitivity-related structural properties, (iii) response time-related structural properties, (iv) stability-related structural properties, and (v) recovery time-related structural properties. Among the above mentioned analytical performances, selectivity, sensitivity and stability are the most important criteria of an analytical method. A detailed discussion will be made on the structural properties of mesoporous materials that are correlated with detection selectivity, sensitivity, response time, stability, and recovery time. The "structure–performance relationship" discussed in this review may provide potential instructions for the development of analytical science in the future.

2. Selectivity-related structural properties

Selectivity describes the capability of analytical methods to discriminate analytes from other compounds in the sample.[68,69] The Western European Laboratory Accreditation Cooperation defines selectivity as the extent to which analytes can be detected in complex sample matrices without interference from other compounds.[68,69] The basic principle to achieve selectivity is to construct recognition subunits that can discriminate the different characteristics between analytes and background compounds.[70,71] At the molecular level, the analyte may show many different characteristics from the background compounds, such as size, shape, hydrophilicity/hydrophobicity, and charge.[60,67] In the past decades, mesoporous materials have been largely employed to discriminate such different characteristics and good selectivity has been achieved.[72–74] The structural properties of mesoporous materials that contribute to the selectivity of analytical methods will be discussed in this section.

2.1 Pore size

Size-selective adsorption of small molecules has been observed in zeolites with micropores long ago.[75–77] However, similar size-based selective adsorption of molecules with larger size such as proteins was beyond reach for a long time due to the lack of porous materials with pore sizes that accommodate larger molecules. The successful development of mesoporous materials makes it possible to realize size-selective adsorption of large molecules for the first time.[78–80] As the size of mesopores ranges from 2 to 50 nm, size-selectivity towards different kinds of analytes can be easily achieved by controlling the pore diameters to allow the analytes to pass in but exclude large interfering compounds (Fig. 2).[73,81,82] In the past decades, considerable efforts have been devoted towards tailoring the size-selectivity, also known as the size-exclusion effect, of mesoporous materials for analytical applications.[83–85]

The size-exclusion effect of mesoporous materials has been widely used in the separation and preconcentration of analytes from complicated sample matrices for further analysis.[85–88] In particular, researchers have combined mesoporous materials with matrix-assisted laser desorption/ionization time of flight mass spectrometry (MALDI-TOF MS) for biofluid proteomics.[74,87,89–91] The human plasma proteome can help researchers to elucidate the molecular basis of biological activities, and much attention has been paid to the proteomic profile in the low-molecular-weight (LMW) range since the LMW peptidome can provide rich disease-specific information. Due to their tunable pore size and large loading capacity, mesoporous materials offer a highly-efficient and easy-to-perform way for selective capture

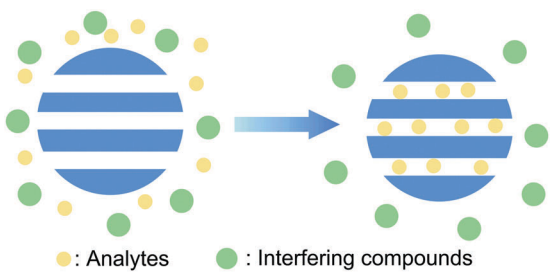

Fig. 2 Schematic illustration of the size-selectivity of mesoporous materials.

and enrichment of the LMW peptidome from biofluids.[86,89,90] In efforts to exploit the applications of the size-exclusion effect of mesoporous materials in LMW peptide analysis, Zou *et al.* pioneered the selective enrichment of the peptidome from human plasma with mesoporous silica in 2007.[37] In this study, mesoporous silicas MCM-41 (pore size around 2 nm), C-SBA-15 (pore size around 8 nm) and L-SBA-15 (pore size around 12 nm) were prepared. The size-exclusion efficiencies of the prepared mesoporous silicas towards high-molecular-weight (HMW) proteins were compared. Lysozyme (14.4 kDa, 3 nm × 3 nm × 4.5 nm) was used as the model of HMW proteins for size-exclusion study. The authors showed that the amounts of lysozyme adsorbed on MCM-41, C-SBA-15 and L-SBA-15 were 63.6 mg mL^{-1}, 191.3 mg mL^{-1} and 420.8 mg mL^{-1}, respectively. These significantly different adsorption efficiencies were due to the different pore sizes of the three kinds of mesoporous silica; that is, the pore size of the MCM-41 mesoporous silica was smaller than the size of lysozyme but C-SBA-15 and L-SBA-15 showed pore sizes well accommodating lysozyme. Therefore, MCM-41 is more efficient in excluding lysozyme, suggesting that MCM-41 can selectively enrich LMW peptides but exclude HMW proteins by the size-exclusion mechanism. The MCM-41 mesoporous silica particles were further used to enrich peptides from native human plasma. For direct analysis of human plasma, strong background signals emerged and only a few peptide peaks could be discriminated (Fig. 3a). However, strong and well-resolved peptide peaks were observed in the mass spectrum in the LMW range (Fig. 3b) after enrichment of the peptides with the MCM-41 mesoporous silica. Moreover, the peaks corresponding to HMW proteins such as human serum albumin that were clearly observed by direct plasma analysis (Fig. 3c) disappeared after treatment with the MCM-41 mesoporous silica (Fig. 3d), which clearly suggested that HMW proteins were efficiently excluded by MCM-41. This study shows

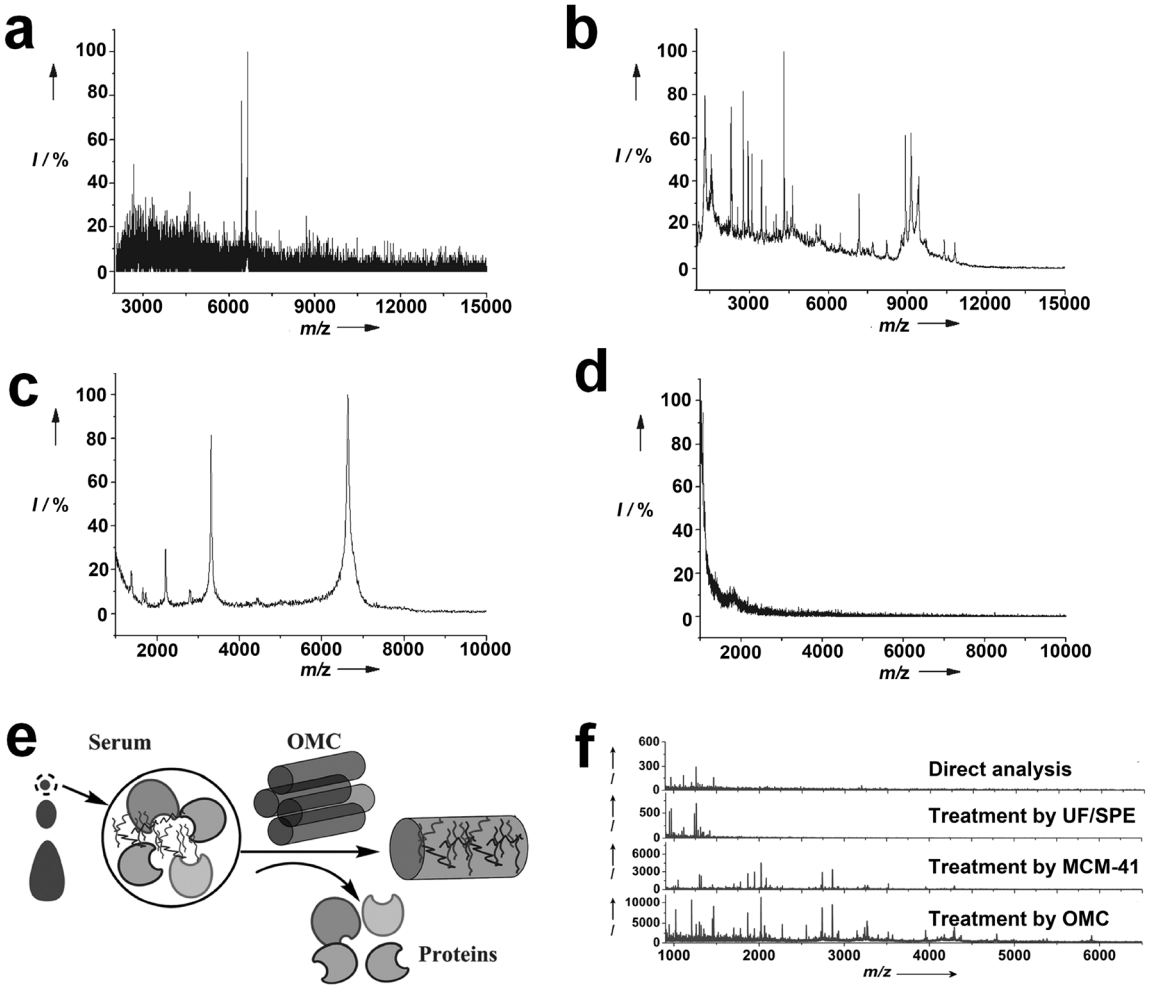

Fig. 3 MALDI-TOF MS analysis of human plasma (a) without and (b) with pretreatment with MCM-41 mesoporous silica particles (in the MW range of 1–15 kDa). MALDI-TOF MS analysis of human plasma (c) without and (d) with pretreatment with MCM-41 mesoporous silica particles (in the MW range of 10–100 kDa). Reprinted with permission from ref. 37. Copyright 2007, Wiley-VCH Verlag GmbH & Co. KGaA, Weinheim. (e) Schematic diagram of the enrichment of serum endogeneous peptides with mesoporous carbon. (f) MALDI-TOF MS analysis of human serum endogeneous peptides without or with pretreatment by US/SPE, MCM-41, and OMC. Reprinted with permission from ref. 89. Copyright 2011, Wiley-VCH Verlag GmbH & Co. KGaA, Weinheim.

that good selectivity can be easily achieved by simply tuning the pore size of mesoporous materials.

Although the directly synthesized mesoporous silica showed good size-exclusion function, researchers found that considerable amounts of analytes are not extracted due to the weak interaction between the pore surface and the analytes.[89] To further improve the enrichment efficiency, researchers have prepared mesoporous materials with both tailored pore sizes and surface properties.[80,89,92,93] Zou *et al.* prepared mesoporous carbon for LMW peptide enrichment (Fig. 3e). They found that the mesoporous carbon displayed a stronger retention of LMW peptides compared to MCM-41 mesoporous silica (Fig. 3f), which was attributed to the hydrophobic interaction between the pore surface and peptides in the mesoporous carbon.[89] In another work, Yu *et al.* synthesized mesoporous silica with different pore sizes and surface modification for insulin enrichment. They showed that mesoporous silica with critical pore sizes and methyl modification was much more efficient in selective enrichment of human insulin than hydrophilic mesoporous silica or mesoporous silica with too large/small pores.[95]

In addition to MALDI-TOF MS, the size-selectivity of mesoporous materials has been widely used in many other analytical techniques.[9,94] In 2009, Sailor *et al.* designed a single mesoporous nanoreactor that can isolate the reaction products from the original analyte in real time for further quantification based on imprinted porous silicon.[9] The reactor consists of two layers of porous films with different pore sizes. The upper layer with larger pore sizes of about 100 nm could trap protease and serve as a nanoreactor. On the other hand, the lower layer with smaller pore sizes of about 6 nm could exclude the proteases but allow the small reaction products to enter for quantification. Pepsin (10 nm × 6 nm × 20 nm) was employed as a model protease and it was loaded into the upper layer through electrostatic adsorption. Substrates such as α-casein in the upper layer were digested by pepsin, and the smaller digestion products diffused into the lower layer, leading to significant changes in the optical reflectivity of the lower layer. With this size-selective nanoreactor, the activity of the proteins could be sensitively quantified without using fluorescently tagged protein substrates.

In the above mentioned methods, the size-selectivity effect of mesoporous materials was utilized to isolate analytes from complicated sample matrices. The most straightforward use of size-selective mesoporous materials allows analytes to enter into mesopores to react with immobilized probes to produce prompt signals. In 2001, Lin and coworkers immobilized amine-sensitive *o*-phthalic hemithioacetal (OPTA) groups on the surfaces of MCM-41 mesoporous silica nanoparticles (OPTA-MSNs) for detecting amines.[85] Due to the size-exclusion effect, only small molecules with amino groups could diffuse into the mesopores and further react with the grafted OPTA groups to produce highly fluorescent isoindole. Small biomolecules such as dopamine and glucosamine can lead to a significant increase in fluorescence intensity from the OPTA-MSN mesoporous sensing system. This study again demonstrates that good selectivity can be easily achieved by controlling the pore size of mesoporous materials.

In addition to mesoporous materials, many other materials, such as polymers and carbon nanotubes, are also widely employed for selective adsorption of analytes based on the size-exclusion mechanism.[96] In adsorption and separation related areas, mesoporous materials, along with polymers, carbon nanotubes, *etc.*, are called restricted access materials (RAMs) since they can retain analytes and exclude large interfering compounds.[96–98] Many of the RAMs are obtained by introducing small pores into conventional sorbents or modifying the surfaces of conventional sorbents with functional groups.[96] Among these ''intelligent'' sorbents, RAMs with mesoporous structure possess unique advantages including tunable pore size and high porosity.[99,100] The tunable pore size makes mesoporous materials suitable for the selective adsorption of a large variety of analytes in a user-defined manner, while the high porosity of mesoporous materials makes it possible to retain large amounts of analytes by a small amount of sorbents, which suggests that high adsorption/separation efficacy can be achieved with mesoporous RAMs. Thus mesoporous materials are widely used as RAMs in separation related applications.

From the above mentioned works, one can get the idea that selectivity can be achieved by controlling the pore size of mesoporous materials to allow the passage of analytes with smaller size but exclude interfering molecules with larger size. Significant achievements have been made in selective adsorption and separation of targets with the size-exclusion effect of mesoporous materials. However, considering that there are usually many interfering molecules with size close to those of the analytes existing in sample matrices, mesoporous materials will retain both the analytes and the interfering molecules. That is, the size-exclusion effect is not selective enough to discriminate the analytes and interfering molecules with similar sizes. In this case, selectivity achieved with the other structural properties of mesoporous materials is preferred, as will be introduced in the following sections.

2.2 Pore shape

It has been reported that zeolites are capable of discriminating molecules with different shapes due to the close matching in shape between the molecules and pores, which was termed ''molecular shape selectivity''.[95,101,102] Researchers have‘ developed the elegant molecular imprinting approach to replicate the shape selectivity observed in zeolites.[103] One of the well-known materials with excellent shape selectivity gifted by molecular imprinting is molecularly imprinted polymers (MIPs).[103,104] MIPs are polymer networks with binding cavities that are well complementary to the analytes. The preparation of MIPs usually involves the copolymerization of cross-linking monomers and functional monomers in the presence of templates, namely analytes or the structural analogs of the analyte. Further removal of the embedded templates from the polymer matrix leaves binding cavities that can rebind to the analytes selectively in preference to other compounds.[105] MIPs with specific recognition function have been widely applied in the adsorption/separation of analytes for analytical applications.[103,106,107]

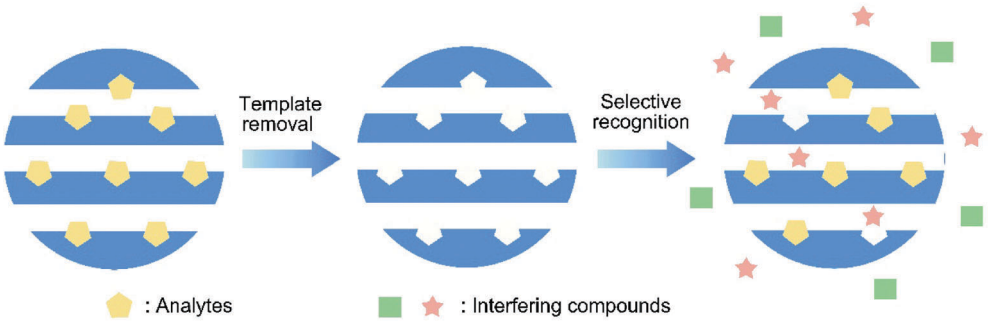

Fig. 4 Schematic illustration of the shape-selectivity of mesoporous materials.

Mesoporous materials possess large surface area, which makes it possible to generate large quantities of binding cavities on the walls of the mesopores. Therefore, the contact possibility between analytes and the binding cavities can be significantly improved by tailoring the large surface area of mesoporous materials. These unique structural properties can make mesoporous materials highly efficient in shape selective recognition of analytes. In the past decades, attempts have been made towards designing imprinted mesoporous materials that combine the advantages of mesoporous materials (fast diffusion, good accessibility) with those of zeolites (shape selectivity, abundant binding cavities) (Fig. 4).[95,108,109] The binding cavities in the pore walls of imprinted mesoporous materials that mimic the shape-selective pores in zeolites are also obtained by molecular imprinting.[110,111] The procedure includes three main steps:[110,112,113] (1) formation of dual-template (mesoporous templates and the analyte analogs) complexes; (2) addition of polymerization monomers for oriented imprinting; and (3) removal of the dual-template complexes to form mesopores and binding cavities. In the synthesis process, a large number of specific binding cavities that closely match the shape of analytes are generated on the pore walls; thus analytes can specifically bind to the imprinted mesoporous materials. In addition to shape-selectivity, the functional groups on the surfaces of the binding cavities may also show binding affinity to the analytes, which further enhances the selectivity of the imprinted mesoporous materials.[61,111,112]

Imprinted mesoporous materials with specific binding cavities are able to discriminate molecules with minor structural differences since only molecules with exactly the same shape can perfectly fill the cavities.[114,115] It has been reported that imprinted mesoporous materials can even achieve enantioselective recognition.[116–121] For instance, Kuhn *et al.* reported the construction of chirally imprinted mesoporous Pt by a simple electrochemical reduction method in which platinum salts were reduced in the presence of chiral template molecules and a liquid crystal phase.[116] The obtained imprinted mesoporous Pt well retained the chiral feature after removing the template molecules. The authors showed that the chirally imprinted mesoporous Pt was able to stereo-selectively recognize isomers such as L-3,4-dihydroxy-phenylalanine and D-3,4-dihydroxy-phenylalanine in a racemic mixture. Compared to the electrochemical reduction method, other strategies[121–123] such as the polymer templating sol–gel approach are more convenient and widely used in the preparation of imprinted mesoporous materials. In one of these works, Mastai and coworkers reported the preparation of chiral mesoporous silica with chiral block copolymers.[121] The designed chiral mesoporous silica was successfully applied in the enantioselective separation of D- or L-valine from racemic solutions. These studies clearly demonstrated the highly specific recognition capabilities of imprinted mesoporous materials with shape-matching cavities. The shape-selectivity of mesoporous materials has been widely explored for analytical applications.

Chang *et al.* developed imprinted mesoporous silica nanoparticles (MSNs) loaded with quantum dots (QDs) as signal transducers for highly selective and sensitive detection of bisphenol A (BPA) (Fig. 5a).[124] The large specific surface area and nano-sized wall thickness of MSNs make it possible to generate binding cavities near the surface and offer high accessibility to BPA. Due to the close proximity between the binding cavities and QDs, fluorescence resonance energy transfer from QDs to BPA was efficiently constructed. In the presence of BPA, a concentration-dependent quenching of QDs' fluorescence was observed. The imprinted mesoporous sensing system was also subjected to BPA structural analogs including 4,4′-biphenol, diethylstilbestrol (DES) and hydroquinone (HQ) (Fig. 5b). The quenching constant of the imprinted mesoporous sensing system to BPA was more than ten times larger than those to BPA analogs, showing that the analogs could not bind to the cavities tightly due to shape mismatch. This study showed that the good potential of imprinted mesoporous materials for highly selective recognition of analytes further provided a general approach for the construction of imprinted mesoporous material based fluorescence sensors.

In addition to the shape-matching effect of binding cavities, the functional groups on the surfaces of the cavities that show binding affinity to analytes can further enhance the binding specificity of imprinted mesoporous sensing systems.[111,114,125,126] Chen *et al.* reported a QD-encapsulating imprinted mesoporous silica with binding cavities that exhibit both shape selectivity and hydrogen bonding interaction with analytes.[114] In that work, a broad-spectrum antibiotic (tetracycline) was employed as the model target. The binding cavities were functionalized with amino groups to provide hydrogen bonding interaction between the cavities and tetracycline. The excited energy of the

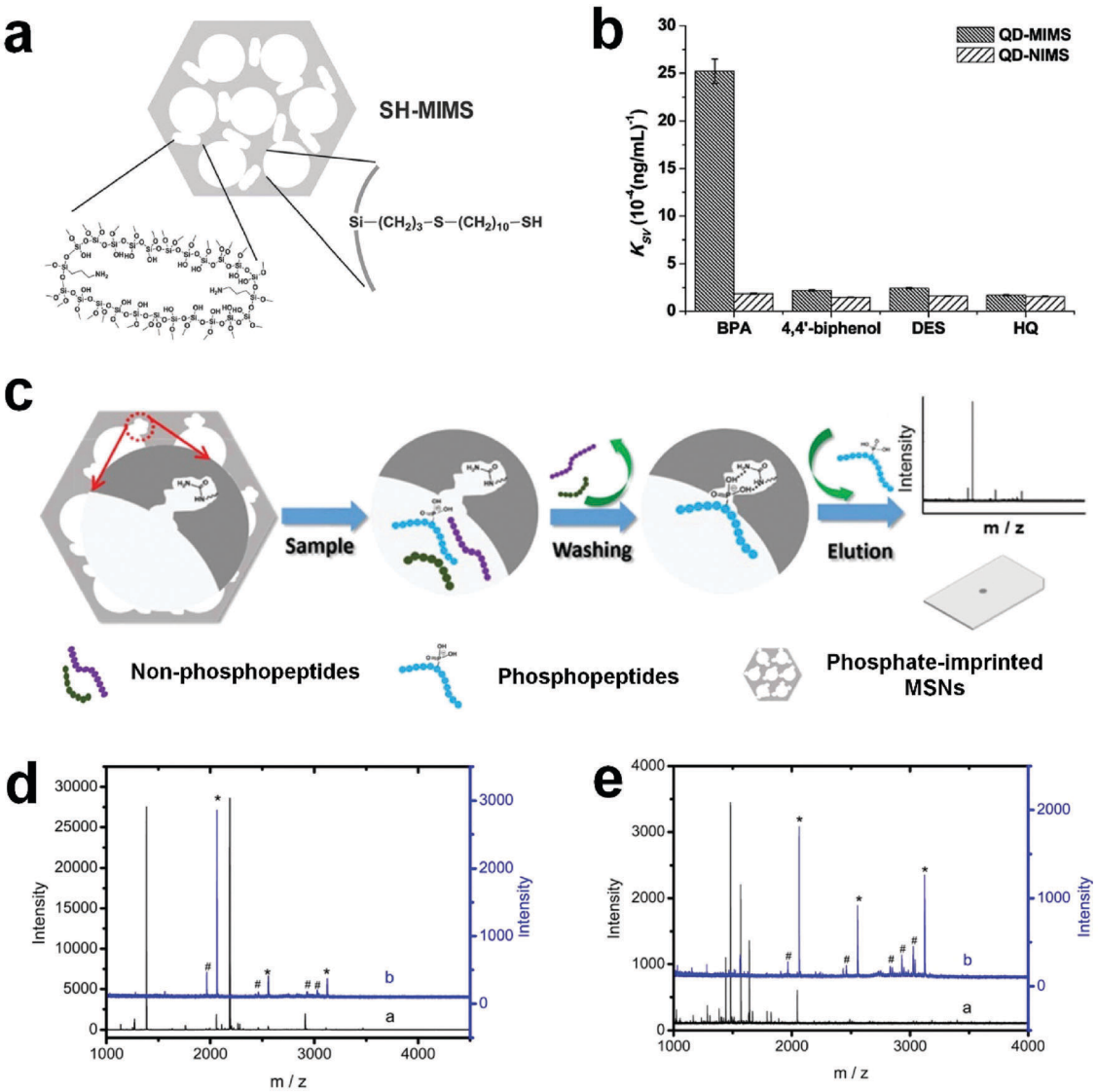

Fig. 5 (a) Schematic illustration of BPA imprinted MSNs. (b) The quenching constants of imprinted MSNs and non-imprinted MSNs in the presence of BPA, 4,4′-biphenol, diethylstilbestrol (DES) and hydroquinone (HQ). Reprinted with permission from ref. 124. Copyright 2012, Royal Society of Chemistry. (c) Schematic representation of MALDI-TOF MS analysis of phosphopeptides after enrichment with phosphate-imprinted MSNs. (d) MALDI-TOF MS spectra of the tryptic digests of β-casein before (black line) and after (blue line) enrichment with the imprinted MSNs. (e) MALDI-TOF MS analysis of a tryptic digest mixture of β-casein and BSA (1 : 100, w/w) before (black line) and after (blue line) enrichment with the imprinted MSNs. + and # represent the phosphopeptides and dephosphorylated peptides, respectively. Reprinted with permission from ref. 61. Copyright 2015, American Chemical Society.

QDs could transfer to the tetracycline trapped in the binding cavities and result in fluorescence quenching for tetracycline detection. The selectivity of the imprinted mesoporous sensing system was tested by measuring the fluorescence intensity in the presence of structural analogs of tetracycline, including chlortetracycline and BPA. Results showed that the structural analogs of tetracycline led to much weaker fluorescence changes compared to tetracycline, showing that the imprinted mesoporous silica displayed good selectivity for tetracycline detection. This study again demonstrated that good selectivity can be achieved by imprinting mesoporous materials with binding cavities that well match the analytes in shape.

Similar to size-selectivity, the shape-selectivity of mesoporous materials has also been largely utilized in MS for the analysis of peptides in biofluids. In 2015, Liu *et al.* developed a dual-template docking oriented molecular imprinting strategy for highly efficient and facile preparation of imprinted mesoporous materials.[110] Later, they synthesized phosphate-imprinted MSNs functionalized with urea groups on the surfaces of the mesopores and the binding cavities.[61] The imprinted mesoporous silica nanoparticles were used to enrich phosphopeptides for protein phosphorylation analysis with MS (Fig. 5c). In addition to the shape-selectivity offered by the binding cavities, the urea groups on the pore surfaces show strong binding affinity to the phosphopeptides because they can act as two-fold donors and form cyclic hydrogen bonds with the phosphopeptides. Using a mixture of the tryptic digests of phosphoprotein β-casein and nonphosphoprotein BSA as the

test sample, they showed that the imprinted mesoporous silica displayed excellent selectivity for phosphopeptides in the presence of interfering nonphosphopeptides at 100-fold higher concentration (Fig. 5d and e). With this method, phosphorylation analysis of a nonfat milk sample was realized. These results clearly confirm the excellent ability of the imprinted mesoporous materials for highly selective recognition of analytes due to the good shape selectivity and molecular interaction offered by the functionalized binding cavities.

The above mentioned studies demonstrated that imprinted mesoporous materials with excellent selectivity can be obtained by molecular imprinting. Imprinted mesoporous materials provide the charming prospect of highly specific antibody-mimicking recognition with specific binding cavities. Also, imprinted mesoporous materials have many advantages such as the size-exclusion effect and excellent stability. Although imprinted mesoporous materials display excellent selectivity, the kinds of currently available imprinted mesoporous materials are rather limited due to the difficulties in the synthesis process, such as the co-assembly of mesoporous templates and analyte analogs. In the past decades, researchers have developed more general and easy-to-perform methods for the preparation of mesoporous materials with specific recognition capabilities based on the surface physicochemical properties of mesoporous materials, as will be discussed in the following section.

2.3 Surface physicochemical properties

Mesoporous materials exhibit abundant surface physicochemical properties and they can be readily functionalized with a great variety of functional molecules on their surfaces,[40,127–129] which endows mesoporous materials with functions beyond their original chemical composition and structure.[22,130] Thus in addition to size and shape, selectivity can also be achieved with surface physicochemical properties by modifying mesoporous materials with chemical molecules or biomolecules with specific recognition functions (Fig. 6). In the past decades, a great variety of targeting molecules, including organic ligands,[70,131–133] DNA molecules,[134–136] aptamers,[137–139] DNAzymes,[140–142] enzymes,[143] peptides and antibodies,[144,145] have been immobilized on the surfaces of mesoporous materials to prepare mesoporous sensing systems for detection of analytes ranging from metal ions to living cells.[12,55] Many interesting sensing strategies such as gated sensing have been developed through the combination of mesoporous materials with other functional molecules.[146,147]

2.3.1 Surface functionalization for the gated sensing approach. Developing stimuli-responsive gated mesoporous materials that can release loaded guest molecules under external stimulation has attracted much attention and these materials are widely used in analytical chemistry.[12,39,60,67,148–152] Gated mesoporous sensing systems are usually prepared by functionalizing the pore entrance of mesoporous materials with switchable gatekeepers that are capable of being "opened" or "closed" in the presence of analytes.[60,153] Martínez-Máñez and coworkers described two basic principles in using gated mesoporous materials for sensing, that is, the "on–off" and "off–on" strategies (Fig. 7).[60,67,146,153] In the "on–off" strategy, mesopores are open and reporter molecules are released into the solution. In the presence of the analyte, gatekeepers on the pore entrance bind to the analytes and close the gate to block the release of reporter molecules.[60] As for the "off–on" strategy, mesoporous materials loaded with reporter molecules are capped with gatekeepers. The presence of the analyte induces the opening of the mesopores and release of the reporter molecules.[12,60] Over the past decades, the Martínez-Máñez group has reported the fabrication of various "on–off" and "off–on" gated mesoporous sensors for the detection of a wide variety of analytes.[67] They also provided very comprehensive reviews about the applications of gated mesoporous silica in the detection of anions, cations, small molecules and biomolecules.[60,67] In this section, gated mesoporous sensing systems will be discussed according to the kinds of gatekeepers (organic molecules, nucleic acids, peptides/proteins, and nanoparticles). Also, since the "off–on" strategy is easy to perform and has been widely explored by researchers, this section will focus on gated mesoporous sensors in the "off–on" manner.

The gatekeepers immobilized on the pore entrance of mesoporous materials for "off–on" control of the mesopores should have several key properties:[12,60,67,154] they should (1) be large

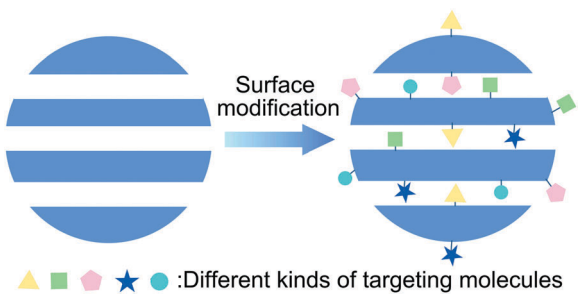

Fig. 6 Schematic illustration of the surface functionalization of mesoporous materials with various targeting molecules.

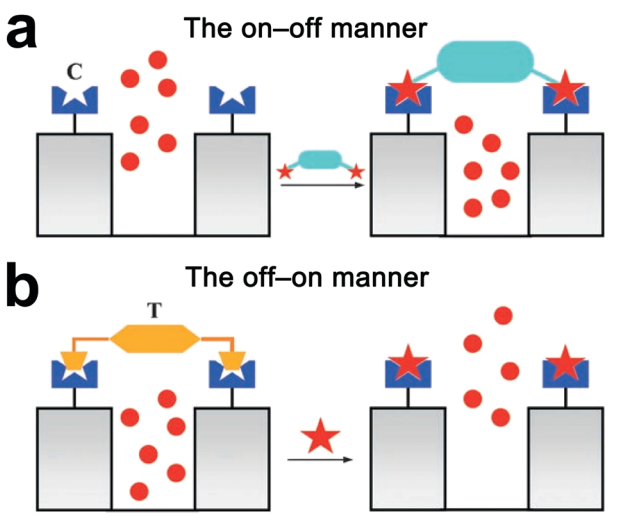

Fig. 7 Schematic illustration of the (a) "on–off" and (b) "off–on" principles of gated mesoporous sensing systems. Reprinted with permission from ref. 146. Copyright 2006, Wiley-VCH Verlag GmbH & Co. KGaA, Weinheim.

enough to cap the mesopores; (2) have selective recognition function; (3) change shape or location upon recognizing analytes; and (4) have functional groups for the immobilization around the pore entrance. In the past decades, molecules with large size and specific recognition function, such as antibodies, aptamers and DNAzymes, have been largely explored to serve as the gatekeepers. Many new gatekeepers have also been developed by the fusion of small molecules that have selective recognition function with large molecules that can cap the mesopores.[12] Nanoparticles functionalized with recognition moieties have also been used as the gatekeepers for the design of gated mesoporous sensors.[155]

2.3.1.1 Organic molecule gated mesoporous sensing systems. Organic molecules have gained increasing attention as gatekeepers due to their synthetic versatility and low cost.[60,156] Small organic molecules with recognition capability are usually integrated with macromolecules to design gatekeepers.[153,157–159] The competitive binding of analytes to the recognizing moieties displaced the gatekeepers to open the mesopores. In 2009, Martínez-Máñez *et al.* pioneered the use of gated mesoporous materials for analytical applications with an "off–on" strategy (Fig. 8a).[157] In that study, they developed an integrated macromolecule-capped MCM-41 mesoporous silica for CH_3Hg^+ detection. The mesoporous silica was loaded with a reporter dye and (3-mercaptopropyl)trimethoxysilane was functionalized on the surface of the MCM-41 mesoporous silica. The mercaptopropyl groups on the surface of the mesoporous silica can react with Hg^{2+}. However, the size of the mercaptopropyl groups is too

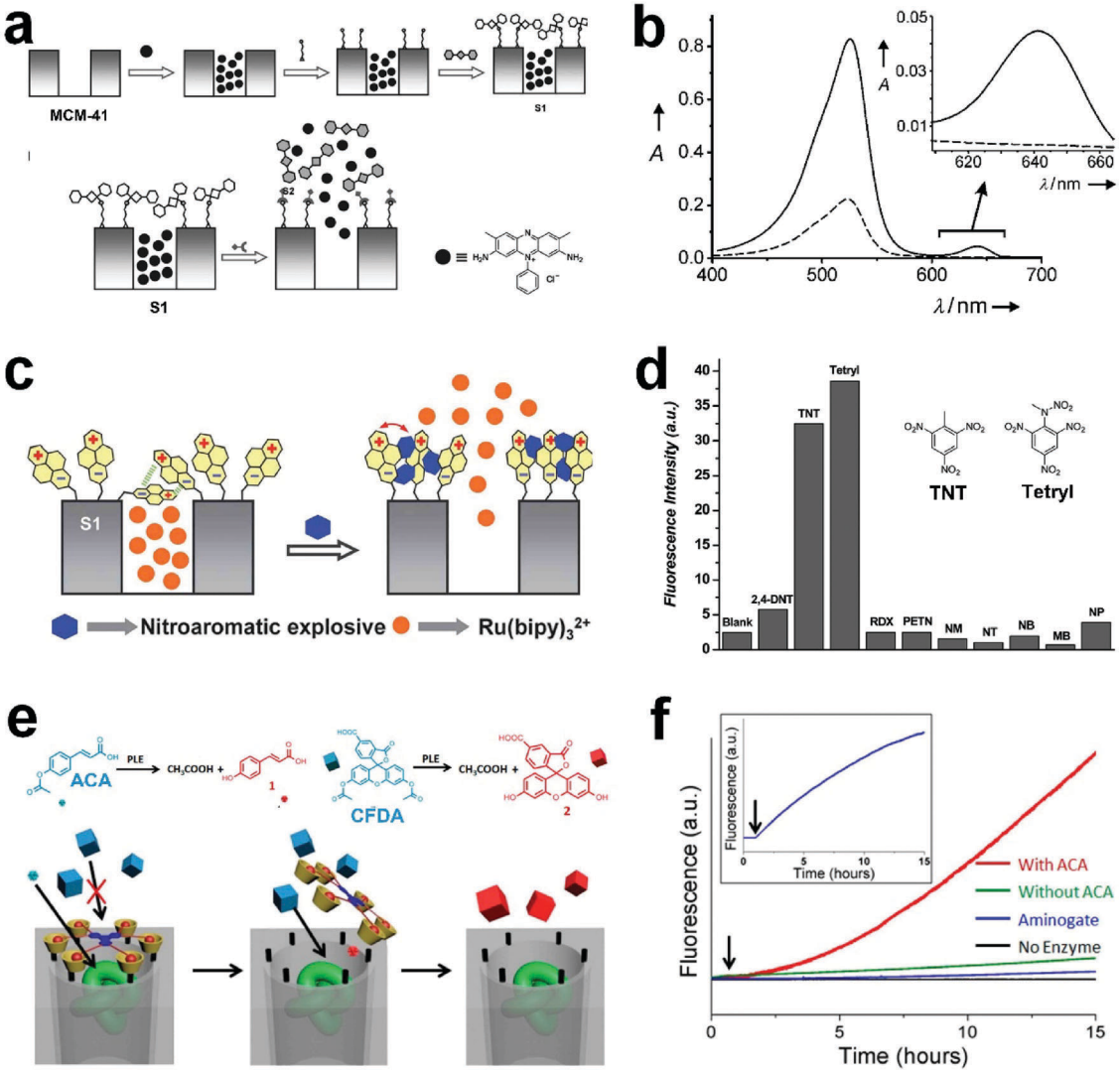

Fig. 8 (a) Schematic illustration of detecting CH_3Hg^+ with gated mesoporous silica in an "off–on" manner. (b) The absorbance of solutions containing gated mesoporous materials in the absence (dotted line) and presence (solid line) of CH_3Hg^+. Reprinted with permission from ref. 157. Copyright 2009, Wiley-VCH Verlag GmbH & Co. KGaA, Weinheim. (c) Schematic representation of sensing a nitroaromatic explosive with pyrene derivative capped mesoporous materials. (d) Fluorescence intensities of the gated mesoporous materials upon addition of nitroaromatic and non-aromatic derivatives. Reprinted with permission from ref. 160. Copyright 2013, Royal Society of Chemistry. (e) Schematic illustration of the sensing mechanism based on supramolecular gated enzyme-encapsulated mesoporous silica nanoparticles. (f) Changes in the fluorescence intensity of the gated mesoporous silica with the addition of different compounds. Reprinted with permission from ref. 164. Copyright 2013, American Chemical Society.

small to cap the mesopores. To solve this problem, a large squaraine derivative was further added to react with the mercaptopropyl groups to form the 2,4-bis(4-dialkylaminophenyl)-3-hydroxy-4-alkylsulfanylcyclobut-2-enone (APC) groups. The bulky APC groups can efficiently close the pores and inhibit the release of the dye. In the presence of CH_3Hg^+, the APC moieties can react with mercury, which led to the coordination of CH_3Hg^+ to the mercaptopropyl group and the release of the large squaraine moiety. As a result, the pores were opened and the loaded dye was released from the mesopores (Fig. 8b). The gated mesoporous sensor was able to distinguish CH_3Hg^+ from Hg^{2+}. Other cations (Pb^{2+}, Cd^{2+}, *etc.*) and various organic species (sodium lauryl sulphate, cysteine, *etc.*) also did not affect the response of the gated mesoporous sensor toward CH_3Hg^+. These results clearly suggested the good selectivity of the developed gated mesoporous sensing systems. Moreover, this study offered a new conception for the design of probes with good selectivity based on mesoporous materials.

Many supramolecules with recognition function have been directly explored as the gatekeepers in the design of gated mesoporous sensors.[153,160–162] Supramolecules that can undergo shape or position changes upon recognizing analytes are ideal gatekeepers. In one of these studies, Martínez-Máñez *et al.* designed a pyrene derivative capped mesoporous sensor for the detection of nitroaromatic explosives (Fig. 8c).[160] In their design, the release of the reporter dye $Ru(bipy)_3^{2+}$ was inhibited by the bulky pyrene moieties immobilized on the pore entrance of MCM-41 mesoporous silica. In the presence of nitroaromatic explosives, pyrene–nitroaromatic complexes were formed, which would push away the bulky pyrene moieties from the pore entrance to release the entrapped dye. The authors showed that nitroaromatic explosives such as tetryl and trinitrotoluene (TNT) were able to induce the release of the loaded dye, whereas other aromatic derivatives induce the negligible release of the dye (Fig. 8d). The good selectivity was ascribed to the strong electron acceptor feature of tetryl and TNT that leads to the formation of charge-transfer compounds between the grafted pyrene moieties and the target tetryl or TNT. The same research group further explored the applications of MCM-41 mesoporous silica capped with tetrathiafulvalene derivatives in the detection of nitroaromatic explosives.[153] The gated mesoporous sensing systems showed ''zero release'' in the absence of the analytes due to the formation of dense tetrathiafulvalene networks around the pore entrance. In the presence of nitroaromatic explosives, charge transfer compounds were formed between the electron-accepting nitroaromatic explosives and the electron-donating tetrathiafulvalene derivatives, which leads to the uncapping of the mesopores and the release of the entrapped dyes. These studies thus clearly demonstrate that good selectivity can be achieved by modifying mesoporous materials with molecules showing specific recognition function.

Zink and coworkers have also designed many interesting gated mesoporous systems.[132,163,164] In one of their studies, they designed an enzyme-encapsulated mesoporous silica modified with a supramolecular gatekeeper that can regulate the access to the loaded enzyme (Fig. 8e).[164] When the analytes opened the gatekeeper and exposed the encapsulated enzymes, a catalytic reaction would be initiated to produce fluorescent molecules. As a proof of concept, mesoporous silica was loaded with porcine liver esterase (PLE) and further functionalized with pH-responsive supramolecules as the gatekeepers. Analytes with small sizes such as 4-acetoxycinnamic acid (ACA) can diffuse into the mesopores to produce acids under the catalysis of the PLE. The pH-sensitive imine bonds within the gatekeepers are cleaved in an acidic environment and molecules with larger sizes can freely diffuse into the mesopores. Once the enzymes loaded into mesopores were accessible, 5-carboxyfluorescein diacetate molecules would diffuse into the mesopores and react with the enzymes, which led to the catalytic production of fluorescent molecules. As a result, the selective and sensitive detection of ACA and 5-carboxyfluorescein diacetate could be realized (Fig. 8f). The developed gated mesoporous sensing systems allow the coexistence of the reporter molecules (enzyme substrates) and the enzymes, and the sensing system can prevent their interaction before the system is selectively activated by the analytes. This study provides a new concept for the design of sensing probes that can simultaneously detect multiple analytes with mesoporous materials, which makes this work highly valuable in areas such as disease diagnosis.

2.3.1.2 Nucleic acid gated mesoporous sensing systems. Nucleic acids are polyanions that have relatively large size and good molecular recognition capability.[165,166] The most famous specific recognition ability of nucleic acids is the classical Watson–Crick base pairing.[167] Moreover, some nucleic acids with unique sequences and structures display extraordinary specific recognition capabilities, such as aptamers[168–171] and DNAzymes.[172,173] Additionally, nucleic acids can also respond to enzymes.[165] Due to their versatile specific recognition function and relatively large sizes, nucleic acids have been extensively combined with mesoporous materials to develop highly selective gated mesoporous sensing systems for the detection of a wide range of analytes, such as metal ions, small molecules, and biomacromolecules.[62,134,136,140,174]

In 2010, Martínez-Máñez *et al.* demonstrated a gated mesoporous sensing system with mesopores that can be uncapped by the hybridization of the gatekeeper nucleic acids with the target oligonucleotide (Fig. 9a).[134] The sensing system was based on fluorescein-loaded MSNs with surface functionalization of (3-aminopropyl)triethoxysilane. The nucleic acid sequence 5′-AAT GCT AGC TAA TCA ATC GGG-3′ was used to cap the mesopores *via* electrostatic interactions with the anchored amines. In the presence of the complementary oligonucleotide, fluorescein was released into the solution due to the hybridization between the gatekeeper and the target complementary oligonucleotide. The developed gated mesoporous sensing system can discriminate the full complementary sequence from other oligonucleotides with a single or two-base mismatch sequence, clearly suggesting its excellent selectivity (Fig. 9b). This study demonstrated a general and easy-to-perform strategy for the construction of target-responsive mesoporous sensing systems, which can further contribute to areas such as drug delivery.

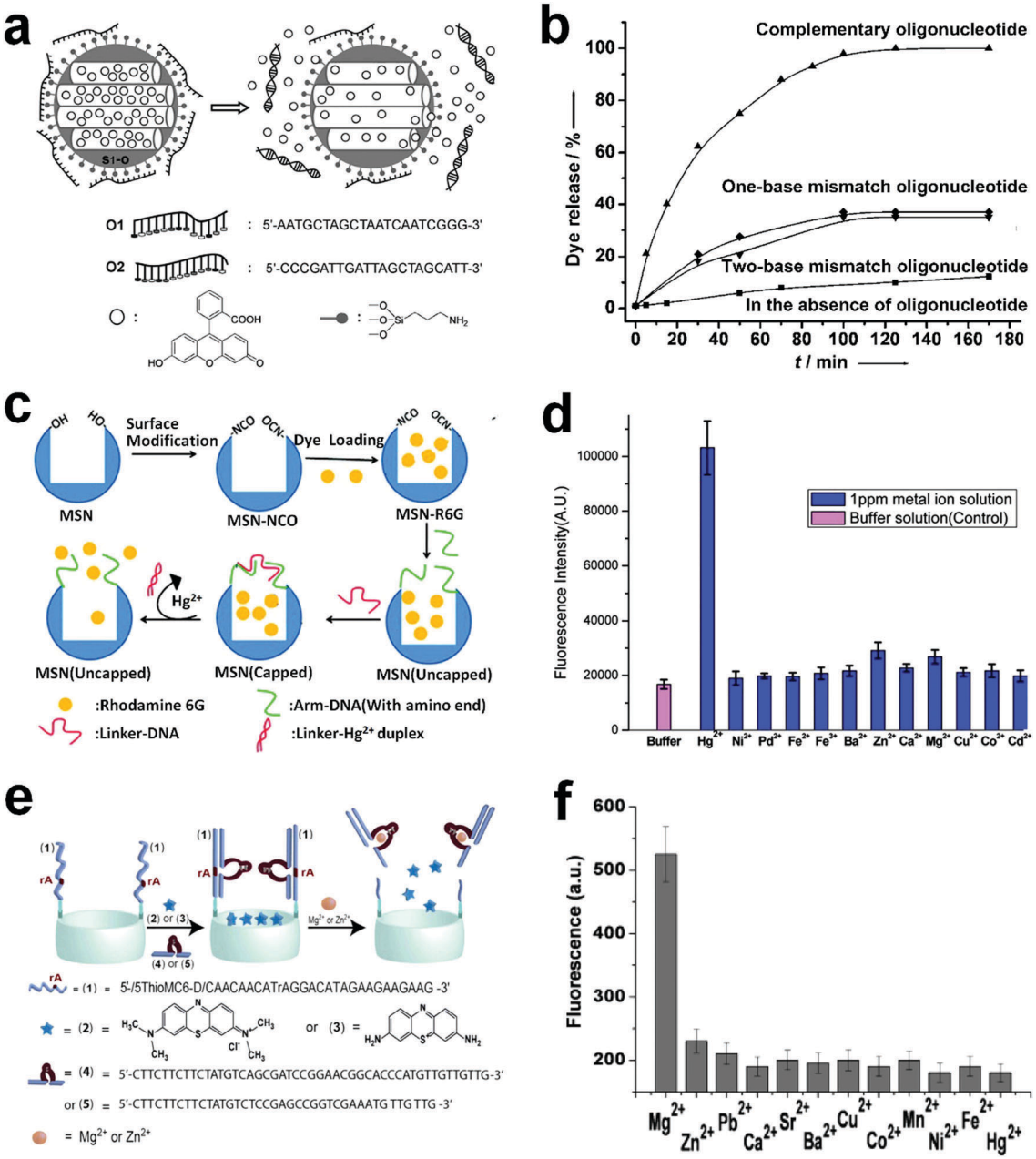

Fig. 9 (a) Schematic illustration of DNA-gated mesoporous silica for the detection of single-stranded oligonucleotides. (b) Fluorescence intensity of the mesoporous sensing system in the presence of a complementary oligonucleotide and oligonucleotides with one or two base mismatches. Reprinted with permission from ref. 134. Copyright 2010, Wiley-VCH Verlag GmbH & Co. KGaA, Weinheim. (c) Schematic illustration of DNA aptamer-gated mesoporous silica for the detection of Hg^{2+}. (d) The response of the aptamer-gated mesoporous probe upon addition of different metal ions. Reprinted with permission from ref. 139. Copyright 2012, American Chemical Society. (e) Schematic illustration of DNAzyme-gated mesoporous silica for the detection of Mg^{2+} or Zn^{2+}. (f) Fluorescence intensity of the DNAzyme-gated mesoporous sensing platform with the addition of different cations. Reprinted with permission from ref. 140. Copyright 2013, American Chemical Society.

As we mentioned above, nucleic acids such as aptamers display specific recognition function beyond Watson–Crick base pairing. In 2012, Tan *et al.* developed DNA aptamer-capped mesoporous silica nanoparticles for the detection of Hg^{2+} (Fig. 9c).[139] In this study, mesoporous silica nanoparticles were loaded with Rhodamine 6G. A short arm-DNA strand labeled with an amino group (5′-GAA GAA CAA CAA AAA-NH_2-3′) was modified on the mesoporous silica nanoparticles. The DNA aptamer that can recognize Hg^{2+} (5′-GTT GTT CTT CCT TTG TTT CCC CTT TCT TTG GTT GTT CTT C-3′) was used to cap the mesopores through hybridizing with the arm-DNA. As Hg^{2+} can bind to two T bases to form a more stable T–Hg^{2+}–T duplex than the aptamer–arm–DNA duplex, the aptamer gatekeeper prefers to bind to Hg^{2+} and open the mesopores. Results show that the mesoporous silica nanoparticles were tightly capped by the aptamer with the negligible release of Rhodamine 6G in the

absence of Hg^{2+}. On the other hand, in the presence of Hg^{2+}, a large release of dye molecules was observed. The gated mesoporous sensor shows good selectivity to Hg^{2+} due to the good specific recognition capability of the DNA aptamer (Fig. 9d). The sensing strategy reported in this study can serve as a new prototype for the construction of highly selective and sensitive sensing systems with aptamers. Moreover, this study can further be promoted to the detection of various targets by simply using the corresponding aptamers.

DNAzymes are single stranded DNA molecules that can catalyze various reactions, such as RNA cleavage.[172,173] Based on the specific cofactor dependence and potent catalytic ability of DNAzymes, Willner *et al.* have developed a series of DNAzyme capped mesoporous silica nanoparticles for the detection of analytes such as metal ions and small biomolecules (Fig. 9e).[140] In one of their studies, mesoporous silica nanoparticles were loaded with methylene blue as the reporter molecules. The substrate strand of the metal ion dependent DNAzymes was immobilized on the pore entrance of the mesoporous silica nanoparticles, and DNAzymes further hybridize with the substrate strand to cap the mesopores. In the presence of target metal ions Mg^{2+} or Zn^{2+}, the DNAzymes bind to the metal ions and further catalyze the specific cleavage of the substrate strands. As a result, the DNAzymes detach from the substrate strands and the mesopores are opened, leading to the release of the reporter molecules. Results showed that enhanced fluorescence can be observed only in the presence of Mg^{2+}, showing good selectivity of the gated mesoporous sensors (Fig. 9f). Since metal ions can serve as the specific cofactor for DNAzymes to cleave the substrate strand,[162,163] the DNAzyme gated mesoporous systems show great potential for the construction of metal ion responsive sensing probes or drug delivery systems.

2.3.1.3 Protein/peptide gated mesoporous sensing systems. Proteins such as antibodies possess both specific recognition capability and relatively large size,[175] making them excellent gatekeepers in the design of gated mesoporous sensing systems.[144,176–178] In 2009, Martínez-Máñez *et al.* described the design of an antibody capped mesoporous system for selective detection of sulfathiazole (Fig. 10a).[176] In this study, mesoporous silica was loaded with $Ru(bipy)_3^{2+}$ as the reporter, and the pore entrance was further functionalized with a hapten, 4-(4-aminobenzenesulfonylamino)benzoic acid. Antibody can bind to the hapten and cap the mesopores to block the diffusion of

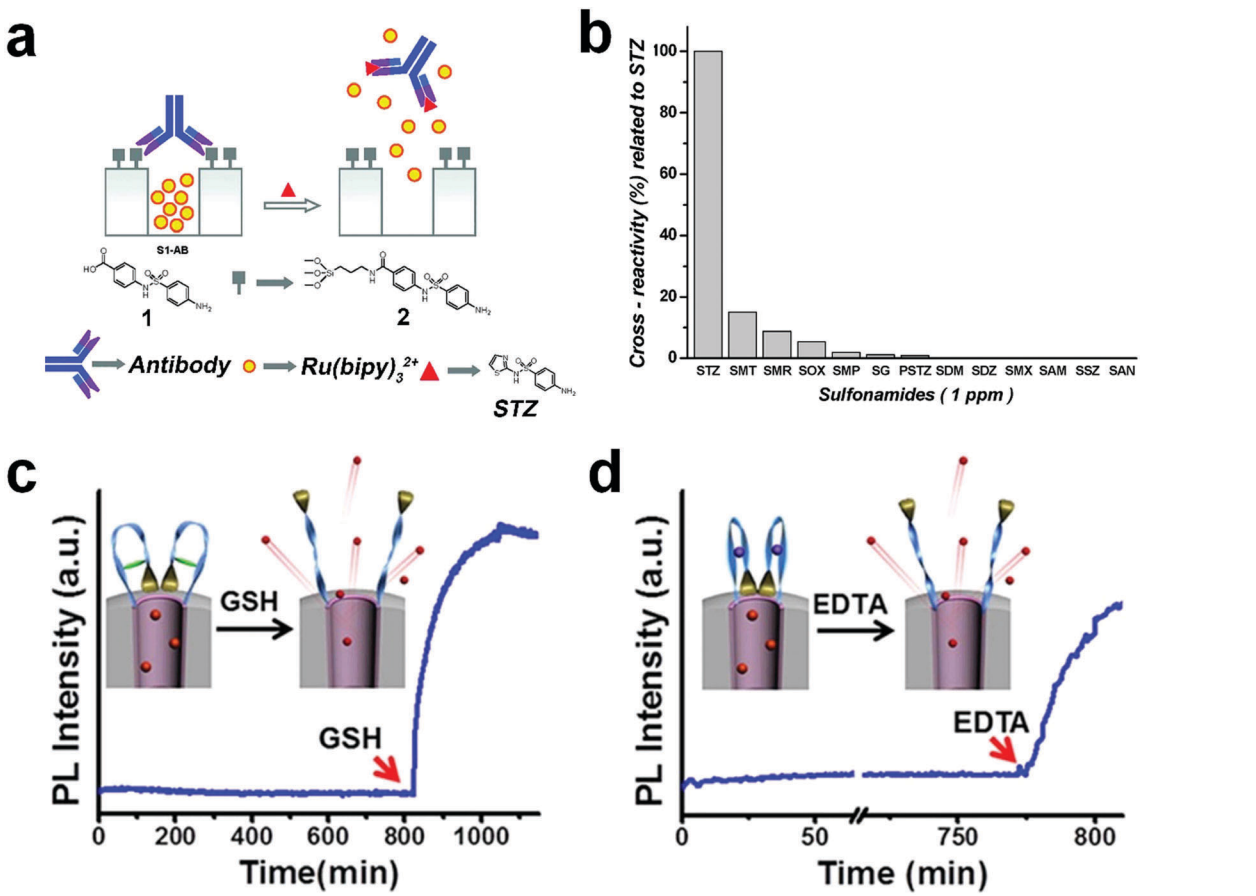

Fig. 10 (a) Schematic representation of antibody capped mesoporous silica for the detection of sulfathiazole. (b) Relative release of dye from the gated mesoporous silica in the presence of different chemicals. Reprinted with permission from ref. 176. Copyright 2009, American Chemical Society. (c) Glutathione detection with Fmoc-CGGC-SS gated mesoporous silica. (d) The detection of Zn^{2+} with Fmoc-CGGC-Zn gated mesoporous silica. Reprinted with permission from ref. 178. Copyright 2014, American Chemical Society.

$Ru(bipy)_3^{2+}$ into the solution. In the presence of sulfathiazole, the antibody was displaced from the mesoporous silica due to its stronger binding affinity to sulfathiazole than to hapten, leading to the release of $Ru(bipy)_3^{2+}$ into the solution (Fig. 10b). The structural analogs of sulfathiazole caused the negligible release of $Ru(bipy)_3^{2+}$, suggesting good selectivity of the antibody-gated mesoporous sensing system (Fig. 10b). This antibody gated mesoporous system can further be promoted to other countless controlled release systems using different cargos and antibodies, making this design highly valuable for a broad range of stimuli-responsive delivery purposes in different areas.

In addition to antibodies, peptides have also been employed as the gatekeepers.[178,179] Lee and co-workers showed that peptide Fmoc-CPGC with a turn structure can efficiently cap the mesopores and inhibit the release of calcein loaded into mesoporous silica, whereas Fmoc-CGGC with a random structure cannot inhibit the release of the entrapped calcein.[178] Based on this phenomenon, they proposed that peptides with conformational conversion between a turn and a random structure can serve as stimuli-responsive gatekeepers. As a proof of concept, they designed Fmoc-CGGC-SS gated mesoporous sensing systems that are responsive to biological stimuli such as glutathione. In the designed systems, the two cysteine units in the peptides were linked *via* a disulfide bond to form a turn-like structure for capping the mesopores (Fig. 10c). With the addition of glutathione, the disulfide bond within Fmoc-CGGC-SS was reduced and the turn-like structure was converted to a random structure, leading to the opening of mesopores and the release of the entrapped calcein. Lee and co-workers further designed another stimuli-responsive system with Zn^{2+} ion stabilized Fmoc-CGGC (Fig. 10d). In the presence of Zn^{2+}, the two thiol groups within CGGC can chelate a Zn^{2+} ion to form a turn structure; thus the mesopores can be efficiently capped. Further addition of EDTA can remove the Zn^{2+} from Fmoc-CGGC-Zn and the peptide is converted to a random structure, leading to the release of the entrapped cargo. This work provides a new way for the design of stimuli-responsive peptide gatekeepers in the construction of gated mesoporous sensing systems, which can contribute to the design of delivery vehicles with user-defined release characteristics.

2.3.1.4 Bio-functionalized nanoparticle gated mesoporous sensing systems. Due to their controllable size and abundant surface properties, nanoparticles functionalized with specific recognizing molecules have also been widely employed as the gatekeepers in the design of gated mesoporous sensing systems.[155,180–186] In 2011, Yang *et al.* described the conception of a novel and general bioresponsive gated mesoporous sensing system by capping mesoporous silica nanoparticles with aptamer functionalized gold nanoparticles (Fig. 11).[155] In this study, mesoporous silica nanoparticles were functionalized with adenosine. The Au nanoparticles were modified with the adenosine triphosphate (ATP) binding aptamer further and they can bind to adenosine to cap the mesopores (Fig. 11a). The binding affinity of the ATP aptamer toward adenosine is much weaker than that toward ATP. Therefore, in the presence of ATP, the Au nanoparticles were displaced from the surfaces of the mesoporous silica nanoparticles due to the competitive displacement reaction (Fig. 11b and c). The gated mesoporous sensing system displayed negligible dye leaching in the absence of ATP, whereas addition of ATP to the system can trigger the considerable release of reporter fluorescein (Fig. 11d). Such target-responsive mesoporous systems can further provide a promising route for the construction of stimuli-responsive

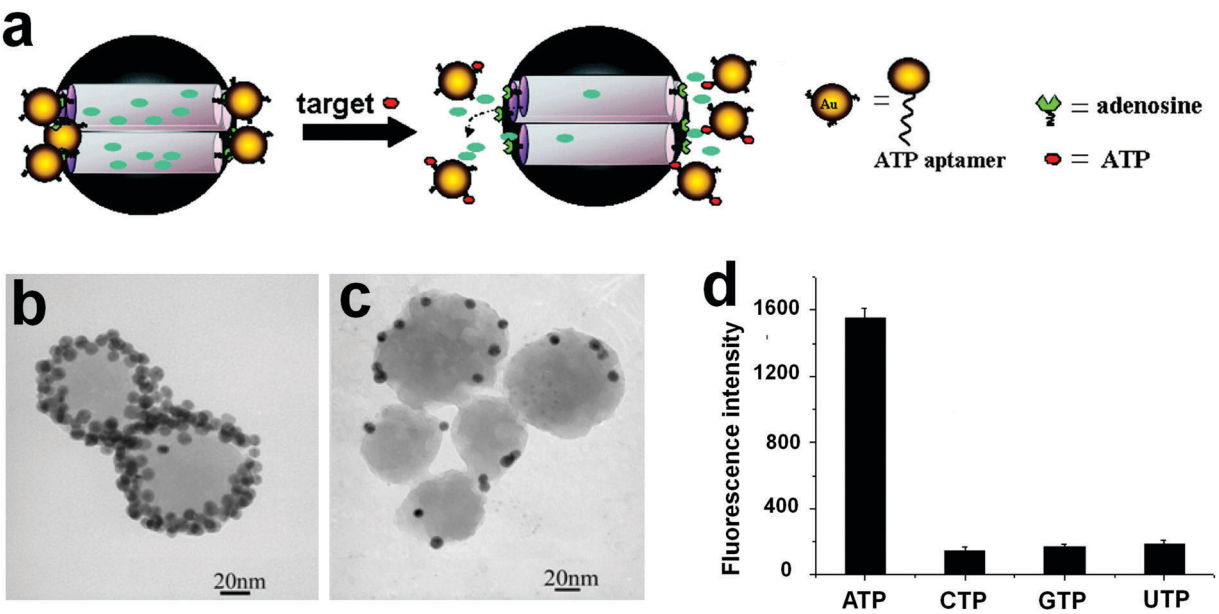

Fig. 11 (a) Schematic illustration of bio-functionalized nanoparticle capped mesoporous silica for the detection of ATP. TEM images of Au-capped mesoporous silica in the absence (b) and presence (c) of ATP. (d) Fluorescence intensity of the released fluorescein in the presence of ATP, CTP, GTP and UTP. Reprinted with permission from ref. 155. Copyright 2011, American Chemical Society.

sensing systems and controlled-delivery nanodevices. Furthermore, considering the good specificity and biocompatibility of aptamers, the gated mesoporous system reported in this study is promising for *in vivo* biosensing and cancer therapy.

2.3.2 Surface functionalization for the binding site–signalling subunit approach. In the above mentioned works, the binding molecules are immobilized on the pore entrance of mesoporous materials as gatekeepers to control the access of mesopores for sensing applications.[60,67] Due to the large inner surface of mesoporous materials, a large variety of binding and signalling subunits have been immobilized on the inner pore surface for the construction of sensing systems.[187–190] The binding subunits can specifically bind to analytes in such a way that the properties of the signalling subunits can be changed to produce signals, such as fluorescence signals.[127,133,147,188,191–193] In 2001, Wirnsberger, Stucky and co-workers demonstrated that dye-functionalized mesoporous thin films can serve as solid-state pH sensors.[194] The pH sensitive dye fluorescein was covalently anchored to the surfaces of the mesopores. The fluorescence intensity of the thin films was dependent on the pH and the observed fluorescence intensity was stronger in a basic environment. Moreover, due to the high porosity of the mesoporous film, the pH sensor displayed fast response in pH sensing. The developed solid-state pH sensors showed high processibility and this design can be further extended to other sensing arrangements including pH sensing microtips.

Martínez-Máñez and co-workers have made much efforts in the design of mesoporous sensing systems with the binding site–signaling subunit approach.[131,147,187,195,196] They reported the grafting of supermolecular receptors onto the inner pore surface of mesoporous silica for the detection of anions such as ATP (Fig. 12a).[147] Mesoporous silica was first treated with 3-aminopropyltriethoxysilane to introduce amino groups onto its surface, and the obtained mesoporous silica was further allowed to react with 9-anthraldehyde for the preparation of mesoporous sensing systems. The binding of 9-anthraldehyde to ATP molecules can lead to efficient quenching of the fluorescence of 9-anthraldehyde (Fig. 12b), leading to the detection of ATP. The addition of structural analogues of ATP including adenosine 5′-diphosphate (ADP) and adenosine 5′-monophosphate (AMP) resulted in much weaker fluorescence quenching than ATP. Other small anions such as chloride, bromide, and phosphate did not cause any significant change to the fluorescence intensity, showing good selectivity of the mesoporous sensing system. The same group further promoted the mesoporous sensing system for the detection of anions such as fatty acids (long-chain carboxylates).[131] In that work, a spacer-substituted 7-urea-phenoxazin-3-one was employed as the signaling

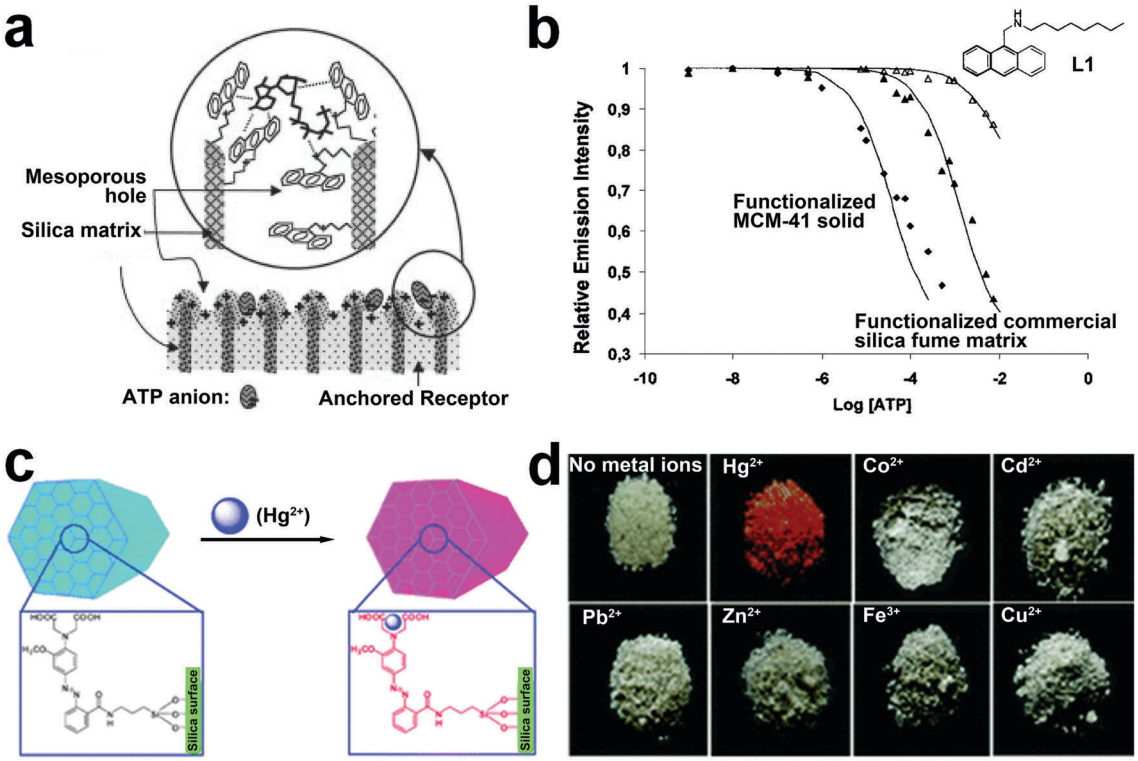

Fig. 12 (a) Schematic illustration of ATP detection with supermolecular receptor functionalized mesoporous silica with the binding site–signaling subunit approach. (b) The fluorescence intensity of supermolecular receptor functionalized mesoporous silica and supermolecular receptor functionalized commercial silica fume matrix upon addition of ATP with different concentrations. Reprinted with permission from ref. 147. Copyright 2002, Wiley-VCH Verlag GmbH & Co. KGaA, Weinheim. (c) Schematic illustration of Hg^{2+} detection with the acyclic receptor functionalized mesoporous silica. (d) Photographs of the acyclic receptor functionalized mesoporous silica with the addition of different kinds of metal ions. Reprinted with permission from ref. 127. Copyright 2008, Royal Society of Chemistry.

receptor and it was modified on the pore surface of the UVM-7 mesoporous silica. The functionalized mesoporous silica showed both fluorescence red-shift and the enhancement of fluorescence intensity upon binding to long-chain carboxylates such as dodecanoate and stearate. Short-chain carboxylates, medium-chain carboxylates, and aromatic, (poly)hydroxy, and polycarboxylic acids do not lead to obvious changes to the fluorescence intensity of the mesoporous sensing system. Anions play crucial roles in chemical reactions and biological processes. The anion sensing strategy developed here may further contribute to fields including reaction kinetics study and biosensing.

In another work, Jung *et al.* reported the preparation of mesoporous silica functionalized with azobenzene-coupled acyclic receptors through the hydrolysis of a triethoxylsilyl group-terminated acyclic receptor.[127] The bridgehead nitrogen atom of the aniline group on the acyclic receptor can form a strong coordination bond with Hg^{2+}, which leads to significant changes to the color of the mesoporous sensing system (Fig. 12c). The functionalized mesoporous silica displayed an obvious color change from light yellow to red within 10 s in the presence of Hg^{2+} (Fig. 12d). However, upon addition of metal ions including Co^{2+}, Cd^{2+}, Pb^{2+}, Zn^{2+}, Fe^{3+} and Cu^{2+}, no obvious color changes of the mesoporous silica powder were observed (Fig. 12d), suggesting that the developed mesoporous probe can be used for selective detection of Hg^{2+}. The reported solid state sensor holds great promise in point of care detection of heavy metal ions.

2.3.3 Surface functionalization for the displacement approach. In addition to gated sensing and binding site–signalling subunit sensing approaches, researchers have also developed the displacement approach for sensing applications.[70,197,198] The mechanism of the displacement approach involves the displacement of the signalling unit from the binding unit by analytes due to the stronger interaction between the binding unit and the analytes.[199–201] Generally, the binding units are immobilized on the surfaces of mesoporous materials through the co-condensation method or post grafting. Signalling reporters, such as organic dye, bind to the binding units *via* electrostatic or covalent interaction.[200] In the presence of analytes, the signalling units are displaced from the binding sites and are released into the solution to produce detectable signals.

In 2005, Martínez-Máñez *et al.* developed a mesoporous sensing system for colorimetric and fluorogenic detection of anions based on the displacement approach (Fig. 13a).[70] In this study, mesoporous silica was covalently functionalized

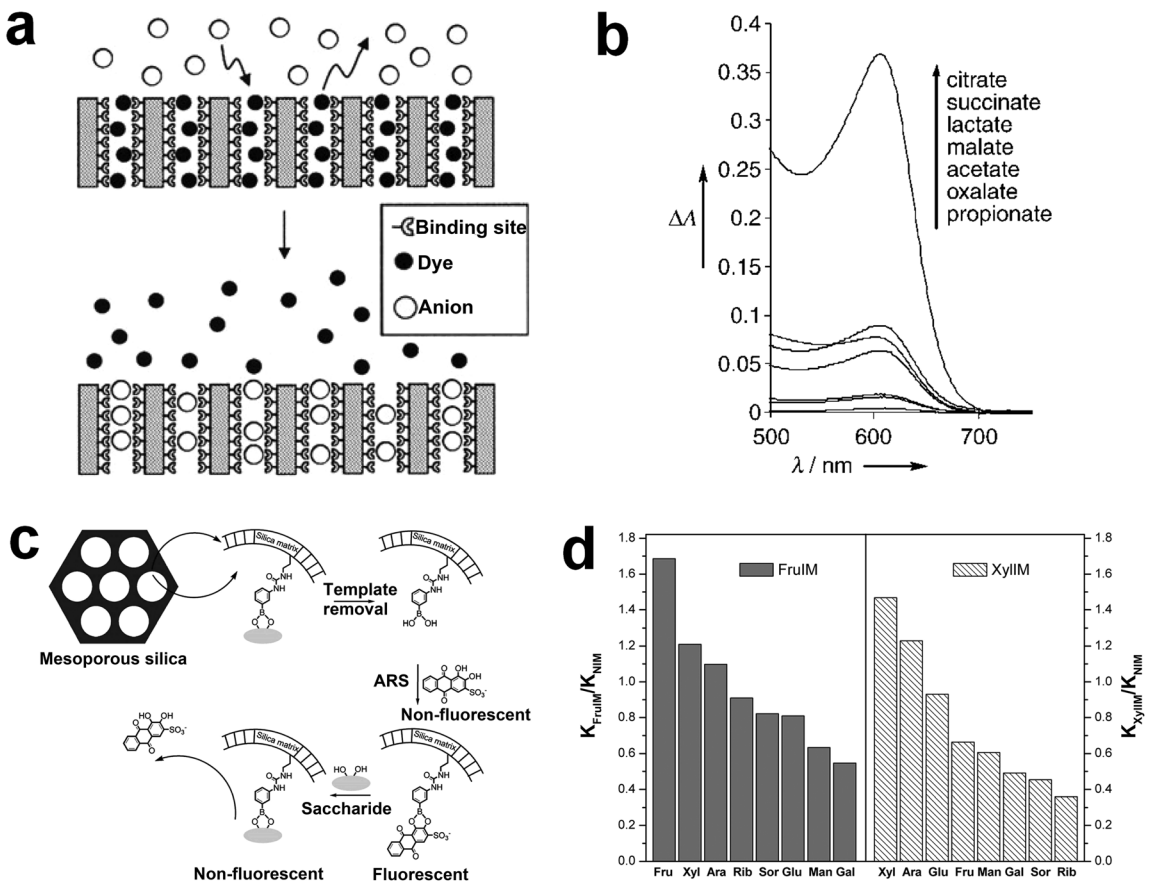

Fig. 13 (a) Schematic illustration of anion detection with a mesoporous sensor through the displacement assays. (b) The absorbance spectra of the mesoporous sensing system in the presence of different carboxylates. Reprinted with permission from ref. 70. Copyright 2005, Wiley-VCH Verlag GmbH & Co. KGaA, Weinheim. (c) Schematic representation of imprinted mesoporous silica for the detection of saccharides in the displacement approach. (d) The quenching constant of the imprinted mesoporous silica and non-imprinted mesoporous silica for saccharides. Reprinted with permission from ref. 197. Copyright 2009, American Chemical Society.

with 2-methylthio-2-imidazoline hydroiodide to serve as the binding units. The signalling reporter methylthymol blue further bound to 2-methylthio-2-imidazoline hydroiodide *via* coordinative interaction. The guanidinium groups of 2-methylthio-2-imidazoline hydroiodide can form hydrogen bonding interactions with carboxyl groups, leading to the displacement and release of the methylthymol blue. As a result, an obvious colour change and significant fluorescence enhancement can be observed (Fig. 13b). In this study, borate has also been selectively detected using mannose as the binding molecule and azoic dye as the reporter molecule. Their work proved that new chromo/fluorogenic probes can be designed based on mesoporous materials functionalized with different binding units through the displacement approach. The same research group has also designed mesoporous chemosensors for detecting other kinds of ions based on the displacement assay.[199,200] In the sensing protocol, different kinds of binding molecules immobilized on the surface of mesoporous silica acted as the binding sites, which can interact with ions through electrostatic attractive forces or hydrogen bonding interaction. Analytes such as nucleotides, Hg^{2+} and a family of carboxylates have been detected with the developed sensing strategy. These studies can open new possibilities for the promotion of mesoporous materials in solid-state/supramolecular chemistry. The countless molecules with recognition function make this approach highly promising in developing new colorimetric or fluorogenic sensors for the detection of a wide range of analytes.

By coupling the signaling unit-displacement strategy with the molecular imprinting technique, Yan *et al.* reported a fluorescent sensor based on imprinted mesoporous silica functionalized with phenylboronic acid for the detection of saccharides.[197] In that work, the phenylboronic acid moiety was used as the saccharide receptor and fluorescent dye Alizarin Red S (ARS) was used as the reporter. The imprinted mesoporous silica was obtained by the co-condensation of triethoxysilane-terminated phenylboronic acid and the saccharide template with tetraethoxysilane. The ARS dye was further covalently conjugated to the inner pore surface to form fluorescent mesoporous silica. With the addition of the analyte saccharide, the ARS was displaced and released from the phenylboronic acid moiety, which resulted in a decrease of fluorescence intensity (Fig. 13c). Also, D-fructose imprinted mesoporous silica (FruIM) and D-xylose imprinted mesoporous silica (XylIM) were prepared. The mesoporous sensors displayed the strongest response to their corresponding templates (Fig. 13d). D-Fructose and D-xylose were successfully quantified even in the presence of structural analogues including D-arabinose, D-glucose and D-galactose, showing good selectivity of the imprinted mesoporous sensing systems. Saccharides are primary biological substances and they play fundamental roles in many biological activities. Also, saccharides are widely used as food and cosmetic additives. This mesoporous sensing system may further find broad applications such as biosensing and food analysis.

3. Sensitivity-related structural properties

Sensitivity is defined as the change in the signal response (optical signals, magnetic signals, electrical signals, *etc.*) induced by a change in the analyte concentration.[68,69,202] For analytical methods with high sensitivity, a small amount of analyte is sufficient to trigger a high signal response. The structural properties of mesoporous materials have been largely explored to improve the sensitivity of many analytical methods.[26,63,203,204] For instance, large pore volumes are widely used to load reporter molecules for signal amplification.[65,140,204] Upon addition of a small amount of analyte, large amounts of reporter molecules can be released and strong signal responses are produced. In this section, the structural properties of mesoporous materials that are conducive to the sensitivity will be discussed. Also, the representative works that achieve high detection sensitivity by making use of the structural properties of mesoporous materials will be introduced.

3.1 Pore volume

The large pore volume of mesoporous materials makes it possible to load large amounts of reporter molecules into the mesopores.[39,60,65,155,203,205] Signal amplification can be easily achieved by triggering the release of reporter molecules with a handful of analytes (Fig. 14). Such signal amplification processes are usually realized with the above mentioned gated mesoporous sensing systems.[60,67] Any molecule with detectable physicochemical properties (fluorescence properties, redox activity, *etc.*) and suitable size can be used as the reporter molecules for signal amplification in the design of mesoporous

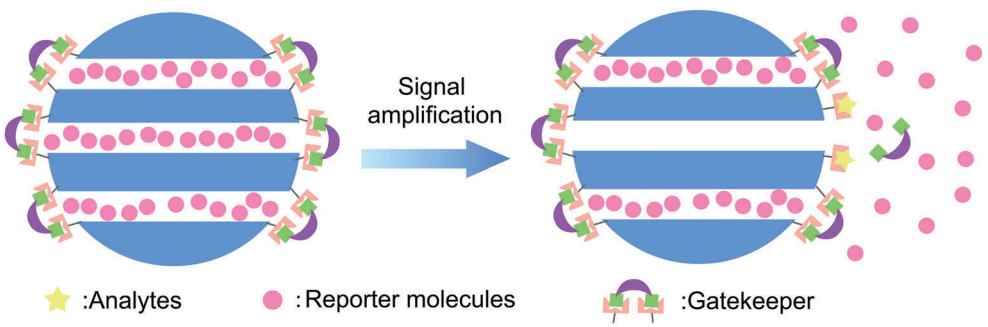

Fig. 14 Schematic illustration of signal amplification based on the large pore volume of mesoporous materials.

sensing systems.[60,185,186] In the past decades, fluorescence molecules, glucose and many other molecules have largely been loaded into mesoporous materials as the reporter molecules.[60,155,203,206,207] Also, a wide range of analytes, such as metal ions, small biomolecules, peptide, proteins, and DNA, have been detected with high sensitivity by making use of the large pore volume of mesoporous materials for signal amplification.[38,67,136,139,208]

3.1.1 Loading fluorescent molecules. Fluorescence analysis offers many advantages, such as easy operation, high spatiotemporal resolution, and noninvasive and real-time analysis, making fluorescence analysis suitable for wide use in analytical science.[62,209] Small organic fluorescent molecules show bright fluorescence, high quantum efficiency and tunable optical properties.[210] Notably, it's easy to load a large amount of small organic fluorescent molecules into the mesopores, and further capping the mesopores with appropriate gatekeepers results in the creation of mesoporous sensing systems with signal amplification capability.[205,211–214] Upon recognizing the analytes, fluorescent molecules are released into the solution to give strong fluorescence signals.[60,62,67]

In 2013, Ju *et al.* reported a sensitive fluorescent probe that consists of dye-loaded mesoporous silica and DNA gatekeepers for the detection of intracellular telomerase activity (Fig. 15a).[62] Telomerase is a ribonucleoprotein that can add the repeated DNA sequence TTAGGG to the 3′ end of telomeres. In cancer cells, the telomerase is overexpressed and thus the telomeres can maintain their length to cause unlimited cell proliferation. Ju and coworkers designed the telomerase-responsive mesoporous probe by wrapping dye-loaded mesoporous silica nanoparticles with DNA molecules containing the TTAGGG sequence (Fig. 15a). In particular, the surfaces of the mesopores were functionalized with a black-hole-quencher (BHQ), and fluorescein was further loaded into the mesoporous silica to serve as the reporter. The DNA strand adsorbed onto the surface of mesoporous silica *via* electrostatic attraction to serve as the gatekeeper. Due to the efficient quenching of fluorescence from fluorescein by BHQ, the mesoporous probe displayed negligible

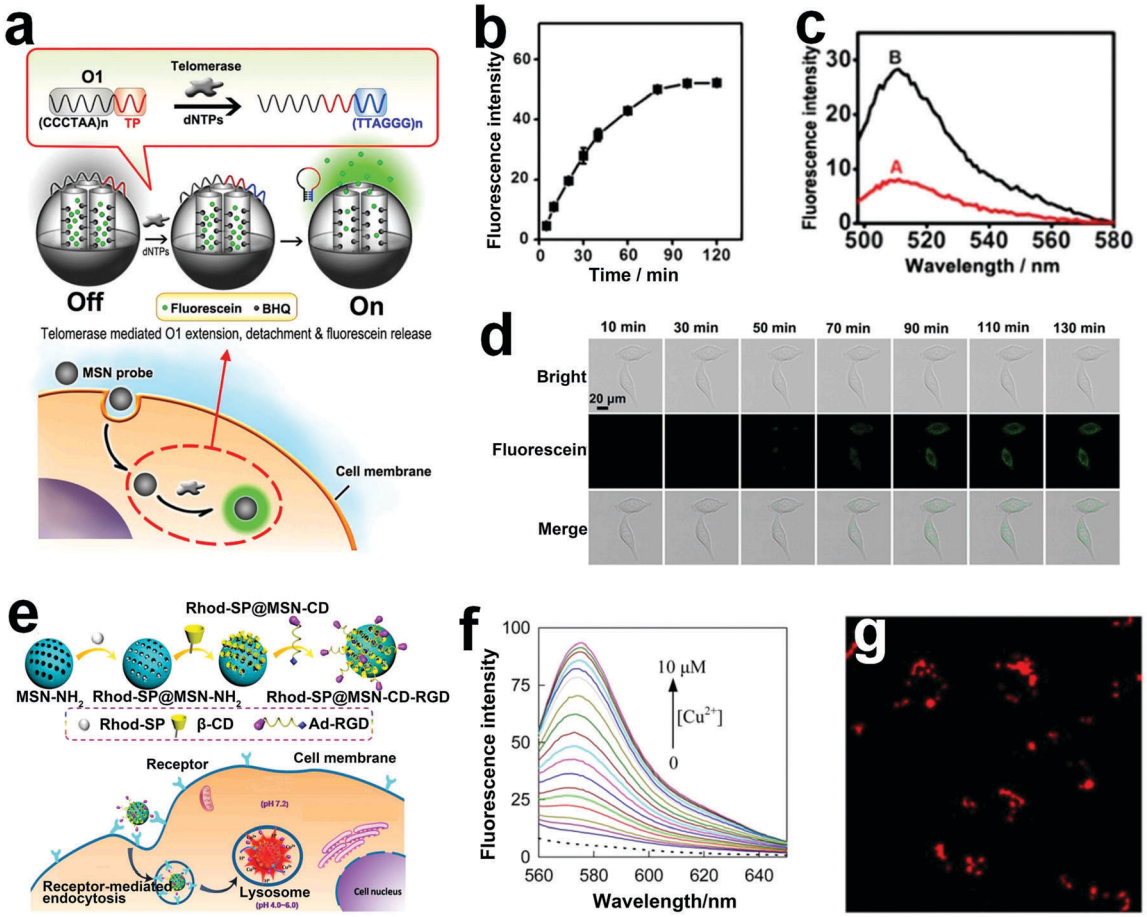

Fig. 15 (a) Schematic illustration of the fluorescein loaded mesoporous probe for intracellular telomerase activity detection. (b) The fluorescence intensities of the mesoporous probe after incubation with telomerase for different times. (c) Fluorescence intensity of the mesoporous probe after incubation with cell extract (A) or with telomerase spiked cell extract (B). (d) Confocal images of HeLa cells incubated with the mesoporous probe at different time points. Reprinted with permission from ref. 62. Copyright 2013, American Chemical Society. (e) Schematic representation of the dual-responsive fluorescence dye Rhod-SP loaded mesoporous probe for Cu^{2+} detection in lysosomes. (f) The fluorescence spectra of the mesoporous probe in the presence of Cu^{2+} with different concentrations at pH = 5.0. (g) Confocal microscopy image of HeLa cells pre-incubated with $CuCl_2$ and then incubated with the mesoporous probe. Reprinted with permission from ref. 210. Copyright 2015, American Chemical Society.

fluorescence in the absence of telomerase. With the addition of telomerase, telomeric repeats can be *in situ* added at the 3′ end of the DNA gatekeeper and drive the detachment of the DNA gatekeeper from the surface of mesoporous silica, resulting in the release of fluorescein and the recovery of fluorescence (Fig. 15b). Telomerase in cell extract was efficiently detected using the developed probe (Fig. 15c). The mesoporous probe was further used for *in situ* imaging of intracellular telomerase. Upon addition of the mesoporous probe, a gradual increase in fluorescence intensity was clearly observed within a single cell (Fig. 15d), showing high sensitivity of the developed mesoporous sensing system. Due to its high sensitivity and good selectivity, this mesoporous probe achieved tracking of intracellular enzyme activity *in situ*. This strategy can further contribute to studying the molecular mechanisms of enzyme involving biological activities.

In addition to commercially available fluorescent dyes, researchers have also designed fluorescent molecules with unique properties to serve as the reporters. Yang and coworkers synthesized a dual-responsive fluorescence dye as reporter molecules for the detection of lysosomal Cu^{2+} (Fig. 15e).[210] The dual-responsive fluorescence dye is made of rhodamine and spiropyran (Rhod-SP), and it can coordinate with Cu^{2+} to form a fluorescent complex under acidic medium. The Rhod-SP was loaded into mesoporous silica nanoparticles, and the RGD peptide was further conjugated on the surface of mesoporous silica for targeted recognition of specific cancer cells (Fig. 15e). Upon activation by lysosomal acidic pH, the Cu^{2+} ions can enter the mesopores and react with Rhod-SP to produce strong fluorescence signals. The as-designed mesoporous probe displayed good response to Cu^{2+} ions in an aqueous solution at a pH of 5 (Fig. 15f). The mesoporous probe was further incubated with HeLa cells, a cell line derived from cervical cancer, to detect the intracellular exchangeable Cu^{2+} ions. Without the addition of $CuCl_2$, a negligible fluorescence signal was visualized. On the other hand, strong fluorescence appeared in cells that were pre-incubated with exogenous $CuCl_2$ (Fig. 15g). The developed mesoporous probe shows good promise in tracking and locating specific targets in living systems, making it valuable in research studies such as understanding the cellular functions and cation physiology.

3.1.2 Loading molecules with redox activity. Molecules with redox activity is another class of commonly used reporters in the design of mesoporous sensing systems.[141,185,207] Glucose is one of the most widely used redox molecules and it can be easily detected with a personal glucose meter (PGM).[38,180,185,186] Tang *et al.* designed a general and easy-to-perform sensing strategy with PGM read out using glucose-loaded mesoporous silica nanoparticles (MSNs) (Fig. 16a).[185] Glucose is loaded into MSNs and a single-stranded DNA molecule (DNA1) is grafted onto the surfaces of the MSNs (DNA1-MSNs). Au nanoparticles modified with another single-stranded DNA molecule (DNA2) (DNA2-AuNPs) are used to cap the mesopores. With the addition of the DNA aptamer as the linker, DNA1 on mesoporous silica and DNA2 on Au nanoparticles hybridize with the aptamer to form a three-strand complex (MSN-AuNPs); thus

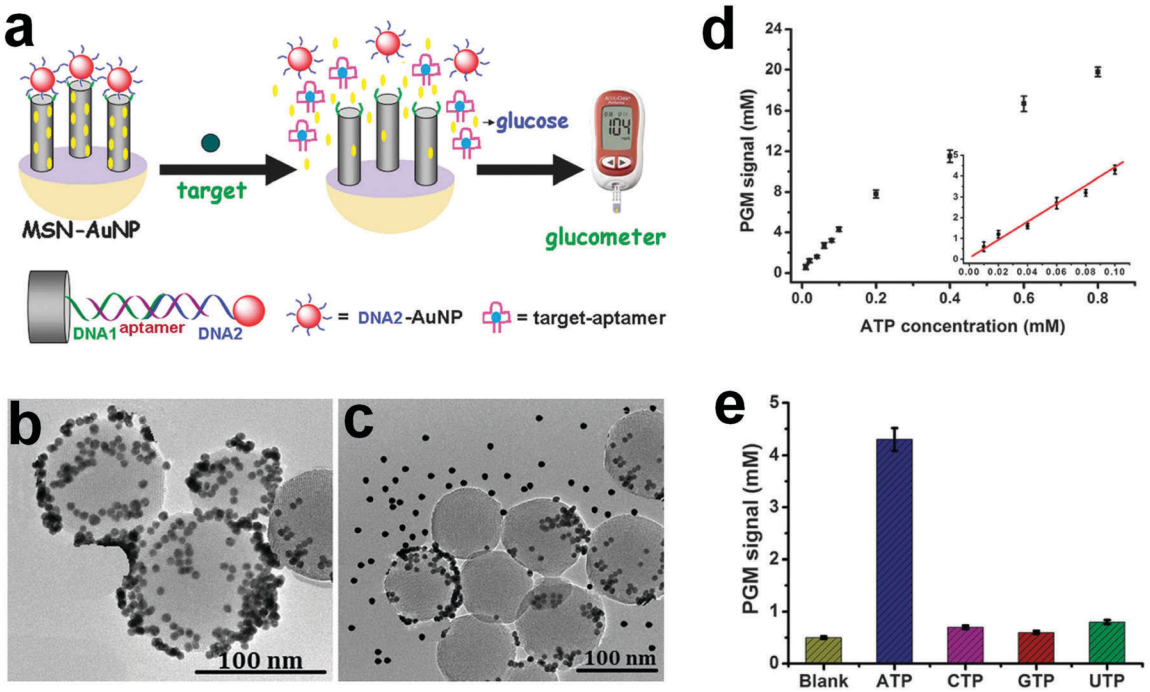

Fig. 16 (a) Schematic illustration of glucose-loaded MSNs combined with PGM read out for analytical applications. TEM images of MSN-AuNPs in the (b) absence and (c) presence of ATP. (d) PGM signal intensities of the mesoporous sensing systems in the presence of ATP with different concentrations. (e) The responses of the mesoporous sensing systems toward ATP, CTP, GTP and UTP. Reprinted with permission from ref. 185. Copyright 2013, Royal Society of Chemistry.

the mesopores are capped by the Au nanoparticles. In the presence of analytes, the DNA aptamer specifically binds to the analytes and the three-strand complex is disrupted, leading to the detachment of gold nanoparticles from mesoporous silica. As a result, the glucose is released into the solution and is further detected using the PGM. As a proof of concept, ATP was used as the model analyte in this study. Upon addition of ATP, Au nanoparticles were efficiently detached from the MSNs due to the specific binding of the DNA aptamer to ATP (Fig. 16b and c). The PGM signal increased gradually with increase of ATP concentration and a detection limit of 8 μM was achieved (Fig. 16d). In addition, ATP analogues including CTP, GTP and UTP induced much weaker glucose release than ATP (Fig. 16e), showing good selectivity of the developed sensor. This strategy can further be promoted to point-of-care detection of many other analytes by simply changing the DNA aptamer.

3.1.3 Loading enzymes. Enzymes exhibit many unique properties such as high catalytic activity and excellent selectivity.[10,215] Benefiting from their highly efficient catalytic capability, enzymes have been widely used in analytical chemistry for signal amplification.[13,198,216] However, the analytical applications of enzymes in their native form are usually hampered by their low stability and difficulties in reuse.[217] Immobilization of enzymes into mesoporous materials have been demonstrated to be one of the most efficient methods to overcome the above mentioned drawbacks.[218,219] Previous studies on enzyme immobilization on mesoporous materials have shown that enzyme confinement in mesopores can increase its stability and reduce denaturation by protein unfolding.[215,217,219] In addition to the intrinsic enzymatic signal amplification, a large amount of enzymes can be loaded into mesoporous materials, which further results in an increase of sensitivity.[13,217,219,220] In the past decades, various types of enzymes have been loaded into mesoporous materials for the design of highly sensitive detection methods.[10,13,198,215]

In 2004, Ju *et al.* constructed an electrochemical sensor by modifying a glassy carbon electrode (GCE) with hemoglobin loaded mesoporous silica (Hb/HMS-GCE).[221] The mesoporous structure offers a favorable microenvironment to facilitate the direct electron transfer between the enzyme and electrode surface. Besides, the immobilized Hb can retain its bioactivity, leading to fast response to both hydrogen peroxide and nitrate. Compared to the bare GCE, HMS modified GCE (HMS-GCE) and Hb modified GCE (Hb-GCE), the Hb/HMS-GCE displayed two couples of stable redox peaks indexed to the redox of Hb (Fig. 17a). Besides, the Hb/HMS-GCE exhibited better reversibility and larger response than the Hb-GCE, suggesting that the immobilization of Hb in mesoporous silica can efficiently facilitate the electron transfer process between the loaded Hb and the GCE. The amperometric responses of the HMS-GCE, Hb-GCE and Hb/HMS-GCE electrodes to H_2O_2 were investigated. As expected, the Hb/HMS-GCE displayed the highest response upon addition of H_2O_2 (Fig. 17b). Moreover, the Hb/HMS-GCE also showed high sensitivity and fast response in the detection of NO_2^- (Fig. 17c), showing great versatility of the developed mesoporous electrochemical sensor in sensing.

Apart from electrochemical sensing, mesoporous materials have also been used in enzyme-linked immunosorbent assay

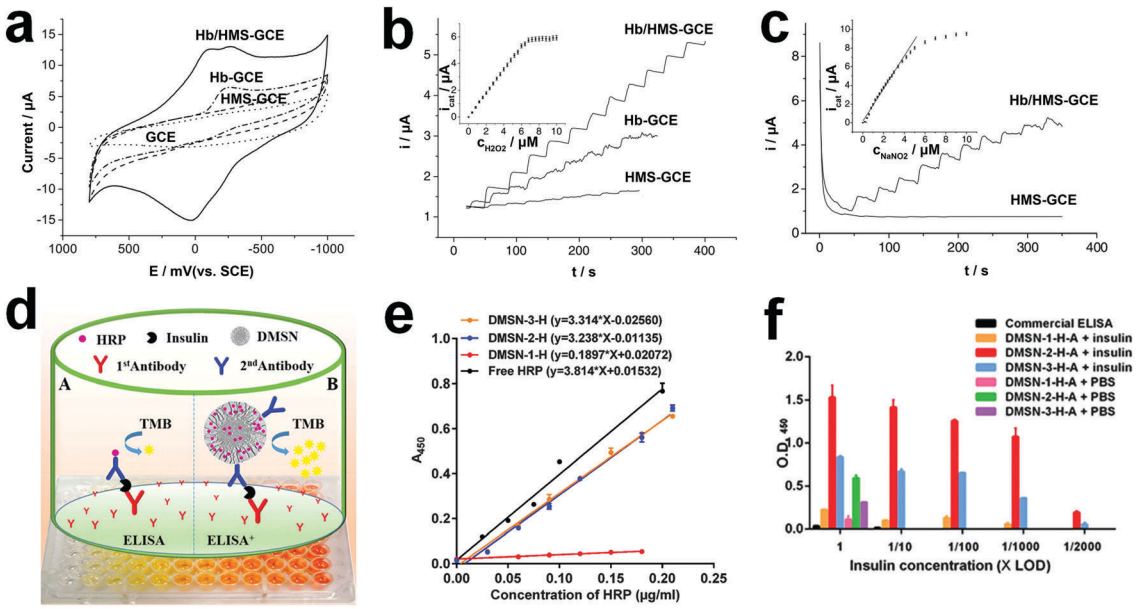

Fig. 17 (a) Cyclic voltammograms of the bare GCE, HMS-GCE, Hb-GCE and Hb/HMS-GCE in PBS (0.1 M, pH = 7.0). (b) Amperometric responses of the HMS-GCE, Hb-GCE and Hb/HMS-GCE upon successive addition of 5 μL H_2O_2 (0.2 mM) to PBS buffer (5.0 mL, 0.1 M). (c) Amperometric responses of the HMS-GCE and Hb/HMS-GCE upon successive addition of 5 μL $NaNO_2$ (0.4 mM) in PBS buffer (5.0 mL, 0.1 M). Reprinted with permission from ref. 221. Copyright 2003, Elsevier B. V. (d) Schematic illustration of traditional ELISA and the DMSN-H involving ELISA. (e) Activity of the DMSN-H relative to free HRP in the presence of TMB/H_2O_2 substrates. (f) Comparison of the responses of traditional ELISA and the DMSN-H involving ELISA at different insulin concentrations. Reprinted with permission from ref. 203. Copyright 2016, Royal Society of Chemistry.

(ELISA) to achieve high sensitivity, stability and reproducibility. In the efforts to develop ultrasensitive ELISA with enzyme-loaded mesoporous materials, Yu *et al.* reported the use of dendritic mesoporous silica nanoparticles (DMSNs) immobilized with horseradish peroxidase (HRP) for the detection of insulin (Fig. 17d).[203] The DMSN-stabilized HRP (DMSN-H) was functionalized with the 2nd antibody for specific recognition of insulin. The insulin was captured by the 1st antibody immobilized on the test plate, and the DMSN-H further bound to the captured insulin. With the addition of the substrates 3,3′,5,5′-tetramethylbenzidine (TMB) and H_2O_2, a significant color change was observed. The activity of the immobilized HRP was largely maintained and the easily accessible pore channels contribute to high enzyme activity (Fig. 17e). Ultrasensitive insulin detection in human serum was realized and a limit of detection (LOD) of 3.85 fg mL^{-1} was achieved, which is 1/2000 of the LOD of a commercial ELISA kit (7.7 pg mL^{-1}) (Fig. 17f). Such a significant decrease in the LOD clearly demonstrates that the large pore volume can contribute to the improvement of detection sensitivity. This study showed great versatility of the large pore volume of mesoporous materials in constructing highly sensitive sensing strategies. The proposed ELISA method based on enzyme loaded mesoporous materials holds good promise for the ultrasensitive detection of bioactive molecules for disease diagnosis.

3.2 Specific surface area

One of the most unique characteristics of mesoporous materials is their large specific surface area.[23,28,222,223] Due to this unique feature, mesoporous materials can provide abundant active sites in detection,[14,26,57] which can significantly increase the probability of contact between analytes and the active sites to produce detectable signals (Fig. 18). This feature is essentially important especially in the case of detection of low abundance analytes.[25,26] That is, the detection sensitivity can be improved by making use of the large specific surface area of mesoporous materials to promote the binding of analytes to the active sites.[14,26,224] The large specific surface area of mesoporous materials has been largely explored to achieve high sensitivity in analytical chemistry.[14,50,64] Many interesting analytical methods have been developed and highly sensitive detection of a wide range of analytes has been achieved in the past years.[26,50,55,57]

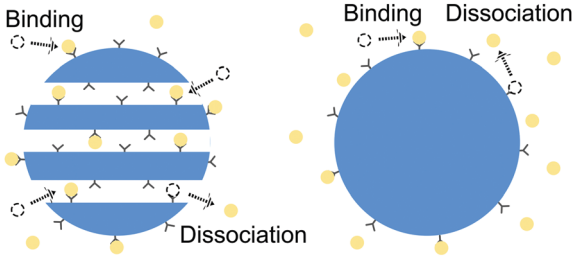

Fig. 18 Schematic illustration of analyte binding to mesoporous materials with abundant surface active sites and nonporous materials with limited surface active sites.

3.2.1 Fluorescence sensing. The large specific surface area of mesoporous materials makes it possible to immobilize large amounts of fluorescent probes on their surfaces, resulting in the creation of abundant active sites for analyte binding.[14,36,55] By making use of the large specific surface area of mesoporous materials, Kim and coworkers designed a mesoporous sensing system for Cu^{2+} detection by modifying a chemodosimeter on the surface of mesoporous silica.[225] In the presence of Cu^{2+}, the chemodosimeter on the surface of mesoporous silica can bind to Cu^{2+} and undergo desulfurization and cyclization to produce strong yellow fluorescence (Fig. 19a). Results showed that the addition of Cu^{2+} into the colloid dispersion of the mesoporous chemodosimeter led to a significantly enhanced fluorescence emission at around 560 nm (Fig. 19b). On the other hand, the mesoporous chemosensor did not show any obvious increase in fluorescence intensity or colour changes in the presence of other metal ions including Li^+, Na^+, K^+, Rb^+, Cs^+, Cd^{2+}, Ag^+, Mg^{2+}, Zn^{2+}, Sr^{2+} and Pb^{2+} (Fig. 19b and c). The designed mesoporous chemodosimeter shows great potential in detecting Cu^{2+} ions in many cases such as in living systems or environmental samples.

Imprinted mesoporous materials with specific binding cavities are widely employed in analytical applications.[61,97,114,124,226–228] Due to their large specific surface area, mesoporous materials can provide abundant binding cavities for recognizing analytes.[55] Xu and coworkers designed a molecularly imprinted mesoporous silica immobilized with carbon dots (M-MIPs@CDs) for highly sensitive and selective detection of TNT (Fig. 19d).[228] The TNT molecules can enter the binding cavities within the pore walls of the mesoporous silica, and the fluorescence of the CDs is quenched due to the electron transfer from the CDs to TNT. With the continuous addition of TNT into the mesoporous sensing system, the fluorescence intensity of the M-MIPs@CDs decreased gradually. A good linear relationship was observed between the fluorescence quenching amount and the TNT concentration ranging from 50 nM to 2.0 μM. The LOD for TNT was determined to be as low as 17 nM. For comparison, a non-mesoporous imprinted fluorescence sensor (MIPs@CDs) was also prepared and used for TNT detection. The LOD of the MIPs@CDs sensor towards TNT was 0.19 μM, which is much higher than the LOD of 17 nM obtained on M-MIPs@CDs. These results clearly demonstrated that the mesoporous structure can significantly improve the detection sensitivity by providing large amounts of accessible binding sites. Due to its simplicity and high sensitivity, the developed sensing strategy has great potential in applications including pollutant analysis and security.

3.2.2 Electrochemical sensing. Electrochemical sensing has many advantages including easy operation, low cost and suitability for point of care detection.[11,13,14,57,64] To improve the sensitivity of electrochemical sensors, one of the most classic methods is to use nanomaterials with large specific surface area to functionalize the electrodes.[14,50,57,229] Mesoporous materials deposited on electrodes can increase the electroactive surface area of the electrodes by several orders of magnitude, thus significantly increasing the sensitivity of the resulting

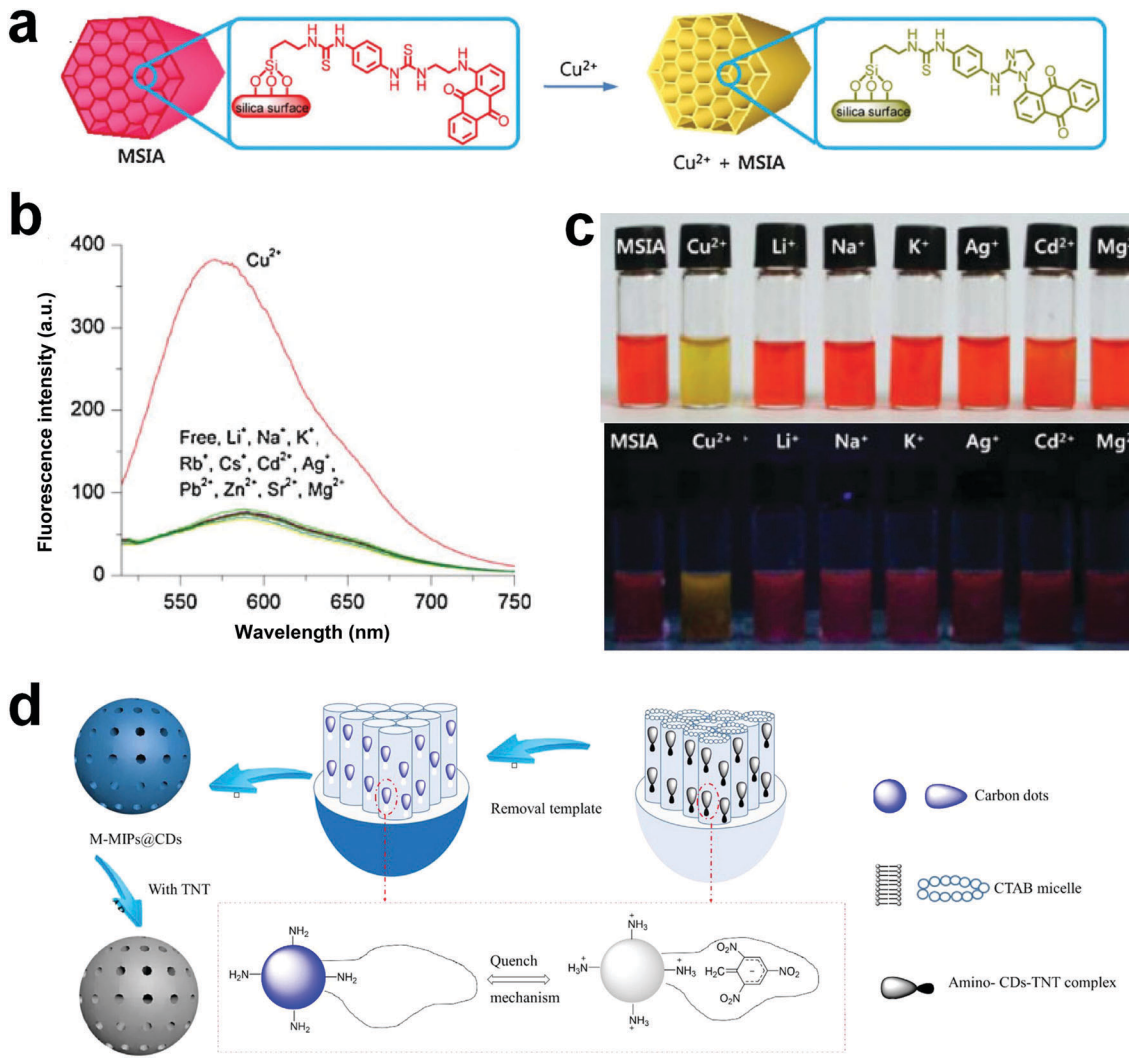

Fig. 19 (a) Schematic illustration of Cu^{2+} detection with the chemodosimeter-immobilized mesoporous chemosensor. (b) Fluorescence spectra of the mesoporous chemosensor in the presence of different metal ions. (c) Photograph and fluorescence images of the mesoporous chemosensor upon addition of different metal ions. Reprinted with permission from ref. 225. Copyright 2008, Wiley-VCH Verlag GmbH & Co. KGaA, Weinheim. (d) Schematic illustration of preparation of a TNT imprinted M-MIPs@CDs mesoporous chemosensor. Reprinted with permission from ref. 228. Copyright 2016, Elsevier B. V.

electrochemical device.[230,231] Moreover, the large specific surface area of mesoporous materials allows the immobilization of other functional reagents that can impart new properties to the electrodes for sensing applications.[13,232] Many kinds of mesoporous materials with large specific surface area and excellent hosting properties have been designed for highly sensitive electrochemical analysis of analytes.[11,233,234]

The gas sensing performance of electrochemical sensors can be greatly improved by mesoporous materials because the large specific surface area of mesoporous materials can provide abundant active sites to promote the contact between the active sites and the gas molecules.[56,235–237] In mesoporous gas sensing systems, gas molecules diffuse into the mesopores of mesoporous materials to react with the electroactive sites, which usually leads to a change in the conductance of the mesoporous sensor.[26,238] Liu and coworkers designed a highly sensitive gas sensor based on hierarchical mesomacroporous SnO_2.[239] The mesomacroporous SnO_2 displayed a large surface area of 23.6 m^2 g^{-1}. The mesoporous structure of SnO_2 can provide large amounts of active sites for surface reactions and the macroporous structure can benefit the diffusion of gas molecules into the sensing film. Several kinds of indoor air pollutants including ethanol, benzene and toluene can react with the surface-bound oxygen on mesomacroporous SnO_2 and release electrons into the sensing film, which results in a change in the conductance of the mesomacroporous SnO_2 sensing film. Compared with traditional nonporous SnO_2, the hierarchical mesomacroporous SnO_2 displayed much higher response to all of the tested gases including ethanol (Fig. 20a), benzene (Fig. 20b) and toluene (Fig. 20c), clearly suggesting that the large specific surface area of the mesomacroporous structure can significantly increase the sensitivity of gas sensors. The detection of the target gas over a wide range of concentrations was also achieved with the mesomacroporous sensor (Fig. 20d).

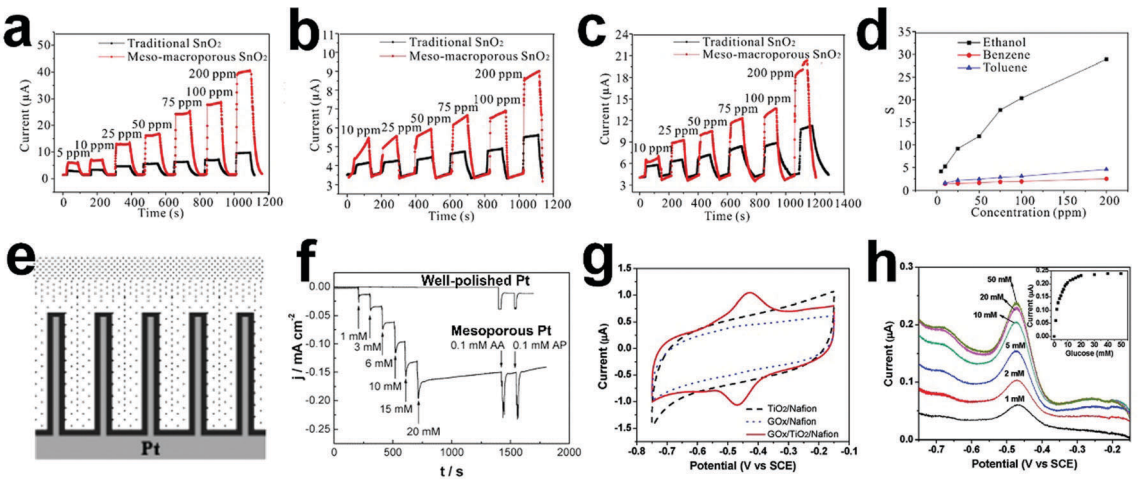

Fig. 20 (a) Real-time responses of a mesomacroporous SnO_2 sensor and a traditional SnO_2 sensor to ethanol, (b) benzene and (c) toluene. (d) The response of the mesomacroporous SnO_2 sensor to the target gas with different concentrations. Reprinted with permission from ref. 239. Copyright 2012, Elsevier B. V. (e) Schematic illustration of the mesoporous Pt electrode. (f) The responses of the flat Pt electrode and the mesoporous Pt electrode to glucose, AA and AP. Reprinted with permission from ref. 242. Copyright 2003, American Chemical Society. (g) Cyclic voltammograms of the TiO_2/Nafion modified GCE, GOx/Nafion modified GCE, and GOx/1DHS TiO_2/Nafion modified GCE in PBS (0.1 M, pH = 7.4). (h) Cathodic branches of the background-subtracted CVs of the GOx/1DHS TiO_2/Nafion modified GCE in the presence of glucose with different concentrations. Reprinted with permission from ref. 251. Copyright 2011, American Chemical Society.

Moreover, compared with the traditional mesoporous SnO_2, the hierarchical mesomacroporous SnO_2 based sensor displayed much shorter response times in gas sensing. The good sensitivity, short response time and facile preparation of the mesomacroporous gas sensor make it valuable in the fabrication of novel gas sensing devices. In addition to gas sensing, mesoporous materials have also been largely employed to modify electrodes for detecting analytes in aqueous solution.[11,64,230,240,241] Metal electrodes with an ordered pore structure possess the unique advantage of ultra-large electroactive surface area, which can boost the faradaic currents several orders of magnitude higher than those of classical flat electrodes.[64] Kim and coworkers constructed mesoporous Pt electrodes with a specific area of 37 $m^2\ g^{-1}$ (Fig. 20e).[242] The electrochemical responses of glucose, L-ascorbic acid (AA), and 4-acetamidophenol (AP) on both flat and the mesoporous Pt electrodes were investigated. The flat Pt electrode responded negligibly to glucose, and only a slight increase in current density was observed in the presence of AA and AP (Fig. 20f). In contrast, the mesoporous Pt electrode gave sensitive response to glucose with concentrations in the range of 0–10 mM. Moreover, the sensitivity of the mesoporous Pt electrode towards glucose was as high as 9.6 μA cm^{-2} mM^{-1}. Additionally, the mesoporous Pt electrode also displayed much higher response to AA and AP than the flat Pt electrode (Fig. 20f). This work clearly demonstrated that mesoporous materials can significantly increase the sensitivity of electrochemical sensors by providing large amounts of electroactive sites. Due to its high sensitivity, good selectivity and stability, the developed mesoporous Pt sensor can serve as a potential candidate for nonenzymatic glucose sensing.

Other metal-free mesoporous materials with good conductivity have also been largely used in electrochemical sensing.[243–246] Ordered mesoporous carbons (OMCs) with superior conductivity, good stability, chemical inertness, and low costs are ideal candidates in the preparation of modified electrodes.[11,231,245–247] Guo *et al.* reported the preparation of OMC-modified GCEs for the detection of morphine.[246] Mesoporous carbons OMC-75, OMC-100, and OMC-125 with surface areas of 903 $m^2\ g^{-1}$, 900 $m^2\ g^{-1}$ and 1155 $m^2\ g^{-1}$ were systematically prepared. The reduction currents of $K_3[Fe(CN)_6]$ on the OMC-75/GC, OMC-100/GC and OMC-125/GC electrodes were determined to be 9.28 mA, 9.47 mA, and 11.68 mA, respectively. These results clearly suggested that OMC-125 with the largest specific surface area produced the highest reduction current, which could be ascribed to the fact that the abundant electroactive sites in OMC-125/GC can facilitate the electrocatalytic reduction of $K_3[Fe(CN)_6]$. This simple comparison test clearly confirms that the large surface area of mesoporous materials can provide large amounts of surface active sites to promote the binding of the analytes to the active size. Thus sensitivity can be efficiently improved by making use of the large specific surface area of mesoporous materials.

In addition to serving as the electroactive units in electroanalysis, mesoporous materials have also been widely employed to immobilize other electroactive molecules for sensing due to their large specific surface area.[10,13,216,223,248–250] For instance, enzymes are usually immobilized on the surfaces of mesoporous materials for electro-biosensing because large amounts of enzymes can be immobilized on electrodes with the assistance of mesoporous materials.[10,13] Additionally, the mesoporous structure can protect the enzymes from denaturing. Kim *et al.* synthesized a novel one-dimensional hierarchically structured TiO_2 (1DHS TiO_2) using multi-walled carbon nanotubes as the template.[251] The 1DHS TiO_2 possessed a large surface area of 218.4 $m^2\ g^{-1}$, and it was used to immobilize glucose oxidase for glucose sensing. The large specific surface area of the 1DHS TiO_2

made it possible to immobilize large amounts of GOx on its surface. The GOx/1DHS TiO_2/Nafion-modified GCE displayed significantly higher response than the TiO_2/Nafion- or GOx/Nafion-modified GCE (Fig. 20g) in PBS solution, clearly suggesting that mesoporous materials can help in improving the detection sensitivity. Direct analysis of glucose with different concentrations was realized (Fig. 20h). Also, the reported mediator-free electrochemical sensor displayed long-term stability in glucose detection. This study shows that mesoporous materials are promising in immobilizing functional guest molecules for the fabrication of novel biosensors.

3.2.3 Microgravimetric sensing. Gravimetric-type sensors can realize analyte detection through direct readout of the frequency shift induced by mass change.[252,253] The sensitivities of gravimetric-type chemical sensors are largely determined by the diffusion, sorption, and/or reaction of analyte molecules on the accessible surfaces of the sensing materials.[254] Since mesoporous materials feature large accessible surface area and good pore connectivity, they can serve as the ideal candidates to construct microgravimetric sensors with high sensitivity.[255] In this section, representative works about using the large specific surface area of mesoporous materials to construct highly sensitive gravimetric-type sensors will be introduced.

Quartz crystal microbalance (QCM) is a kind of well established gravimetric-type sensor and it can determine a small electrode-mass change down to the nano-gram level.[252,256] Moreover, QCM shows advantages including fast response, low cost and small dimensions. The QCM has been widely used in the detection of trace amounts of analytes, especially chemical vapors.[257] To detect chemical vapors with relatively small molecular weight, adsorption materials that possess large specific surface area should be used to provide the maximum variation of mass.[252,258] Mesoporous materials with large accessible surface area can allow more molecules to be adsorbed to generate a higher mass-adding-induced frequency-shift sensing signal. Li *et al.* developed a high-performance integrated QCM sensor for the detection of trinitrotoluene (TNT) vapors.[254] In this study, mesoporous silica SBA-15 with a specific surface area of 385 $m^2 g^{-1}$ was prepared and further functionalized with hexafluoro-2-propanol (HFIP) for the efficient capture of TNT (Fig. 21a). With the introduction of 45 ppt of TNT vapor into the testing chamber, the frequency of the QCM sensor significantly decreased by about 2.6 Hz (Fig. 21b). Such high sensitivity can be attributed to the abundant adsorption sites towards TNT provided by the large specific surface area of the functionalized mesoporous silica. Stronger single output was observed when the amount of TNT vapor was increased to 90 ppt and 135 ppt. Fig. 21c shows that H_2O also causes obvious signal changes, which may cause false positive signals in a humid environment. Nevertheless, the QCM sensor displayed good selectivity towards TNT (Fig. 21c). The developed QCM sensor shows good potential in areas such as security inspection and pollutant analysis.

Kimura *et al.* reported the modification of the Au electrode in a normal QCM system with mesoporous silica to improve the sensing performance (Fig. 21d).[252] The performances of normal QCM and the developed meso-QCM system in the detection of chemical vapors including CH_3CH_2OH and CH_3CHO were compared. For normal QCM, frequency shifts were barely observed with the injection of CH_3CH_2OH with concentrations as high as 1000 ppb. However, a frequency shift was distinctly observed for the meso-QCM system in the presence of CH_3CH_2OH with a concentration of 100 ppb (Fig. 21e), clearly suggesting that the large surface area of mesoporous materials can lead to the enhancement of QCM sensitivity. The meso-QCM system also displayed good sensitivity in the detection of CH_3CHO. Most excitingly, the meso-QCM system could quantitatively analyze mixed vapors of CH_3CH_2OH/CH_3CHO and calculate the concentration of each component (Fig. 21f). This method is extensively useful for quantitative analysis of gases and vaporized molecules of different components.

3.2.4 Mass spectrometry. Preconcentration is an efficient method to improve the detection sensitivity by collecting low abundance analytes from complex sample matrices to obtain detectable signals.[137,171] To achieve highly-efficient preconcentration, adsorbents should possess abundant binding sites to promote the adsorption of trace analytes.[259,260] Mesoporous materials feature large specific surface area and can provide abundant binding sites for efficient adsorption of analytes from sample solutions.[261,262] Mesoporous materials have been largely explored for the preconcentration of analytes with low abundance to improve the sensitivity of mass spectrometry (MS).[61,74,86,89,92,263,264] In this section, several preconcentration analyses that make use of the large specific surface area of mesoporous materials to improve the detection sensitivity of MS will be discussed.

Li *et al.* reported the enrichment of phosphopeptides from biological samples with their developed Ti^{4+}-immobilized graphene/mesoporous silica composites (Ti^{4+}-MGMSs).[265] The mesoporous composites display large surface areas and large amounts of immobilized Ti^{4+} for the adsorption of phosphopeptides. High efficiencies were observed in the enrichment of phosphopeptides from both a β-casein tryptic digest (0.5 μM) and from a β-casein tryptic digest/α-casein mixture (mass ratio 1 : 500). Moreover, after enriching phosphopeptides with the Ti^{4+}-derived mesoporous composites from β-casein digest solution with ultra-low concentration (0.5 aM), a phosphopeptide signal with a signal-to-noise ratio over 10 was observed. Such a low detection limit and high sensitivity could be attributed to the abundant binding sites provided by the large surface area of Ti^{4+}-MGMSs. The developed MS strategy holds good promise in proteomics and disease diagnosis.

Compared to Ti^{4+} ions, mesoporous TiO_2 is much more specific in recognizing phosphoproteins or phosphopeptides because the metal oxides display more specific and reversible chemisorption of phosphate groups on their amphoteric surface.[259,266–268] Wang *et al.* reported a novel method for the preparation of magnetic mesoporous Fe_3O_4@mTiO_2 microspheres with a highly accessible mesoporous TiO_2 layer.[268] The Fe_3O_4@mTiO_2 microspheres can specifically bind to phosphopeptides through the classical bridging bidentate bonds between the surfaces of TiO_2 mesopores and the phosphoric acid groups. The preconcentration efficiency of the Fe_3O_4@mTiO_2 microspheres

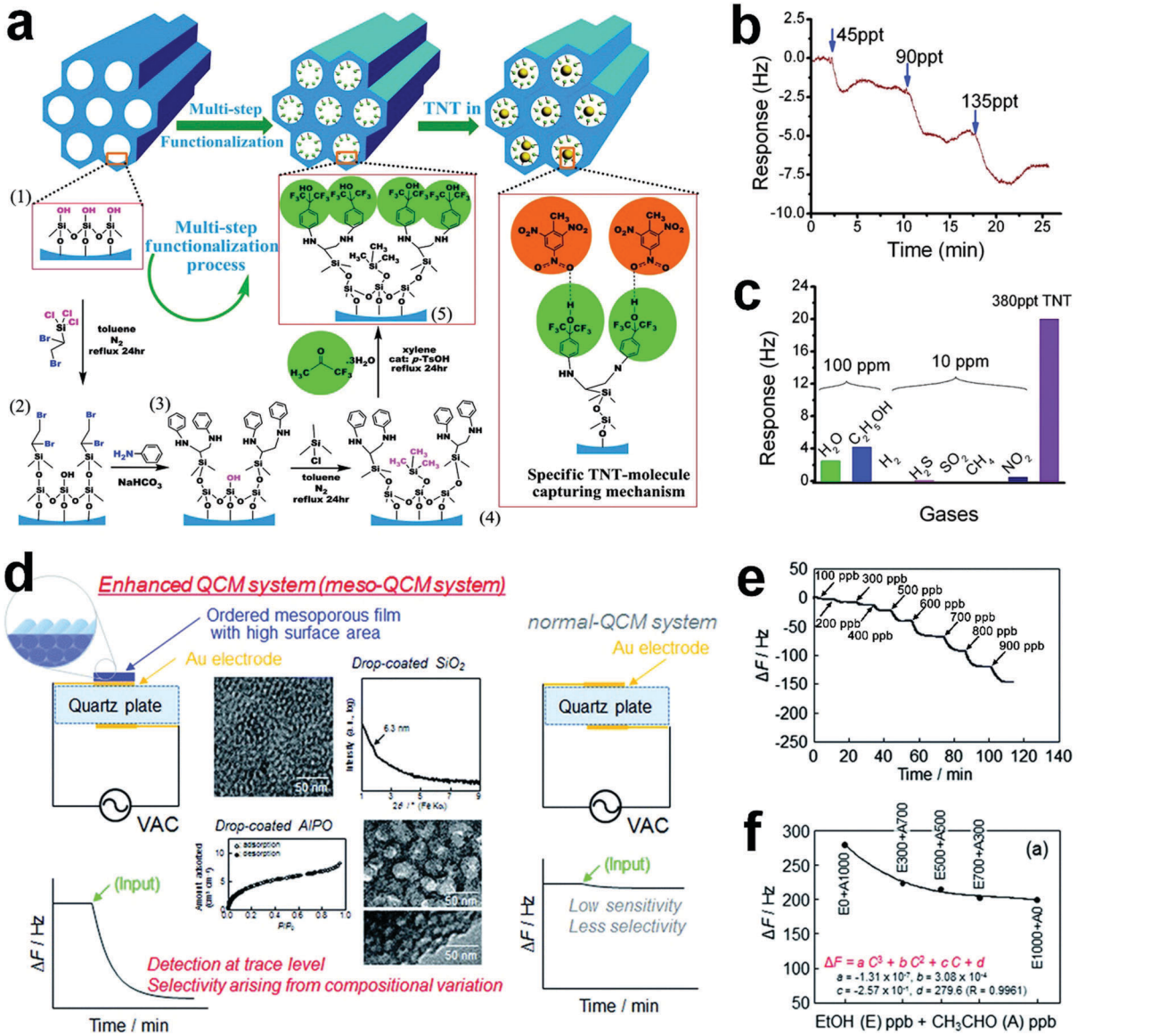

Fig. 21 (a) Schematic representation of a hexafluoro-2-propanol (HFIP) modified SBA-15 mesoporous QCM sensor for TNT sensing. (b) Responses of the QCM sensor upon addition of TNT with concentrations of 45 ppt, 90 ppt and 135 ppt. (c) Responses of the QCM sensor to different kinds of chemical vapors. Reprinted with permission from ref. 254. Copyright 2011, American Chemical Society. (d) Schematic representation of the meso-QCM system. (e) Responses of the meso-QCM system with the addition of CH_3CH_2OH at different concentrations. (f) The frequency changes of the meso-QCM system upon changing the mixing rate of CH_3CH_2OH and CH_3CHO vapors. Reprinted with permission from ref. 252. Copyright 2014, Royal Society of Chemistry.

was compared with that of non-mesoporous TiO_2 coated Fe_3O_4 (Fe_3O_4@TiO_2) microspheres. The non-mesoporous Fe_3O_4@TiO_2 microspheres gave an enrichment capacity of 20 mg g^{-1}. In contrast, the enrichment capacity of the Fe_3O_4@mTiO_2 was as high as 225 mg g^{-1}, much higher than that of the non-mesoporous Fe_3O_4@TiO_2 microspheres. The significantly increased adsorption capacity can be ascribed to the abundant binding sites provided by the large specific surface area of the mesoporous TiO_2. Due to the good enrichment capacity of the Fe_3O_4@mTiO_2 microspheres, the target phosphopeptide in the complex samples can be easily adsorbed and further separated. The authors showed that a signal-to-noise ratio as high as 56 was obtained even in the presence of only 10 fmol β-casein. These results demonstrated that the Fe_3O_4@mTiO_2 microspheres exhibited extreme sensitivity due to the abundant binding sites provided by the mesoporous structure. The outstanding feature of the Fe_3O_4@mTiO_2 microspheres demonstrated that sensitivity can be improved by increasing the amount of surface active sites. The prepared Fe_3O_4@mTiO_2 microspheres have good potential in mass spectrometric analysis of phosphopeptides.

4. Response-time-related structural properties

The response time is the time taken for a sensor to respond to a step concentration change from a certain concentration value

to another value.[68,69] Mesoporous materials with large specific surface area provide abundant active sites that can bind to analytes and convert the binding events into measurable signals.[26,57,63] The large specific surface can significantly increase the probability of binding of the analytes to the active sites; thus the response time can be shortened.[56,224] Also, it should be noted that analytes have to diffuse into the mesopores to reach the active sites regardless of the sensing principles.[26] That is, the response time of mesoporous sensors is also influenced by the diffusion of analytes in mesopores. Previous studies demonstrated that porous materials with large pore sizes and connected channels favor molecular diffusion and thus ensure a fast response.[59,64,269–272] Therefore, in addition to specific surface area, pore size and pore connectivity can also influence the response time.

4.1 Specific surface area

Mesoporous materials have large specific surface area and can provide enormous binding sites for the detection of analytes.[14,55,57] The abundant binding sites can significantly increase the probability of contact between analytes and the binding sites to produce detectable signals, thus contributing to shortening the response time (Fig. 22).[26,56] Several previous studies have demonstrated that the large specific surface area of mesoporous sensors can provide fast response in detection.[26,63,273] Pellicer *et al.* prepared two different crystalline mesoporous WO_3 replicas using SBA-15 and KIT-6 mesoporous silicas as the templates for NO_2 gas detection.[273] Brunauer–Emmett–Teller (BET) surface analyses (Fig. 23a) showed that the specific surface areas of the WO_3 KIT-6 and SBA-15 replicas were 48.2 m^2 g^{-1} and 12.6 m^2 g^{-1}, respectively. As expected, the WO_3 KIT-6 replica is more sensitive than the SBA-15 replica in NO_2 detection (Fig. 23b). Moreover, in the presence of NO_2 with the same concentration, the signal on the WO_3 KIT-6 replica reached equilibrium much more rapidly than that on the WO_3 SBA-15 replica (Fig. 23b). The response time of WO_3 KIT-6 was estimated to be half of that of WO_3 SBA-15. The shorter response time to NO_2 gas by the WO_3 KIT-6 replica was due to the fact that the KIT-6 replica had a higher surface area than the SBA-15 replica. Therefore, the number of active sites that were accessible to the NO_2 gas in the WO_3 KIT-6 mesoporous sensor was much larger than that in the WO_3 SBA-15 mesoporous sensor. These results thus confirmed that the response time of a mesoporous sensor can be largely influenced by the specific surface area of the employed mesoporous materials.

The influence of the specific surface area of a mesoporous sensor on the response time was also investigated by other researchers. Deng, Zhao and co-workers developed OMCs with two-dimensional hexagonal mesostructure and unique buckled large mesopores *via* a micelle fusion-aggregation assembly method using poly(ethylene oxide)-*block*-polystyrene (PEO-*b*-PS) diblock copolymers as the template (Fig. 23c).[63] The pore size of the OMCs was fine-tuned from 26.2 to 36.3 nm by simply using diblock copolymers with different hydrophobic PS segment lengths. Moreover, the pore volume and specific surface area of the OMCs could reach as high as 0.54 cm^3 g^{-1} and 571 m^2 g^{-1}, respectively. The applications of the prepared OMCs in sensing NH_3 at room temperature were investigated. The OMCs (carbon-PEO117-*b*-PS198) with a high density of surface active sites (0.188 nm^{-2}) displayed a quick response to 5 ppm of NH_3 in 2 min (Fig. 23d). Mesoporous carbon C-FDU-15 was also prepared and its NH_3 sensing performance was compared with that of carbon-PEO117-*b*-PS97. Both the C-FDU-15 and carbon-PEO117-*b*-PS97 OMCs displayed similar two dimensional (2D) hexagonal mesoporous structures. The densities of surface active sites of C-FDU-15 and carbon-PEO117-*b*-PS97 are 0.083 nm^{-2} and 0.131 nm^{-2}, respectively. The response time of the C-FDU-15 based sensor to NH_3 input of 15 ppm exceeded 7 min, much longer than that of the carbon-PEO117-*b*-PS97 based sensor (6 min). This study clearly demonstrates that mesoporous materials with large surface area can shorten the response time of the mesoporous sensor towards analytes.

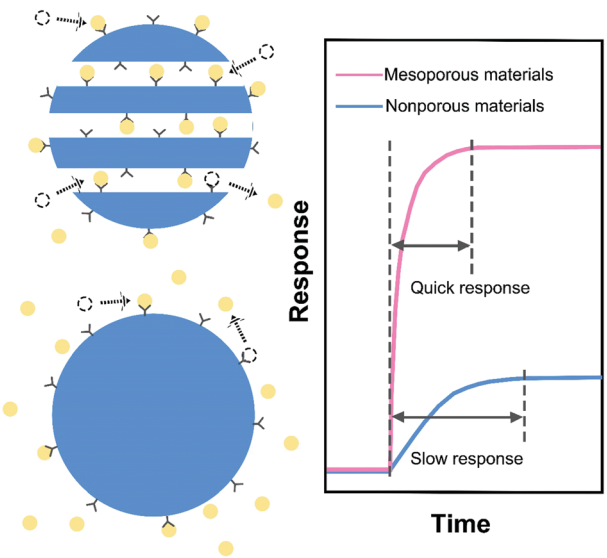

Fig. 22 Schematic illustration of the response of mesoporous sensing systems and nonporous sensing systems to analytes.

4.2 Pore size

As mentioned above, analytes need to diffuse into mesoporous materials to reach the active sites regardless of the sensing principles.[26] Pore size is one of the important factors that influence the diffusion rate of analytes in mesoporous sensors (Fig. 24).[26,63] Sakai *et al.* theoretically illustrated the theory of gas diffusion in mesoporous film sensors in detail. When the pores are in the range from 2 to 100 nm, the target gas moves in the film on the basis of Knudsen diffusion. The increase of the pore size will promote gas diffusion in the film and shorten the response time.[274]

In 2004, Vallet-Regí *et al.* studied the influence of the pore size of MCM-41 mesoporous silica on the diffusion of guest molecules and they found that the diffusion rate of molecules decreased as the pore size decreased.[275] In this study, MCM-41 mesoporous silicas with pore sizes of 3.6 nm, 3.3 nm, 2.7 nm

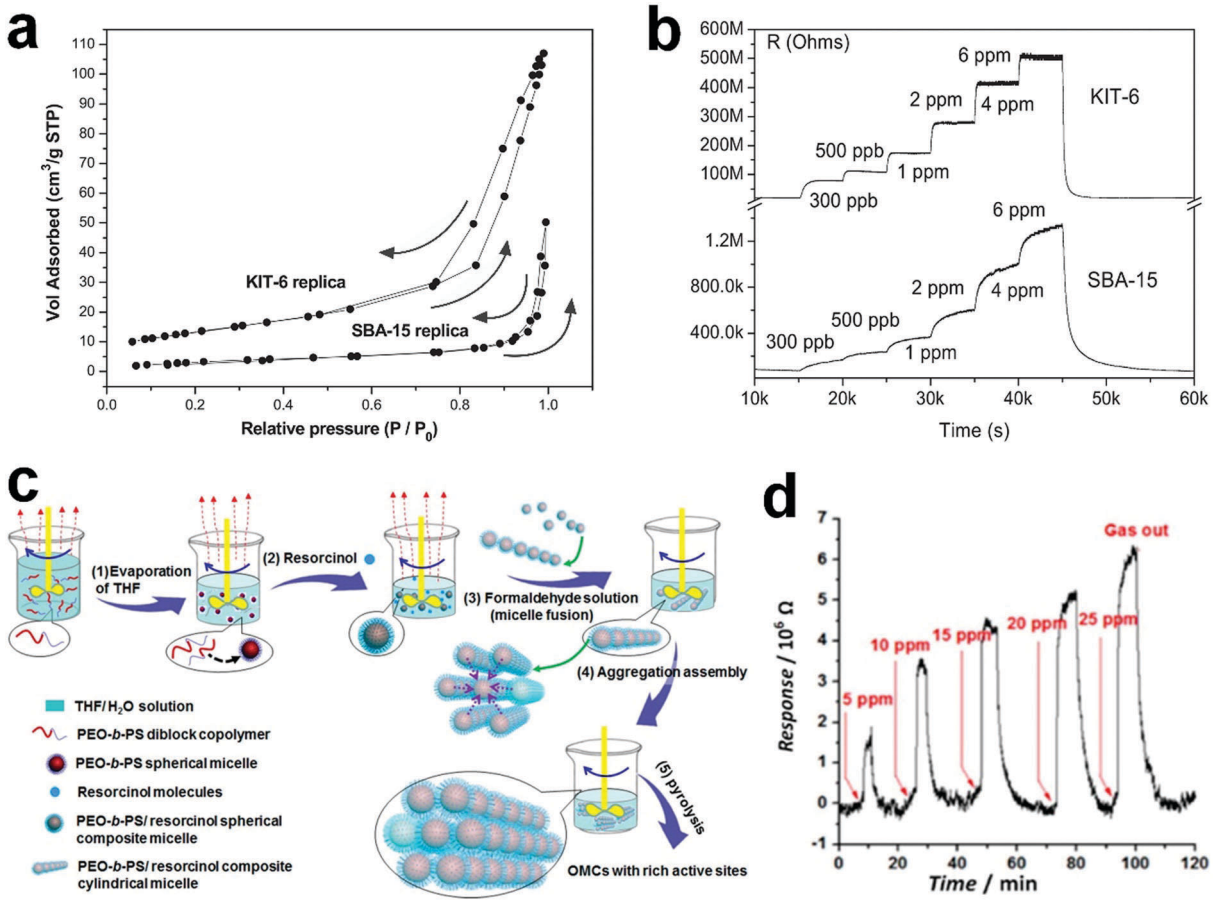

Fig. 23 (a) The N_2 adsorption curves of the KIT-6 and SBA-15 based mesoporous WO_3. (b) Responses of KIT-6 and SBA-15 WO_3 replica samples in the presence of NO_2 with different concentrations. Reprinted with permission from ref. 273. Copyright 2007, Wiley-VCH Verlag GmbH & Co. KGaA, Weinheim. (c) Schematic representation of the formation of the mesoporous carbon materials with rich active sites. (d) The response and recovery curves of the carbon-PEO117-*b*-PS198 sensor to NH_3 at different concentrations. Reprinted with permission from ref. 63. Copyright 2016, American Chemical Society.

and 2.5 nm were systematically synthesized using alkyltrimethylammonium surfactants with different chain lengths as the soft-templates. The mesoporous silicas were loaded with ibuprofen as the guest molecules and the amounts of ibuprofen delivered into the solution were monitored. Results showed that the liberation rate increased from 5 mg h^{-1} for a pore size of 2.5 nm to 24 mg h^{-1} for a pore size of 3.6 nm. This fivefold increase in the release rate indicated that the diffusion rate of guest molecules increased significantly with increase of the pore size of mesoporous materials. Other studies also showed that the diffusion rate of guest molecules in mesopores increased with increase of pore size.[269,276,277] For instance, Lindén and coworkers prepared a series of ordered porous silicas (μSBA-3, mSBA-3 and MCM-41) exhibiting 2D hexagonal structures with cylindrical pores.[269] The pore sizes of μSBA-3, mSBA-3 and MCM-41 were 1.7 nm, 2.6 nm and 3.3 nm, respectively. The absorption and release behaviors of ibuprofen on these porous silicas were monitored. The MCM-41 mesoporous silica with the largest pore size (3.3 nm) exhibited the highest ibuprofen adsorption capacity with a loading degree of up to 41 wt % (Fig. 25a). The majority of ibuprofen loaded into the MCM-41 mesoporous silica was released within 24 h, whereas the μSBA-3 and mSBA-3 silicas with smaller pore size all displayed total release times in the range of 100 h (Fig. 25b). The absorption and release rates of ibuprofen increase in the order μSBA-3 < mSBA-3 < MCM-41, indicating that increasing the pore size can promote the diffusion of guest molecules.

Deng and coworkers reported the synthesis of highly ordered mesoporous WO_3 with large pore size and showed that a mesoporous WO_3-based gas sensor displayed a short response time in H_2S sensing.[270] The pore size of the prepared mesoporous WO_3 was 10.9 nm and the surface area was 121 m^2 g^{-1}. The dynamic responses of the mesoporous sensor to H_2S gas with different concentrations (0.25–200 ppm) were monitored (Fig. 25c). With the injection of H_2S gas into the test chamber, the intensity of the signal increased rapidly. A short response time of 2 s was observed in the detection of a low concentration H_2S with the mesoporous WO_3-based H_2S gas sensor (Fig. 25d). This study clearly suggested that the uniform large mesopores contributed to the fast diffusion of H_2S to achieve short response times. The synthesized mesoporous WO_3 has potential use as a gas sensor in fields such as environmental monitoring and food safety.

Furthermore, the Zhao group reported the preparation of ordered mesoporous ZnO with uniform large mesopores that

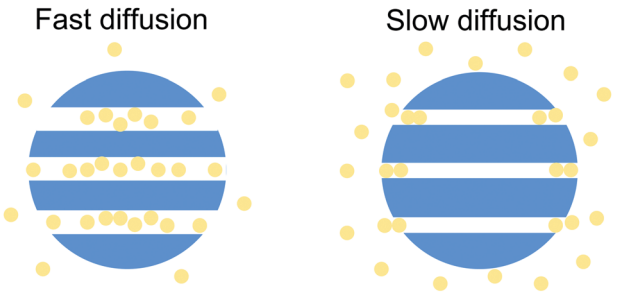

Fig. 24 Schematic illustration of molecular diffusion in mesoporous materials with relatively large and small pore sizes.

exhibited excellent ethanol sensing performance with fast response.[59] The mesoporous ZnO with a pore size of 29.0 nm was synthesized through a citric acid assisted soft template strategy. The obtained mesoporous ZnO displayed a continuous and crystalline framework with open pore channels, ensuring the rapid diffusion of analytes within the mesopores. The dynamic electrical response of a mesoporous ZnO-based gas sensor to ethanol gas was investigated. A non-mesoporous ZnO-based sensor was employed for comparison. As expected, the mesoporous ZnO-based gas sensor exhibited a much stronger response than the non-mesoporous ZnO based sensor (Fig. 25e). Moreover, the mesoporous ZnO-based gas sensor also exhibited a response time of 6 s (Fig. 25f), much shorter than the response time obtained on the non-mesoporous ZnO based sensor (11 s). These results thus clearly show that large pore size can contribute to facilitating molecular diffusion and shortening the response time.

4.3 Pore connectivity

Interconnected mesopores provide the necessary conditions for facile diffusion of analytes within the mesopores to increase the probability of contact between the analytes and the binding sites to produce detectable signals (Fig. 26), which is especially critical when the sensing reactions are diffusion-controlled.[26,64,271,278] Previous studies have reported that mass transport is usually more efficient in ordered mesoporous architectures than in disordered mesoporous structures because the optimized communication between the pores can lead to fast diffusion of guest molecules.[64,271,278] Thus interconnected mesopores can afford fast diffusion of guest molecules and shorten the response time in detection. Many researchers have investigated the influence of pore connectivity on the diffusion of guest molecules in mesoporous materials.[64,272,279,280]

Sanchez, Walcarius and coworkers prepared a series of mesoporous films displaying *p6m* (2D hexagonal), *P*63/*mmc* (3D hexagonal), and *Pm*3*n* (3D cubic) mesoporous structures, as illustrated in Fig. 27a.[271] The influence of pore connectivity on the permeability of analytes to the redox probes was studied by cyclic voltammetry. In the presence of analytes such as $Ru(bpy)_3^{2+}$ (Fig. 27b) or FcMeOH (Fig. 27c), the *P*63/*mmc* (3D hexagonal) and *Pm*3*n* (3D cubic) mesoporous silica films with interconnected pores displayed significantly higher response than the *p6m* (2D hexagonal) film, suggesting that the interconnected pores allowed faster molecular diffusion. These results showed that 3D mesoporous films displayed much better permeability than the 2D hexagonal mesoporous film, which could be attributed to the fact that the interconnected mesopores in the 3D mesoporous films allowed fast diffusion of the redox probes. In another study, Wu *et al.* prepared highly ordered mesoporous silica films with a 2D hexagonal structure (channel-type mesopores) and a 3D hexagonal structure (cage-type mesopores).[278] The 3D hexagonal mesoporous silica film exhibited an ink-bottle porous structure with ideal interconnectivity, whereas the 2D hexagonal mesoporous silica film only possessed small pores within the pore wall to serve as open windows to connect the mesochannels. The mesoporous silica films were loaded with fluorescein isothiocyanate (FITC) and the release of FITC was monitored. Results showed that the half-life value for the steady release of FITC from the 3D hexagonal and 2D hexagonal mesoporous silica films were 60 min and 92 min, respectively. These results indicate that interconnected mesopores can allow fast diffusion of guest molecules.

Fast response in the detection of analytes has been largely achieved with interconnected mesoporous sensors in the past years. El-Safty *et al.* reported the use of 3D mesoporous monoliths (cage-type mesopores) functionalized with different kinds of binding receptors for highly sensitive and selective detection of toxic ions in a few minutes.[272] The cage monoliths with spherical nanosized cavities show efficient transport of toxic ions to the inner active sites. Due to the interconnected mesopores, the mesoporous sensor displayed short response times (30 s $< t <$ 3 min) in the detection of Pb^{2+}, Cd^{2+}, Sb^{3+}, and Hg^{2+} ions. In another study, 3D cubic and 2D hexagonal mesoporous WO_3 were used for the detection of NO_2 gas.[266] A five times faster response was observed on the 3D cubic mesoporous WO_3 as compared to the 2D hexagonal mesoporous WO_3, which was attributable to the higher pore interconnectivity in the 3D cubic mesoporous WO_3. These studies show that mesoporous materials with inter-connected mesopores favor fast molecular diffusion and show good promise in the construction of sensors with rapid response and low cost.

5. Stability-related structural properties

Generally, nanomaterial-based sensors involve the immobilization of reporter molecules or binding molecules on the outer surfaces of nanoparticles, which inevitably suffers signal fluctuation caused by the detachment or diffusion of the anchored molecules.[55] As for mesoporous material based sensors (Fig. 28), binding molecules or reporter molecules can be loaded into the mesopores or immobilized on their inner surfaces.[55,60,70,131,136,204] The unique mesoporous structure offers protection to the binding molecules or reporter molecules to enhance the stability of the mesoporous sensor. As a result, the functional binding sites and signalling subunits are protected from the outer environment, which greatly enhances the signal stability and eliminates the false positive signals.[191,272,281]

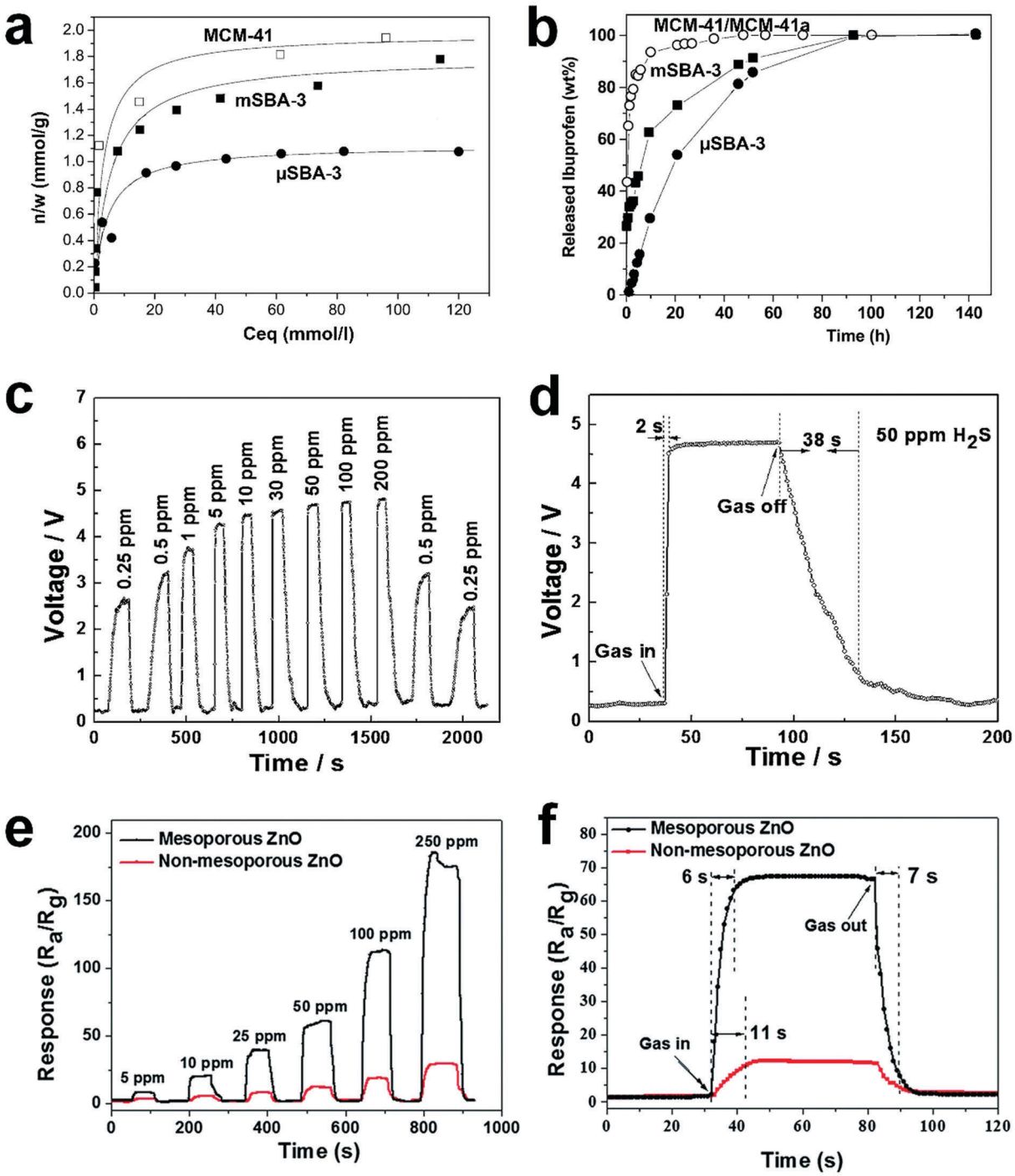

Fig. 25 (a) The adsorption isotherms of ibuprofen on MCM-41, mSBA-3 and μSBA-3 porous silicas. (b) The release curves of ibuprofen from MCM-41, mSBA-3 and μSBA-3 porous silica. Note: MCM-41a is the aged MCM-41. The MCM-41 and MCM-41a exhibited very similar release behavior; thus in (b) the same curve was used for MCM-41 and MCM-41a in the original paper. Reprinted with permission from ref. 269. Copyright 2004, American Chemical Society. (c) Response and recovery curves of a mesoporous WO_3-based gas sensor to H_2S with different concentrations. (d) Response and recovery curves of a mesoporous WO_3 sensor to H_2S with a concentration of 50 ppm. Reprinted with permission from ref. 270. Copyright 2014, Wiley-VCH Verlag GmbH & Co. KGaA, Weinheim. (e) Response and recovery curves of a mesoporous ZnO-based sensor and a non-mesoporous ZnO-based sensor to ethanol vapor with different concentrations. (f) Response and recovery curves of a mesoporous ZnO-based sensor and a non-mesoporous ZnO-based sensor to ethanol with a concentration of 50 ppm. Reprinted with permission from ref. 59. Copyright 2016, Royal Society of Chemistry.

Many studies have reported that mesoporous sensors displayed long-term stability due to the protective effect provided by their unique mesoporous structure.[272,281] Han *et al.* reported the preparation of mesoscopic and molecular scale periodic organosilicas functionalized with bis(rhodamine Schiff-base derivative) that can selectively bind to Cu^{2+} (BRhPMOs).[191]

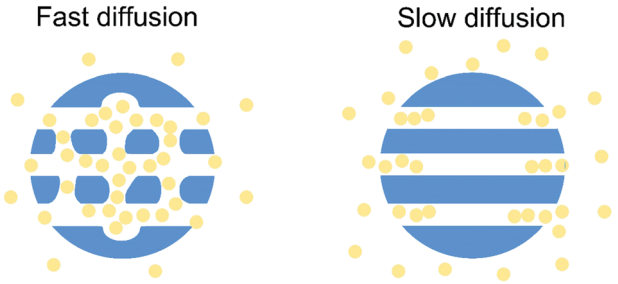

Fig. 26 Schematic illustration of the diffusion of guest molecules into mesoporous materials with the interconnected (left) and non-connected (right) mesopores.

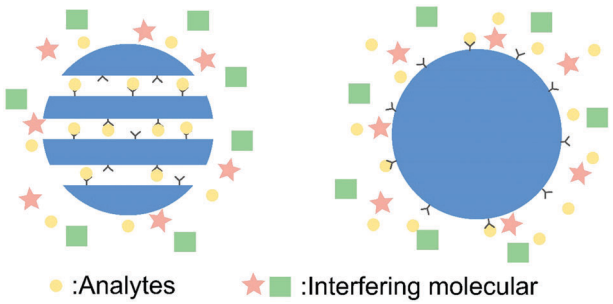

Fig. 28 Schematic illustration of detection of analytes with active sites on the inner surfaces of mesoporous materials and outer surfaces of nonporous materials.

In the absence of Cu^{2+}, the BRh chromophores were non-fluorescent. With the addition of Cu^{2+}, the BRh chromophores bound to Cu^{2+} and the ring of rhodamine moieties opened, resulting in strong fluorescence (Fig. 29a). The changes in fluorescence intensity from different BRh chromophores with time upon light irradiation were further monitored (Fig. 29b). The free R6G and the Cu^{2+}-chelated BRh-Si_4 lost about 25% and 21% of their initial fluorescence intensities, respectively. In contrast, the Cu^{2+}-chelated BRhPMOs did not display any obvious photobleaching under strong irradiation. These results indicated that the Cu^{2+}-chelated BRh chromophores immobilized on the surfaces of the mesopores exhibited excellent photostability under long-term irradiation. The excellent optical stability of Cu^{2+}-chelated BRhPMOs was ascribed to the protective mesoporous silica networks that could protect the inner immobilized fluorophores from exoteric quenching factors such as oxygen.

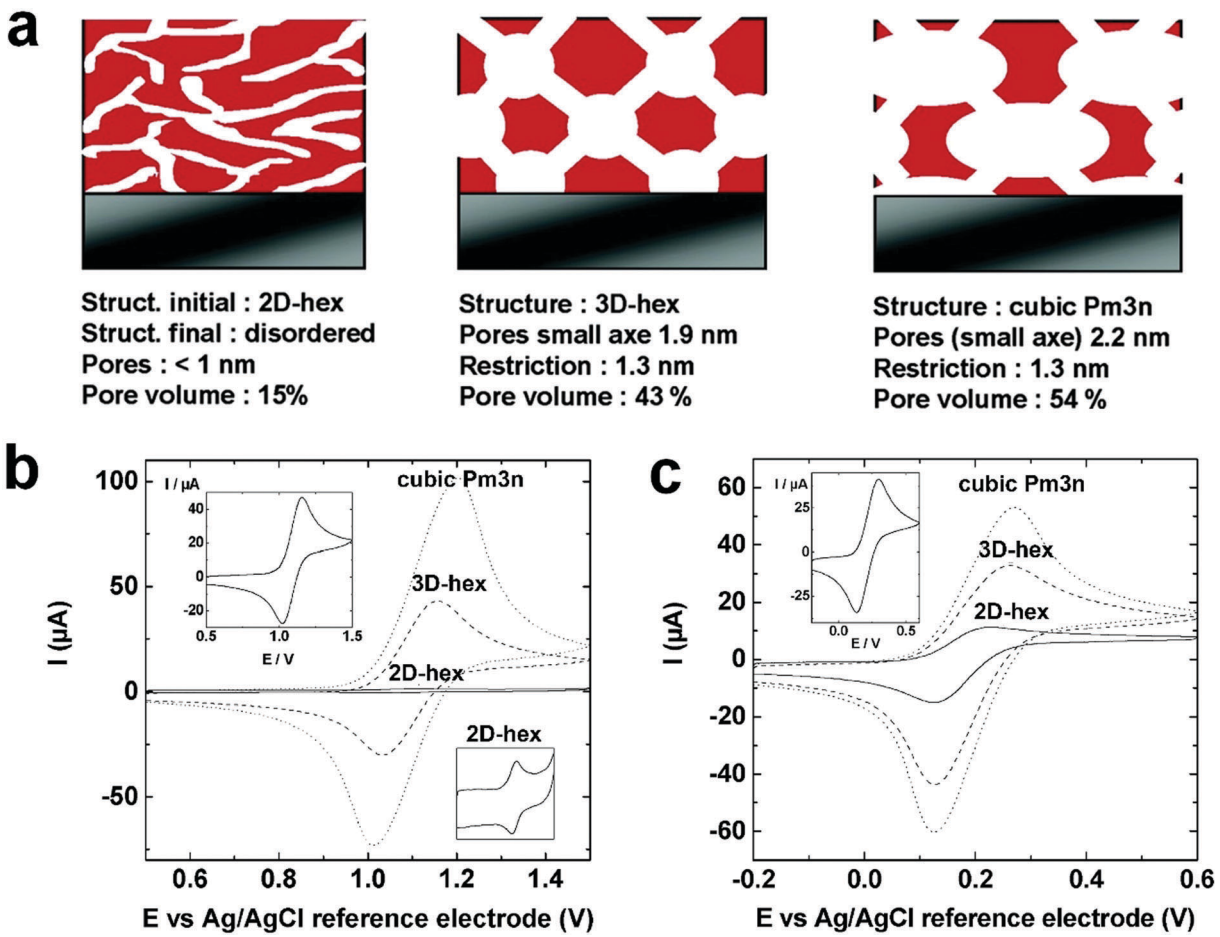

Fig. 27 (a) Schematic illustration of the structures and porosity characteristics of 2D-Hex, 3D-hexagonal and 3D cubic *Pm3n* mesoporous silica films. Cyclic voltammetric curves of ITO electrodes covered with different mesoporous silica thin films in 0.05 M hydrogen phthalate solutions containing 0.5 mM $Ru(bpy)_3^{2+}$ (b) and FcMeOH (c). Reprinted with permission from ref. 271. Copyright 2007, American Chemical Society.

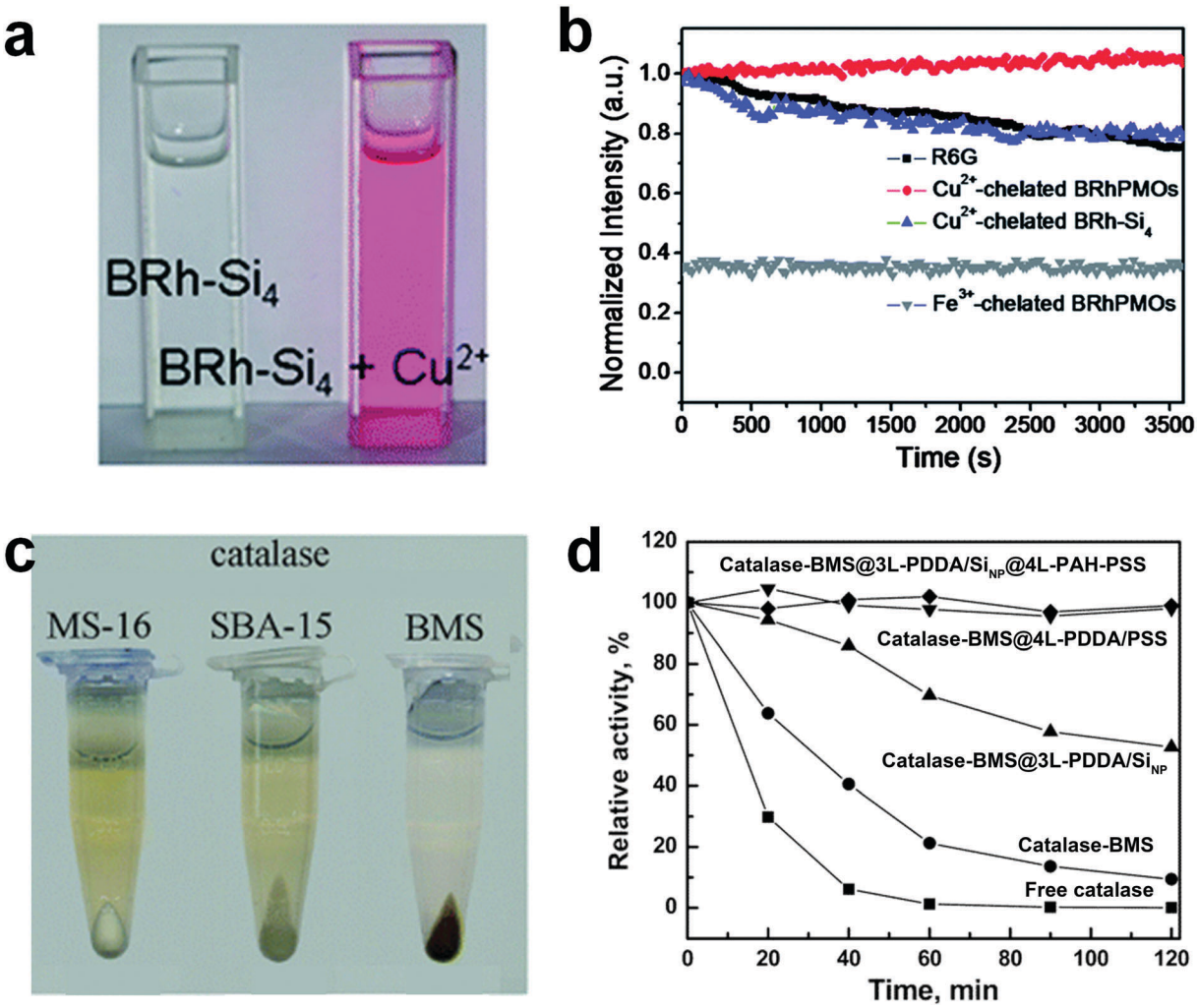

Fig. 29 (a) Photograph of BRh–Si_4 in THF before (left) and after (right) the addition of copper ions. (b) Photostability of R6G, Cu^{2+}-chelated BRhPMOs, Cu^{2+}-chelated BRh–Si_4 and Fe^{3+}-chelated BRhPMOs. Reprinted with permission from ref. 191. Copyright 2013, Royal Society of Chemistry. (c) Photographs of the color changes of the MS-16, SBA-15 and BMS mesoporous silicas following the immobilization of catalase. (d) Stability of free catalase, catalase-BMS particles, catalase-BMS particles coated with three PDDA/Si_{NP} bilayers, catalase-BMS particles coated with four PDDA/PSS bilayers, and catalase-BMS particles coated with three PDDA/Si_{NP} bilayers as well as four PAH/PSS bilayers in the presence of protease. Reprinted with permission from ref. 283. Copyright 2005, American Chemical Society.

Mesoporous materials bearing enzymes have been widely applied in biosensing applications.[10,13,282] Previous studies have demonstrated that the unique mesoporous structure contributes to the retention of enzyme activity. Ackerman, Liu and coworkers investigated the effect of mesoporous silica encapsulation on the specific activity of organophosphorus hydrolase (OPH).[220] For the free OPH in solution, results showed that the 145 days of storage caused a serious decrease (about 77%) to the specific activity of OPH. In contrast, the specific activity of OPH entrapped in the mesoporous silica decreased only 38% after the same storage. These results clearly suggest that the mesoporous structure can lead to the improvement of the stability of sensors. The rational design in this study can provide new strategies for the stabilization of biomolecules for a broad range of applications.

Caruso *et al.* prepared bimodal mesoporous silica (BMS) displaying a series of pore sizes of 2–3 nm and 10–40 nm.[283] Various enzymes, including catalase, peroxidase, cytochrome *C*, and lysozyme, were immobilized into BMS and the enzyme-loaded BMS was further encapsulated by multilayered nanocomposite thin shells. Due to the presence of relatively larger pores (10–40 nm) in BMS, much higher enzyme immobilization capacity was achieved on BMS spheres compared to MS-16 and SBA-15 mesoporous silicas (Fig. 29c). Moreover, the enzyme-loaded BMS spheres were further exposed to proteases to test the stability of the enzyme. Compared to free enzyme (Fig. 29d), the activity of the enzyme encapsulated in BMS was efficiently retained and no obvious decrease of enzyme activity was observed within 2 h. The encapsulated catalase also exhibits enhanced stability under reaction conditions over a wide pH range (pH 5–10) and retains an activity of 70% after 25 successive batch reactions. This study clearly demonstrates that the mesoporous structure can improve the stability of enzyme-based sensing systems.

6. Recovery time-related structural properties

Reusability is important for the practical use of a sensor because good reusability can significantly lower the costs.[127,272,284] The unique structural properties of mesoporous materials can contribute to the short recovery times and good reusability of mesoporous sensors.[63,128,270] The recovery of mesoporous sensors involves the detachment of analytes and the outward diffusion of analytes from mesoporous sensors to the solution or the air.[128] The recovery time of a sensor is the time it takes for the signal to return to its initial value upon decreasing the analyte concentration to zero.[68] Similar to the response time, the recovery time of a mesoporous sensor is correlated with the pore size and pore connectivity of mesoporous materials since these two structural properties significantly influence the diffusion of the analytes.

6.1 Pore size

Many previous studies have demonstrated that large pore sizes can lead to short recovery times by promoting the outward diffusion of detached analytes.[59,63,239,270,272,285] In one of these studies, Deng *et al.* prepared ordered mesoporous carbons that showed two-dimensional (2D) hexagonal mesopores and unique buckled large mesopores.[63] They investigated the application of the mesoporous carbons in NH_3 sensing. The mesoporous carbon (carbon-PEO_{117}-*b*-PS_{198}) consists of cylindrical mesopores with a pore size of about 26.2 nm. The mesoporous carbon-based gas sensor displayed good reversibility in NH_3 sensing and the sensor could be efficiently recovered in 4 min. For comparison, the mesoporous carbons C-FDU-15 and carbon-PEO_{117}-*b*-PS_{97} were also prepared and used for NH_3 sensing. The C-FDU-15 and carbon-PEO_{117}-*b*-PS_{97} mesoporous carbons display similar 2D hexagonal mesopores to those of the

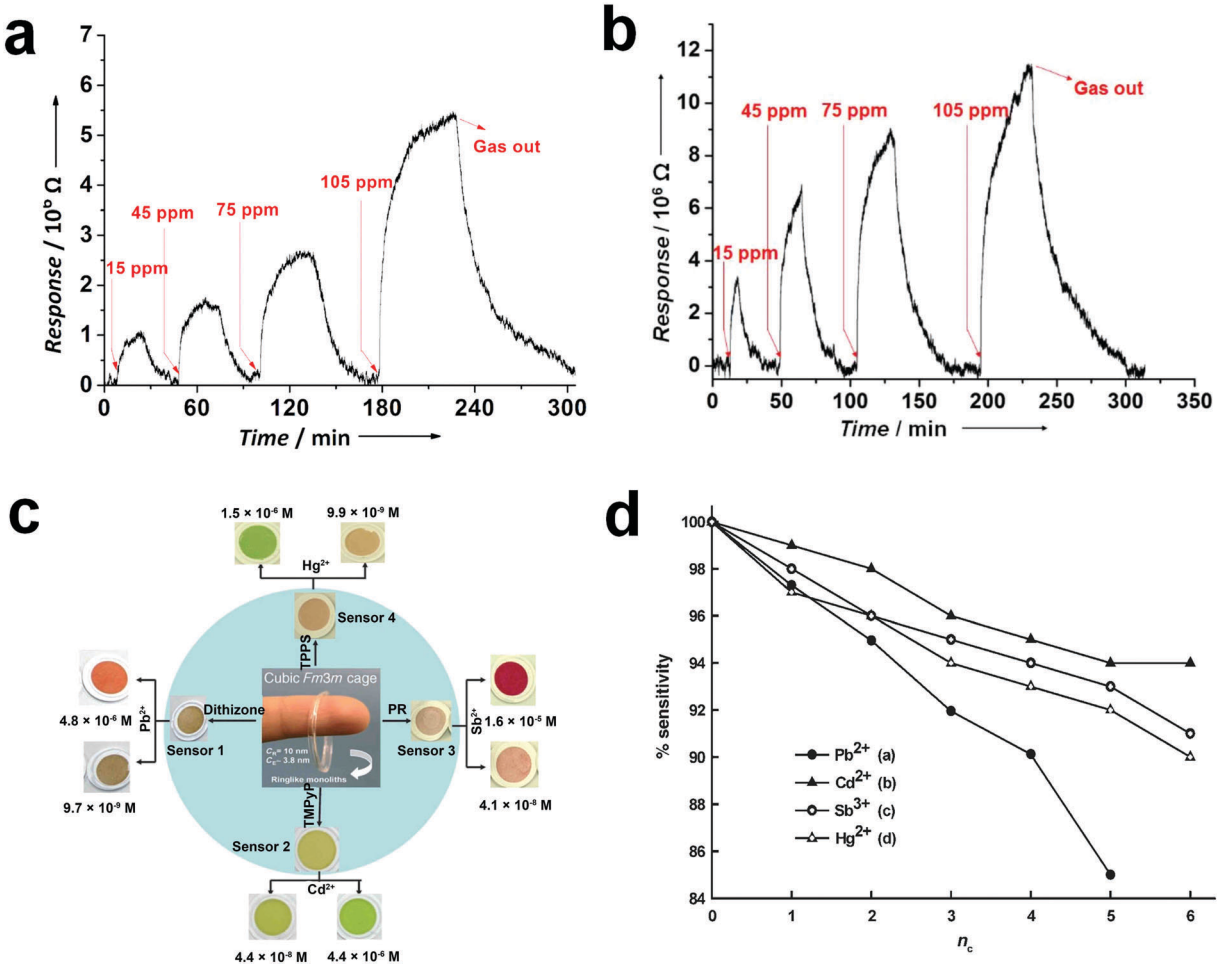

Fig. 30 (a) Response and recovery curves of the mesoporous carbon C-FDU-15 sensor to NH_3 at different concentrations. (b) Response and recovery curves of the mesoporous carbon-PEO117-*b*-PS_{97} to NH_3 at different concentrations. Reprinted with permission from ref. 63. Copyright 2016, American Chemical Society. (c) Schematic illustration of the colorimetric mesoporous sensors and the color changes of the corresponding sensors to different heavy metals. (d) Reproducibility of the cage sensors after complexation–regeneration cycles of analyte ions. The number of cycles is abbreviated as n_c. Reprinted with permission from ref. 272. Copyright 2006, Wiley-VCH Verlag GmbH & Co. KGaA, Weinheim.

carbon-PEO_{117}-*b*-PS_{198}. On the other hand, the pore sizes of the C-FDU-15 and carbon-PEO_{117}-*b*-PS_{97} mesoporous carbons are much smaller, 3.3 nm and 13.8 nm, respectively. The recovery times of the C-FDU-15 based sensor (Fig. 30a) and the carbon-PEO_{117}-*b*-PS_{97} based sensor (Fig. 30b) all exceeded 15 min, much longer than that of carbon-PEO_{117}-*b*-PS_{198}. This study suggests that large pore size can shorten the recovery time of mesoporous sensors by promoting the outward diffusion of analytes.

6.2 Pore connectivity

Good pore connectivity can also enhance the outward diffusion of analytes and lead to good recovery of mesoporous sensors. El-Safty and coworkers prepared a mesoporous monolith with 3D cage-typed mesopores for the detection of toxic ions (Fig. 30c).[272] The mesoporous monolith displayed spherical cavities and the mesopores were well-interconnected. Different kinds of binding receptors were grafted onto the inner surface of the mesoporous monolith for the sensing of Pb^{2+}, Cd^{2+}, Sb^{3+}, and Hg^{2+}. The mesoporous monolith-based sensor displayed a short response time ($t < 3$ min) and good reusability in sensing applications. The reusability was investigated by the designed cycles of repeated exquisite-detection–regeneration procedures. During the treatment, stripping agents such as EDTA were used to remove the metal ions trapped on the surfaces of the mesopores. Results showed that the mesoporous sensor was efficiently regenerated without resulting in obviously reduced response within several cycles (Fig. 30d). The slight decrease of detection sensitivity was ascribed to the deleterious effect of the employed stripping agents on the recognition subunits in the repeated exquisite-detection–regeneration cycles. This work provided a potential analytical tool for monitoring toxic metal ions in environmental samples.

7. Summary and outlook

In the past decades, impressive progress has been achieved in exploring mesoporous materials for analytical applications. The variety of analytical methods developed with mesoporous materials is ultra-large, which can be ascribed to the vast choice of available mesoporous materials with user-defined structures and properties. In exploring the analytical applications of mesoporous materials, many studies have demonstrated that the structural properties of mesoporous materials can be rationally tailored to improve the performance of analytical methods. Understanding the ''structure–performance relationship'' is of great importance for developing analytical methods with excellent performance based on mesoporous materials. In this review, the connections between the structural properties of mesoporous materials and some of the important analytical performances have been discussed. We summarized the structural properties, including pore size, pore shape, specific surface area, pore volume, *etc.*, that can contribute to the improvement of the selectivity, sensitivity, response time, stability and recovery time of analytical methods, which may provide potential instructions for the design of analytical methods with mesoporous materials.

Although certain connections exist between the structural properties of mesoporous materials and their analytical performance, challenges remain in the design of analytical methods. When designing analytical systems with mesoporous materials, many factors need to be taken into account because the structural properties may be incompatible in improving the analytical performance. For instance, an increase of pore size can facilitate molecular diffusion and afford a shorter response or recovery time, whereas a decrease of specific surface area caused by the increase of pore size inevitably leads to a decrease of surface active sites and the compromise of detection sensitivity. A balance between the structural properties of mesoporous materials should be achieved to optimize their analytical performance. On the other hand, the influence of the structural properties on the analytical performance is qualitatively investigated in the past decades. More quantitative studies need to be conducted in the coming years. The future development of the analytical applications of mesoporous materials requires the close collaboration of materials scientists and analytical chemists. By this way, the targets of good selectivity, high sensitivity, fast response, long-term stability, easy recovery and low cost can be achieved with mesoporous materials.

Conflicts of interest

There are no conflicts to declare.

Acknowledgements

This work was supported by the National Natural Science Foundation of China (21675120), the National Key R&D Program of China (2017YFA0208000, 2016YFF0100800), the National Postdoctoral Program for Innovative Talents (BX20180223), the National Basic Research Program of China (973 Program, Grant 2015CB932600) and the Ten Thousand Talents Program for Young Talents. Q. Yuan thanks the large-scale instrument and equipment sharing foundation of Wuhan University.

Notes and references

1 T. Yanagisawa, T. Shimizu, K. Kuroda and C. Kato, *Bull. Chem. Soc. Jpn.*, 1990, **63**, 988–992.
2 C. Kresge, M. Leonowicz, W. J. Roth, J. Vartuli and J. Beck, *Nature*, 1992, **359**, 710–712.
3 D. Zhao, J. Feng, Q. Huo, N. Melosh, G. H. Fredrickson, B. F. Chmelka and G. D. Stucky, *Science*, 1998, **279**, 548–552.
4 M. R. Benzigar, S. N. Talapaneni, S. Joseph, K. Ramadass, G. Singh, J. Scaranto, U. Ravon, K. Al-Bahilyc and A. Vinu, *Chem. Soc. Rev.*, 2018, **47**, 2680–2721.
5 Y. Wan and D. Zhao, *Chem. Rev.*, 2007, **107**, 2821–2860.
6 S. H. Wu, C. Y. Mou and H. P. Lin, *Chem. Soc. Rev.*, 2013, **42**, 3862–3875.

7 Y. Chen and J. Shi, *Adv. Mater.*, 2016, **28**, 3235–3272.
8 T. J. Barton, L. M. Bull, W. G. Klemperer, D. A. Loy, B. McEnaney, M. Misono, P. A. Monson, G. Pez, G. W. Scherer and J. C. Vartuli, *Chem. Mater.*, 1999, **11**, 2633–2656.
9 M. M. Orosco, C. Pacholski and M. J. Sailor, *Nat. Nanotechnol.*, 2009, **4**, 255–258.
10 Z. Zhou and M. Hartmann, *Chem. Soc. Rev.*, 2013, **42**, 3894–3912.
11 J. C. Ndamanisha and L. P. Guo, *Anal. Chim. Acta*, 2012, **747**, 19–28.
12 N. Song and Y. W. Yang, *Chem. Soc. Rev.*, 2015, **44**, 3474–3504.
13 M. Etienne, L. Zhang, N. Vilà and A. Walcarius, *Electroanalysis*, 2015, **27**, 2028–2054.
14 A. Walcarius, *Chem. Soc. Rev.*, 2013, **42**, 4098–4140.
15 L. Pan, Q. He, J. Liu, Y. Chen, M. Ma, L. Zhang and J. Shi, *J. Am. Chem. Soc.*, 2012, **134**, 5722–5725.
16 Y. Wu, G. Cheng, K. Katsov, S. W. Sides, J. Wang, J. Tang, G. H. Fredrickson, M. Moskovits and G. D. Stucky, *Nat. Mater.*, 2004, **3**, 816–822.
17 G. Buntkowsky, H. Breitzke, A. Adamczyk, F. Roelofs, T. Emmler, E. Gedat, B. Grünberg, Y. Xu, H. H. Limbach and I. Shenderovich, *Phys. Chem. Chem. Phys.*, 2007, **9**, 4843–4853.
18 Y. Chen, S. Wang, J. Ye, D. Li, Z. Liu and X. Wu, *Nanoscale*, 2014, **6**, 9563–9567.
19 Q. Yuan, A. X. Yin, C. Luo, L. D. Sun, Y. W. Zhang, W. T. Duan, H. C. Liu and C. H. Yan, *J. Am. Chem. Soc.*, 2008, **130**, 3465–3472.
20 F. Goettmann and C. Sanchez, *J. Mater. Chem.*, 2007, **17**, 24–30.
21 R. Ravindra, S. Zhao, H. Gies and R. Winter, *J. Am. Chem. Soc.*, 2004, **126**, 12224–12225.
22 Z. Li, J. C. Barnes, A. Bosoy, J. F. Stoddart and J. I. Zink, *Chem. Soc. Rev.*, 2012, **41**, 2590–2605.
23 Y. Shi, Y. Wan and D. Zhao, *Chem. Soc. Rev.*, 2011, **40**, 3854–3878.
24 W. Li, Q. Yue, Y. Deng and D. Zhao, *Adv. Mater.*, 2013, **25**, 5129–5152.
25 R. Zhang, A. A. Elzatahry, S. S. Al-Deyab and D. Zhao, *Nano Today*, 2012, **7**, 344–366.
26 T. Wagner, S. Haffer, C. Weinberger, D. Klaus and M. Tiemann, *Chem. Soc. Rev.*, 2013, **42**, 4036–4053.
27 Y. Chen, H. Chen and J. Shi, *Adv. Mater.*, 2013, **25**, 3144–3176.
28 C. Gérardin, J. Reboul, M. Bonne and B. Lebeau, *Chem. Soc. Rev.*, 2013, **42**, 4217–4255.
29 L. L. Li, W. T. Duan, Q. Yuan, Z. X. Li, H. H. Duan and C. H. Yan, *Chem. Commun.*, 2009, 6174–6176.
30 Q. Yuan, Q. Liu, W. G. Song, W. Feng, W. L. Pu, L. D. Sun, Y. W. Zhang and C. H. Yan, *J. Am. Chem. Soc.*, 2007, **129**, 6698–6699.
31 K. Ma, H. Sai and U. Wiesner, *J. Am. Chem. Soc.*, 2012, **134**, 13180–13183.
32 Y. Chen, H. R. Chen and J. L. Shi, *Acc. Chem. Res.*, 2013, **47**, 125–137.
33 J. S. Lee, S. H. Joo and R. Ryoo, *J. Am. Chem. Soc.*, 2002, **124**, 1156–1157.
34 Q. Huo, D. I. Margolese and G. D. Stucky, *Chem. Mater.*, 1996, **8**, 1147–1160.
35 M. E. Davis, *Nature*, 2002, **417**, 813.
36 I. Sierra and D. Pérez-Quintanilla, *Chem. Soc. Rev.*, 2013, **42**, 3792–3807.
37 R. Tian, H. Zhang, M. Ye, X. Jiang, L. Hu, X. Li, X. Bao and H. Zou, *Angew. Chem., Int. Ed.*, 2007, **46**, 962–965.
38 Z. Qiu, J. Shu and D. Tang, *Anal. Chem.*, 2017, **89**, 5152–5160.
39 P. Yang, S. Gai and J. Lin, *Chem. Soc. Rev.*, 2012, **41**, 3679–3698.
40 L. L. Li, M. Xie, J. Wang, X. Li, C. Wang, Q. Yuan, D. W. Pang, Y. Lu and W. Tan, *Chem. Commun.*, 2013, **49**, 5823–5825.
41 Y. Chen, Q. Meng, M. Wu, S. Wang, P. Xu, H. Chen, Y. Li, L. Zhang, L. Wang and J. Shi, *J. Am. Chem. Soc.*, 2014, **136**, 16326–16334.
42 M. Wu, Q. Meng, Y. Chen, Y. Du, L. Zhang, Y. Li, L. Zhang and J. Shi, *Adv. Mater.*, 2015, **27**, 215–222.
43 J. Lu, M. Liong, Z. Li, J. I. Zink and F. Tamanoi, *Small*, 2010, **6**, 1794–1805.
44 Y. Wang, X. Hu, J. Dai, J. Wang, Y. Tan, X. Yang, S. Yang, Q. Yuan and Y. Zhang, *J. Mater. Chem. B*, 2017, **5**, 6794–6800.
45 X. Hu, Y. Wang, Y. Tan, J. Wang, H. Liu, Y. Wang, S. Yang, M. Shi, S. Zhao and Y. Zhang, *Adv. Mater.*, 2017, **29**, 1605235.
46 M. Vallet-Regí, M. Colilla and B. González, *Chem. Soc. Rev.*, 2011, **40**, 596–607.
47 K. S. Lakhi, D. Park, K. Albahily, W. S. Cha, B. Viswanathan, J. Choy and A. Vinu, *Chem. Soc. Rev.*, 2017, **46**, 72–101.
48 A. Corma, *Chem. Rev.*, 1997, **97**, 2373–2420.
49 Y. Yang, W. Yin, S. Wu, X. Yang, W. Xia, Y. Shen, Y. Huang, A. Cao and Q. Yuan, *ACS Nano*, 2015, **10**, 1240–1248.
50 A. Walcarius, *TrAC, Trends Anal. Chem.*, 2012, **38**, 79–97.
51 M. W. Ambrogio, C. R. Thomas, Y. L. Zhao, J. I. Zink and J. F. Stoddart, *Acc. Chem. Res.*, 2011, **44**, 903–913.
52 M. Liong, J. Lu, M. Kovochich, T. Xia, S. G. Ruehm, A. E. Nel, F. Tamanoi and J. I. Zink, *ACS Nano*, 2008, **2**, 889–896.
53 B. Hatton, K. Landskron, W. Whitnall, D. Perovic and G. A. Ozin, *Acc. Chem. Res.*, 2005, **38**, 305–312.
54 C. Sanchez, P. Belleville, M. Popall and L. Nicole, *Chem. Soc. Rev.*, 2011, **40**, 696–753.
55 W. S. Han, H. Y. Lee, S. H. Jung, S. J. Lee and J. H. Jung, *Chem. Soc. Rev.*, 2009, **38**, 1904–1915.
56 M. Tiemann, *Chem. – Eur. J.*, 2007, **13**, 8376–8388.
57 A. Walcarius, *Electroanalysis*, 2015, **27**, 1303–1340.
58 F. Hoffmann, M. Cornelius, J. Morell and M. Fröba, *Angew. Chem., Int. Ed.*, 2006, **45**, 3216–3251.
59 X. Zhou, Y. Zhu, W. Luo, Y. Ren, P. Xu, A. A. Elzatahry, X. Cheng, A. Alghamdi, Y. Deng and D. Zhao, *J. Mater. Chem. A*, 2016, **4**, 15064–15071.
60 F. Sancenón, L. Pascual, M. Oroval, E. Aznar and R. Martínez-Máñez, *ChemistryOpen*, 2015, **4**, 418–437.
61 Y. Chen, D. Li, Z. Bie, X. He and Z. Liu, *Anal. Chem.*, 2016, **88**, 1447–1454.
62 R. Qian, L. Ding and H. Ju, *J. Am. Chem. Soc.*, 2013, **135**, 13282–13285.

63 W. Luo, T. Zhao, Y. Li, J. Wei, P. Xu, X. Li, Y. Wang, W. Zhang, A. A. Elzatahry, A. Alghamdi, Y. H. Deng, L. J. Wang, W. Jiang, Y. Liu, B. Kong and D. Y. Zhao, *J. Am. Chem. Soc.*, 2016, **138**, 12586–12595.
64 A. Walcarius and A. Kuhn, *TrAC, Trends Anal. Chem.*, 2008, **27**, 593–603.
65 I. I. Slowing, B. G. Trewyn, S. Giri and V. Y. Lin, *Adv. Funct. Mater.*, 2007, **17**, 1225–1236.
66 T. Ma, L. Liu and Z. Yuan, *Chem. Soc. Rev.*, 2013, **42**, 3977–4003.
67 C. Coll, A. Bernardos, R. N. Martínez-Máñez and F. L. Sancenón, *Acc. Chem. Res.*, 2012, **46**, 339–349.
68 V. Bochenkov and G. Sergeev, *Met. Oxide Nanostruct. Their Appl.*, 2010, **3**, 31–52.
69 H. L. Pardue, *Anal. Chim. Acta*, 1989, **216**, 69–107.
70 M. Comes, G. Rodríguez-López, M. D. Marcos, R. Martínez-Máñez, F. Sancenón, J. Soto, L. A. Villaescusa, P. Amorós and D. Beltrán, *Angew. Chem., Int. Ed.*, 2005, **44**, 2918–2922.
71 Y. Shin, J. Liu, L. Q. Wang, Z. Nie, W. D. Samuels, G. E. Fryxell and G. J. Exarhos, *Angew. Chem., Int. Ed.*, 2000, **39**, 2702–2707.
72 A. Katiyar and N. G. Pinto, *Small*, 2006, **2**, 644–648.
73 Y. J. Han, G. D. Stucky and A. Butler, *J. Am. Chem. Soc.*, 1999, **121**, 9897–9898.
74 H. Qin, L. Zhao, R. Li, R. A. Wu and H. Zou, *Anal. Chem.*, 2011, **83**, 7721–7728.
75 D. W. Breck, W. G. Eversole, R. M. Milton, T. B. Reed and T. L. Thomas, *J. Am. Chem. Soc.*, 1956, **78**, 5963–5972.
76 R. M. Barrer and D. A. Ibbitson, *Trans. Faraday Soc.*, 1944, **40**, 195–206.
77 U. Olsbye, S. Svelle, M. Bjørgen, P. Beato, T. V. Janssens, F. Joensen, S. Bordiga and K. P. Lillerud, *Angew. Chem., Int. Ed.*, 2012, **51**, 5810–5831.
78 D. M. Schlipf, S. E. Rankin and B. L. Knutson, *ACS Appl. Mater. Interfaces*, 2013, **5**, 10111–10117.
79 Y. Li, H. D. Tolley and M. L. Lee, *Anal. Chem.*, 2009, **81**, 4406–4413.
80 H. H. Yiu, C. H. Botting, N. P. Botting and P. A. Wright, *Phys. Chem. Chem. Phys.*, 2001, **3**, 2983–2985.
81 Q. Yue, J. Li, W. Luo, Y. Zhang, A. A. Elzatahry, X. Wang, C. Wang, W. Li, X. Cheng and A. Alghamdi, *J. Am. Chem. Soc.*, 2015, **137**, 13282–13289.
82 D. Van Gough, A. Wolosiuk and P. V. Braun, *Nano Lett.*, 2009, **9**, 1994–1998.
83 M. Kruk, V. Antochshuk, J. R. Matos, L. P. Mercuri and M. Jaroniec, *J. Am. Chem. Soc.*, 2002, **124**, 768–769.
84 Z. Sun, Y. Deng, J. Wei, D. Gu, B. Tu and D. Zhao, *Chem. Mater.*, 2011, **23**, 2176–2184.
85 V. S. Y. Lin, C. Y. Lai, J. Huang, S. A. Song and S. Xu, *J. Am. Chem. Soc.*, 2001, **123**, 11510–11511.
86 J. Tan, W. J. Zhao, J. K. Yu, S. Ma, M. J. Sailor and J. M. Wu, *Adv. Healthcare Mater.*, 2012, **1**, 742–750.
87 R. Terracciano, F. Casadonte, L. Pasqua, P. Candeloro, E. Di Fabrizio, A. Urbani and R. Savino, *Talanta*, 2010, **80**, 1532–1538.
88 A. Bouamrani, Y. Hu, E. Tasciotti, L. Li, C. Chiappini, X. Liu and M. Ferrari, *Proteomics*, 2010, **10**, 496–505.
89 H. Qin, P. Gao, F. Wang, L. Zhao, J. Zhu, A. Wang, T. Zhang, R. A. Wu and H. Zou, *Angew. Chem., Int. Ed.*, 2011, **50**, 12218–12221.
90 X. Huang, Q. Liu, J. Fu, Z. Nie, K. Gao and G. Jiang, *Anal. Chem.*, 2016, **88**, 4107–4113.
91 Q. Min, R. a. Wu, L. Zhao, H. Qin, M. Ye, J. J. Zhu and H. Zou, *Chem. Commun.*, 2010, **46**, 6144–6146.
92 Y. Hu, Y. Peng, K. Lin, H. Shen, L. C. Brousseau III, J. Sakamoto, T. Sun and M. Ferrari, *Nanoscale*, 2011, **3**, 421–428.
93 C. Lei, O. Noonan, S. Jambhrunkar, K. Qian, C. Xu, J. Zhang, A. Nouwens and C. Yu, *Small*, 2014, **10**, 2413–2418.
94 Y. Li, H. D. Tolley and M. L. Lee, *J. Chromatogr. A*, 2010, **1217**, 8181–8185.
95 M. Hartmann, *Angew. Chem., Int. Ed.*, 2004, **43**, 5880–5882.
96 H. D. Faria, L. C. C. Abrão, M. G. Santos, A. F. Barbosa and E. C. Figueiredo, *Anal. Chim. Acta*, 2017, **959**, 43–65.
97 P. Sadílek, D. Šatínský and P. Solich, *TrAC, Trends Anal. Chem.*, 2007, **26**, 375–384.
98 J. Jeromenok and J. Weber, *Langmuir*, 2013, **29**, 12982–12989.
99 Y. C. Liu, Y. Lu and Z. Liu, *Chem. Sci.*, 2012, **3**, 1467–1471.
100 F. Wang, Y. F. Guan, S. Zhang and Y. Xia, *J. Chromatogr. A*, 2012, **1246**, 76–83.
101 L. I. Devriese, L. Cools, A. Aerts, J. A. Martens, G. V. Baron and J. F. Denayer, *Adv. Funct. Mater.*, 2007, **17**, 3911–3917.
102 C. H. Christensen, K. Johannsen, I. Schmidt and C. H. Christensen, *J. Am. Chem. Soc.*, 2003, **125**, 13370–13371.
103 A. Sarafraz-Yazdi and N. Razavi, *TrAC, Trends Anal. Chem.*, 2015, **73**, 81–90.
104 Y. Ge and A. P. F. Turner, *Chem. – Eur. J.*, 2009, **15**, 8100–8107.
105 G. Vasapollo, R. D. Sole, L. Mergola, M. R. Lazzoi, A. Scardino, S. Scorrano and G. Mele, *Int. J. Mol. Sci.*, 2011, **12**, 5908–5945.
106 A. Martín-Esteban, *Fresenius' J. Anal. Chem.*, 2001, **370**, 795–802.
107 S. Tokonami, H. Shiigi and T. Nagaoka, *Anal. Chim. Acta*, 2009, **641**, 7–13.
108 M. Amjadi and R. Jalili, *Biosens. Bioelectron.*, 2017, **96**, 121–126.
109 M. Li, H. Liu and X. Ren, *Biosens. Bioelectron.*, 2017, **89**, 899–905.
110 Y. Chen, X. Li, D. Yin, D. Li, Z. Bie and Z. Liu, *Chem. Commun.*, 2015, **51**, 10929–10932.
111 R. Horikawa, H. Sunayama, Y. Kitayama, E. Takano and T. Takeuchi, *Angew. Chem., Int. Ed.*, 2016, **55**, 13023–13027.
112 A. Katz and M. E. Davis, *Nature*, 2000, **403**, 286–289.
113 S. Wang, D. Yin, W. Wang, X. Shen, J. J. Zhu, H. Y. Chen and Z. Liu, *Sci. Rep.*, 2016, **6**, 22757.
114 L. Zhang and L. Chen, *ACS Appl. Mater. Interfaces*, 2016, **8**, 16248–16256.
115 X. Pan, X. He and Z. Liu, *Anal. Chim. Acta*, 2018, **1019**, 65–73.
116 C. Wattanakit, Y. B. Saint Côme, V. Lapeyre, P. A. Bopp, M. Heim, S. Yadnum, S. Nokbin, C. Warakulwit, J. Limtrakul and A. Kuhn, *Nat. Commun.*, 2014, **5**, 3325.

117 D. Coutinho, A. O. Acevedo, G. R. Dieckmann and K. J. Balkus Jr, *Microporous Mesoporous Mater.*, 2002, **54**, 249–255.
118 P. Paik, A. Gedanken and Y. Mastai, *Microporous Mesoporous Mater.*, 2010, **129**, 82–89.
119 S. Lacasta, V. Sebastián, C. Casado, Á. Mayoral, P. Romero, Á. Larrea, E. Vispe, P. López-Ram-de-Viu, S. Uriel and J. Coronas, *Chem. Mater.*, 2011, **23**, 1280–1287.
120 T. Yutthalekha, C. Warakulwit, J. Limtrakul and A. Kuhn, *Electroanalysis*, 2015, **27**, 2209–2213.
121 P. Paik, A. Gedanken and Y. Mastai, *ACS Appl. Mater. Interfaces*, 2009, **1**, 1834–1842.
122 K. Haupt and K. Mosbach, *Chem. Rev.*, 2000, **100**, 2495–2504.
123 B. M. Jung, M. S. Kim, W. J. Kim and J. Y. Chang, *Chem. Commun.*, 2010, **46**, 3699–3701.
124 Y. Kim, J. B. Jeon and J. Y. Chang, *J. Mater. Chem.*, 2012, **22**, 24075–24080.
125 D. Li, Y. Chen and Z. Liu, *Chem. Soc. Rev.*, 2015, **44**, 8097–8123.
126 Z. Liu and H. He, *Acc. Chem. Res.*, 2017, **50**, 2185–2193.
127 E. Kim, H. E. Kim, S. J. Lee, S. S. Lee, M. L. Seo and J. H. Jung, *Chem. Commun.*, 2008, 3921–3923.
128 X. Pan, Y. Chen, P. Zhao, D. Li and Z. Liu, *Angew. Chem., Int. Ed.*, 2015, **54**, 6173–6176.
129 Q. Yuan, Y. Zhang, T. Chen, D. Lu, Z. Zhao, X. Zhang, Z. Li, C. H. Yan and W. Tan, *ACS Nano*, 2012, **6**, 6337–6344.
130 Z. Zhang, D. Balogh, F. Wang, S. Y. Sung, R. Nechushtai and I. Willner, *ACS Nano*, 2013, **7**, 8455–8468.
131 A. B. Descalzo, K. Rurack, H. Weisshoff, R. Martínez-Máñez, M. D. Marcos, P. Amorós, K. Hoffmann and J. Soto, *J. Am. Chem. Soc.*, 2005, **127**, 184–200.
132 K. Patel, S. Angelos, W. R. Dichtel, A. Coskun, Y. W. Yang, J. I. Zink and J. F. Stoddart, *J. Am. Chem. Soc.*, 2008, **130**, 2382–2383.
133 D. R. Radu, C. Y. Lai, J. W. Wiench, M. Pruski and V. S. Y. Lin, *J. Am. Chem. Soc.*, 2004, **126**, 1640–1641.
134 E. Climent, R. Martínez-Máñez, F. Sancenón, M. D. Marcos, J. Soto, A. Maquieira and P. Amorós, *Angew. Chem., Int. Ed.*, 2010, **49**, 7281–7283.
135 K. Ren, J. Wu, Y. Zhang, F. Yan and H. Ju, *Anal. Chem.*, 2014, **86**, 7494–7499.
136 Y. Wang, M. Lu, J. Zhu and S. Tian, *J. Mater. Chem. B*, 2014, **2**, 5847–5853.
137 H. Shen, J. Wang, H. Liu, Z. Li, F. Jiang, F. B. Wang and Q. Yuan, *ACS Appl. Mater. Interfaces*, 2016, **8**, 19371–19378.
138 M. Oroval, E. Climent, C. Coll, R. Eritja, A. Aviñó, M. D. Marcos, F. Sancenón, R. Martínez-Máñez and P. Amorós, *Chem. Commun.*, 2013, **49**, 5480–5482.
139 Y. Zhang, Q. Yuan, T. Chen, X. Zhang, Y. Chen and W. Tan, *Anal. Chem.*, 2012, **84**, 1956–1962.
140 Z. Zhang, D. Balogh, F. Wang and I. Willner, *J. Am. Chem. Soc.*, 2013, **135**, 1934–1940.
141 L. Fu, J. Zhuang, W. Lai, X. Que, M. Lu and D. Tang, *J. Mater. Chem. B*, 2013, **1**, 6123–6128.
142 Z. Zhang, F. Wang, D. Balogh and I. Willner, *J. Mater. Chem. B*, 2014, **2**, 4449–4455.
143 E. Aznar, R. Villalonga, C. Giménez, F. Sancenón, M. D. Marcos, R. Martínez-Máñez, P. Díez, J. M. Pingarrón and P. Amorós, *Chem. Commun.*, 2013, **49**, 6391–6393.
144 A. Schlossbauer, J. Kecht and T. Bein, *Angew. Chem., Int. Ed.*, 2009, **48**, 3092–3095.
145 E. Climent, D. Gröninger, M. Hecht, M. A. Walter, R. Martínez-Máñez, M. G. Weller, F. Sancenón, P. Amorós and K. Rurack, *Chem. – Eur. J.*, 2013, **19**, 4117–4122.
146 R. Casasús, E. Aznar, M. D. Marcos, R. Martínez-Máñez, F. Sancenón, J. Soto and P. Amorós, *Angew. Chem., Int. Ed.*, 2006, **45**, 6661–6664.
147 A. B. Descalzo, D. Jimenez, M. D. Marcos, R. Martinez-Manez, J. Soto, J. El Haskouri, C. Guillem, D. Beltran, P. Amoros and M. V. Borrachero, *Adv. Mater.*, 2002, **14**, 966–969.
148 C. Y. Lai, B. G. Trewyn, D. M. Jeftinija, K. Jeftinija, S. Xu, S. Jeftinija and V. S. Y. Lin, *J. Am. Chem. Soc.*, 2003, **125**, 4451–4459.
149 Q. He, Y. Gao, L. Zhang, Z. Zhang, F. Gao, X. Ji, Y. Li and J. Shi, *Biomaterials*, 2011, **32**, 7711–7720.
150 X. Li, T. Zhai, P. Gao, H. Cheng, R. Hou, X. Lou and F. Xia, *Nat. Commun.*, 2018, **9**, 40.
151 W. Fan, B. Shen, W. Bu, F. Chen, Q. He, K. Zhao, S. Zhang, L. Zhou, W. Peng and Q. Xiao, *Biomaterials*, 2014, **35**, 8992–9002.
152 J. Lu, M. Liong, J. I. Zink and F. Tamanoi, *Small*, 2007, **3**, 1341–1346.
153 Y. Salinas, M. V. Solano, R. E. Sørensen, K. R. Larsen, J. Lycoops, J. O. Jeppesen, R. Martínez-Máñez, F. Sancenón, M. D. Marcos and P. Amorós, *Chem. – Eur. J.*, 2014, **20**, 855–866.
154 S. Saha, K. F. Leung, T. D. Nguyen, J. F. Stoddart and J. I. Zink, *Adv. Funct. Mater.*, 2007, **17**, 685–693.
155 C. L. Zhu, C. H. Lu, X. Y. Song, H. H. Yang and X. R. Wang, *J. Am. Chem. Soc.*, 2011, **133**, 1278–1281.
156 S. Angelos, Y. W. Yang, K. Patel, J. F. Stoddart and J. I. Zink, *Angew. Chem., Int. Ed.*, 2008, **47**, 2222–2226.
157 E. Climent, M. D. Marcos, R. Martínez-Máñez, F. Sancenón, J. Soto, K. Rurack and P. Amorós, *Angew. Chem., Int. Ed.*, 2009, **48**, 8519–8522.
158 B. Lozano-Torres, L. Pascual, A. Bernardos, M. D. Marcos, J. O. Jeppesen, Y. Salinas, R. Martínez-Máñez and F. Sancenón, *Chem. Commun.*, 2017, **53**, 3559–3562.
159 I. Candel, A. Bernardos, E. Climent, M. D. Marcos, R. Martínez-Máñez, F. Sancenon, J. Soto, A. Costero, S. Gil and M. Parra, *Chem. Commun.*, 2011, **47**, 8313–8315.
160 Y. Salinas, A. Agostini, É. Pérez-Esteve, R. Martínez-Máñez, F. Sancenón, M. D. Marcos, J. Soto, A. M. Costero, S. Gil and M. Parra, *J. Mater. Chem. A*, 2013, **1**, 3561–3564.
161 Y. L. Sun, Y. Zhou, Q. L. Li and Y. W. Yang, *Chem. Commun.*, 2013, **49**, 9033–9035.
162 Y. L. Choi, J. Jaworski, M. L. Seo, S. J. Lee and J. H. Jung, *J. Mater. Chem.*, 2011, **21**, 7882–7885.
163 R. Hernandez, H. R. Tseng, J. W. Wong, J. F. Stoddart and J. I. Zink, *J. Am. Chem. Soc.*, 2004, **126**, 3370–3371.
164 M. Xue and J. I. Zink, *J. Am. Chem. Soc.*, 2013, **135**, 17659–17662.

165 J. Liu, Z. Cao and Y. Lu, *Chem. Rev.*, 2009, **109**, 1948–1998.
166 J. Wang, Q. Ma, X. X. Hu, H. Liu, W. Zheng, X. Chen, Q. Yuan and W. Tan, *ACS Nano*, 2017, **11**, 8010–8017.
167 J. Wang, Q. Ma, W. Zheng, H. Liu, C. Yin, F. Wang, X. Chen, Q. Yuan and W. Tan, *ACS Nano*, 2017, **11**, 8185–8191.
168 J. Wang, Y. Wei, X. Hu, Y. Y. Fang, X. Li, J. Liu, S. Wang and Q. Yuan, *J. Am. Chem. Soc.*, 2015, **137**, 10576–10584.
169 H. M. Meng, H. Liu, H. Kuai, R. Peng, L. Mo and X. B. Zhang, *Chem. Soc. Rev.*, 2016, **45**, 2583–2602.
170 W. Jie and Y. Quan, *Sci. China: Chem.*, 2017, **60**, 687–688.
171 J. Wang, H. Shen, X. Hu, Y. Li, Z. Li, J. Xu, X. Song, H. Zeng and Q. Yuan, *Adv. Sci.*, 2016, **3**, 1500289.
172 Z. Li, J. Wang, Y. Li, X. Liu and Q. Yuan, *Mater. Chem. Front.*, 2018, **2**, 423–436.
173 W. Zhou, R. Saran and J. Liu, *Chem. Rev.*, 2017, **117**, 8272–8325.
174 Y. Wang, L. Jiang, L. Chu, W. Liu, S. Wu, Y. Wu, X. He and K. Wang, *Biosens. Bioelectron.*, 2017, **87**, 459–465.
175 J. Wang, Q. Ma, H. Liu, Y. Wang, H. Shen, X. Hu, C. Ma, Q. Yuan and W. Tan, *Anal. Chem.*, 2017, **89**, 12764–12770.
176 E. Climent, A. Bernardos, R. Martínez-Máñez, A. Maquieira, M. D. Marcos, N. Pastor-Navarro, R. Puchades, F. Sancenón, J. Soto and P. Amorós, *J. Am. Chem. Soc.*, 2009, **131**, 14075–14080.
177 M. Chen, C. Huang, C. He, W. Zhu, Y. Xu and Y. Lu, *Chem. Commun.*, 2012, **48**, 9522–9524.
178 J. Lee, H. Kim, S. Han, E. Hong, K. H. Lee and C. Kim, *J. Am. Chem. Soc.*, 2014, **136**, 12880–12883.
179 P. D. Thornton and A. Heise, *J. Am. Chem. Soc.*, 2010, **132**, 2024–2028.
180 D. Tang, Y. Lin, Q. Zhou, Y. Lin, P. Li, R. Niessner and D. Knopp, *Anal. Chem.*, 2014, **86**, 11451–11458.
181 L. Chen, Y. Wen, B. Su, J. Di, Y. Song and L. Jiang, *J. Mater. Chem.*, 2011, **21**, 13811–13816.
182 Y. Wen, L. Xu, C. Li, H. Du, L. Chen, B. Su, Z. Zhang, X. Zhang and Y. Song, *Chem. Commun.*, 2012, **48**, 8410–8412.
183 B. Zhang, B. Liu, J. Liao, G. Chen and D. Tang, *Anal. Chem.*, 2013, **85**, 9245–9252.
184 Z. Gao, D. Tang, M. Xu, G. Chen and H. Yang, *Chem. Commun.*, 2014, **50**, 6256–6258.
185 L. Hou, C. Zhu, X. Wu, G. Chen and D. Tang, *Chem. Commun.*, 2014, **50**, 1441–1443.
186 Q. Tan, R. Zhang, R. Kong, W. Kong, W. Zhao and F. Qu, *Microchim. Acta*, 2018, **185**, 44.
187 M. Comes, M. D. Marcos, R. Martínez-Máñez, M. C. Millán, J. V. Ros-Lis, F. Sancenon, J. Soto and L. A. Villaescusa, *Chem. – Eur. J.*, 2006, **12**, 2162–2170.
188 K. Sarkar, K. Dhara, M. Nandi, P. Roy, A. Bhaumik and P. Banerjee, *Adv. Funct. Mater.*, 2010, **19**, 223–234.
189 M. K. Nazeeruddin, D. Di Censo, R. Humphry-Baker and M. Grätzel, *Adv. Funct. Mater.*, 2006, **16**, 189–194.
190 Q. Lv, G. Li, Z. Cheng, H. Lu and X. Gao, *Environ. Sci.: Processes Impacts*, 2014, **16**, 116–123.
191 X. Qiu, S. Han, Y. Hu, M. Gao and H. Wang, *J. Mater. Chem. A*, 2014, **2**, 1493–1501.
192 J. Tan, H. F. Wang and X. P. Yan, *Biosens. Bioelectron.*, 2009, **24**, 3316–3321.
193 W. Warkocki, S. A. Elsafty, M. A. Shenashen, E. A. Elshehy, H. Yamaguchi and N. Akhtar, *J. Mater. Chem.*, 2015, **3**, 17578–17589.
194 G. Wirnsberger, B. J. Scott and G. D. Stucky, *Chem. Commun.*, 2001, 119–120.
195 M. Comes, M. D. Marcos, R. Martínez-Máñez, F. Sancenón, J. Soto, L. A. Villaescusa, P. Amorós and D. Beltrán, *Adv. Mater.*, 2004, **16**, 1783–1786.
196 B. García-Acosta, M. Comes, J. L. Bricks, M. A. Kudinova, V. V. Kurdyukov, A. I. Tolmachev, A. B. Descalzo, M. D. Marcos, R. Martínez-Máñez and A. Moreno, *Chem. Commun.*, 2006, 2239–2241.
197 J. Tan, H. F. Wang and X. P. Yan, *Anal. Chem.*, 2009, **81**, 5273–5280.
198 A. Wada, S.i. Tamaru, M. Ikeda and I. Hamachi, *J. Am. Chem. Soc.*, 2009, **131**, 5321–5330.
199 M. Comes, E. Aznar, M. Moragues, M. D. Marcos, R. Martínez-Máñez, F. Sancenón, J. Soto, L. A. Villaescusa, L. Gil and P. Amorós, *Chem. – Eur. J.*, 2009, **15**, 9024–9033.
200 J. V. Ros-Lis, R. Casasús, M. Comes, C. Coll, M. D. Marcos, R. Martínez-Máñez, F. Sancenón, J. Soto, P. Amorós and J. E. Haskouri, *Chem. – Eur. J.*, 2008, **14**, 8267–8278.
201 A. B. Descalzo, D. Jiménez, J. El Haskouri, D. Beltrán, P. Amorós, M. D. Marcos, R. Martínez-Máñez and J. Soto, *Chem. Commun.*, 2002, 562–563.
202 K. S. Booksh and B. R. Kowalski, *Anal. Chem.*, 1994, **66**, 782A–791A.
203 C. Lei, C. Xu, A. Nouwens and C. Yu, *J. Mater. Chem. B*, 2016, **4**, 4975–4979.
204 E. Climent, L. Mondragón, R. Martínez-Máñez, F. Sancenón, M. D. Marcos, J. R. Murguía, P. Amorós, K. Rurack and E. Pérez-Payá, *Angew. Chem., Int. Ed.*, 2013, **52**, 8938–8942.
205 R. R. Castillo, A. Baeza and M. Vallet-Regí, *Biomater. Sci.*, 2017, **5**, 353–377.
206 J. Li, X. Qin, Z. Yang, H. Qi, Q. Xu and G. Diao, *Talanta*, 2013, **104**, 116–121.
207 M. Yang, H. Li, A. Javadi and S. Gong, *Biomaterials*, 2010, **31**, 3281–3286.
208 X. He, Y. Zhao, D. He, K. Wang, F. Xu and J. Tang, *Langmuir*, 2012, **28**, 12909–12915.
209 J. Wang, T. Wei, X. Li, B. Zhang, J. Wang, C. Huang and Q. Yuan, *Angew. Chem., Int. Ed.*, 2014, **53**, 1616–1620.
210 Y. Li, Y. Zhao, W. Chan, Y. Wang, Q. You, C. Liu, J. Zheng, J. Li, S. Yang and R. Yang, *Anal. Chem.*, 2015, **87**, 584–591.
211 A. Ribes, E. Aznar, A. Bernardos, M. D. Marcos, P. Amorós, R. Martínez-Máñez and F. Sancenon, *Chem. – Eur. J.*, 2017, **23**, 8581–8584.
212 M. Oroval, C. Coll, A. Bernardos, M. D. Marcos, R. Martinez-Manez, D. G. Shchukin and F. Sancenón, *ACS Appl. Mater. Interfaces*, 2017, **9**, 11332–11336.
213 À. Ribes, S. Santiago-Felipe, A. Bernardos, M. D. Marcos, T. Pardo, F. Sancenón, R. Martínez-Máñez and E. Aznar, *ChemistryOpen*, 2017, **6**, 653–659.

214 S. E. Sayed, M. Licchelli, R. Martínez-Máñez and F. Sancenón, *Chem. – Asian J.*, 2017, **12**, 2670–2674.
215 M. Hasanzadeh, N. Shadjou, M. Eskandani and M. de la Guardia, *TrAC, Trends Anal. Chem.*, 2012, **40**, 106–118.
216 C. Xu, Z. Song, Q. Xiang, J. Jin and X. Feng, *Nanoscale*, 2016, **8**, 7391–7395.
217 M. Hartmann and X. Kostrov, *Chem. Soc. Rev.*, 2013, **42**, 6277–6289.
218 L. Bayne, R. V. Ulijn and P. J. Halling, *Chem. Soc. Rev.*, 2013, **42**, 9000–9010.
219 E. Magner, *Chem. Soc. Rev.*, 2013, **42**, 6213–6222.
220 C. Lei, Y. Shin, J. Liu and E. J. Ackerman, *J. Am. Chem. Soc.*, 2002, **124**, 11242–11243.
221 Z. Dai, S. Liu, H. Ju and H. Chen, *Biosens. Bioelectron.*, 2004, **19**, 861–867.
222 Y. Deng, J. Wei, Z. Sun and D. Zhao, *Chem. Soc. Rev.*, 2013, **42**, 4054–4070.
223 D. Fattakhova Rohlfing, J. Rathouský, Y. Rohlfing, O. Bartels and M. Wark, *Langmuir*, 2005, **21**, 11320–11329.
224 S. J. Kim, S. J. Choi, J. S. Jang, N. H. Kim, M. Hakim, H. L. Tuller and I. D. Kim, *ACS Nano*, 2016, **10**, 5891–5899.
225 H. J. Kim, S. J. Lee, S. Y. Park, J. H. Jung and J. S. Kim, *Adv. Mater.*, 2008, **20**, 3229–3234.
226 S. Xu and H. Lu, *Biosens. Bioelectron.*, 2015, **73**, 160–166.
227 S. Shinde, Z. El-Schich, A. Malakpour, W. Wan, N. Dizeyi, R. Mohammadi, K. Rurack, A. Gjörloff Wingren and B. R. Sellergren, *J. Am. Chem. Soc.*, 2015, **137**, 13908–13912.
228 S. Xu and H. Lu, *Biosens. Bioelectron.*, 2016, **85**, 950–956.
229 D. Wang, J. Wang, Z. E. Liu, X. Yang, X. Hu, J. Deng, N. Yang, Q. Wan and Q. Yuan, *ACS Appl. Mater. Interfaces*, 2015, **8**, 28265–28273.
230 Y. Yamauchi, A. Tonegawa, M. Komatsu, H. Wang, L. Wang, Y. Nemoto, N. Suzuki and K. Kuroda, *J. Am. Chem. Soc.*, 2012, **134**, 5100–5109.
231 K. M. Zeinu, H. Hou, B. Liu, X. Yuan, L. Huang, X. Zhu, J. Hu, J. Yang, S. Liang and X. Wu, *J. Mater. Chem. A*, 2016, **4**, 13967–13979.
232 A. L. Lee, C. T. Gee, B. P. Weegman, S. A. Einstein, A. R. Juelfs, H. L. Ring, K. R. Hurley, S. M. Egger, G. Swindlehurst and M. Garwood, *ACS Nano*, 2017, **11**, 5623–5632.
233 R. A. Naikoo, S. U. Bhat, M. A. Mir and R. Tomar, *Microporous Mesoporous Mater.*, 2017, **243**, 229–238.
234 J. Zhang, P. Tang, T. Liu, Y. Feng, C. Blackman and D. Li, *J. Mater. Chem. A*, 2017, **5**, 10387–10397.
235 V. K. Tomer, N. Thangaraj, S. Gahlot and K. Kailasam, *Nanoscale*, 2016, **8**, 19794–19803.
236 P. Wang, Z. Zheng, X. Cheng, L. Sui, S. Gao, X. Zhang, Y. Xu, H. Zhao and L. Huo, *J. Mater. Chem. A*, 2017, **5**, 19846–19856.
237 V. K. Tomer and S. Duhan, *J. Mater. Chem. A*, 2016, **4**, 1033–1043.
238 R. Malik, V. K. Tomer, V. Chaudhary, M. S. Dahiya, A. Sharma, S. Nehra, S. Duhan and K. Kailasam, *J. Mater. Chem. A*, 2017, **5**, 14134–14143.
239 H. Li, F. Meng, J. Liu, Y. Sun, Z. Jin, L. Kong, Y. Hu and J. Liu, *Sens. Actuators, B*, 2012, **166**, 519–525.
240 M. Zhou, J. Ding, L. P. Guo and Q. K. Shang, *Anal. Chem.*, 2007, **79**, 5328–5335.
241 J. Zang, C. X. Guo, F. Hu, L. Yu and C. M. Li, *Anal. Chim. Acta*, 2011, **683**, 187–191.
242 S. Park, T. D. Chung and H. C. Kim, *Anal. Chem.*, 2003, **75**, 3046–3049.
243 N. Thinakaran, S. Subramani, T. Priya, N. Dhanalakshmi, T. Vineesh and V. Kathikeyan, *Electroanalysis*, 2017, **29**, 1903–1910.
244 G. P. Mane, S. N. Talapaneni, K. S. Lakhi, H. Ilbeygi, U. Ravon, K. Al-Bahily, T. Mori, D. H. Park and A. Vinu, *Angew. Chem., Int. Ed.*, 2017, **56**, 8481–8485.
245 C. Fu, D. Yi, C. Deng, X. Wang, W. Zhang, Y. Tang, F. Caruso and Y. Wang, *Chem. Mater.*, 2017, **29**, 5286–5293.
246 X. Bo, W. Xie, J. C. Ndamanisha, J. Bai and L. Guo, *Electroanalysis*, 2009, **21**, 2549–2555.
247 L. Zhu, C. Tian, R. Yang and J. Zhai, *Electroanalysis*, 2008, **20**, 527–533.
248 M. Hasanzadeh, M. H. Pournaghi-Azar, N. Shadjou and A. Jouyban, *RSC Adv.*, 2014, **4**, 4710–4717.
249 M. Hasanzadeh, M. H. Pournaghi-Azar, N. Shadjou and A. Jouyban, *Electrochim. Acta*, 2013, **89**, 660–668.
250 L. Ding and B. Su, *J. Electroanal. Chem.*, 2015, **736**, 83–87.
251 P. Si, S. Ding, J. Yuan, X. W. Lou and D. H. Kim, *ACS Nano*, 2011, **5**, 7617–7626.
252 T. Kimura, N. L. Torad and Y. Yamauchi, *J. Mater. Chem. A*, 2014, **2**, 8196–8200.
253 R. A. Wallace, M. J. Sepaniak, N. V. Lavrik and P. G. Datskos, *Anal. Chem.*, 2017, **89**, 6272–6276.
254 P. Xu, H. Yu and X. Li, *Anal. Chem.*, 2011, **83**, 3448–3454.
255 Y. Zhu, J. Chen, H. Li, Y. Zhu and J. Xu, *Sens. Actuators, B*, 2014, **193**, 320–325.
256 G. Fang, G. Liu, Y. Yang and S. Wang, *Sens. Actuators, B*, 2016, **230**, 272–280.
257 Y. Ogimoto, R. Selyanchyn, N. Takahara, S. Wakamatsu and S. W. Lee, *Sens. Actuators, B*, 2015, **215**, 428–436.
258 J. Tang, N. L. Torad, R. R. Salunkhe, J. H. Yoon, A. Hossain, M. Shahriar, S. X. Dou, J. H. Kim, T. Kimura and Y. Yamauchi, *Chem. – Asian J.*, 2014, **9**, 3238–3244.
259 J. Wang, H. Shen, C. Huang, Q. Ma, Y. Tan, F. Jiang, C. Ma and Q. Yuan, *Nano Res.*, 2017, **10**, 145–156.
260 W. Teng, Z. Wu, J. Fan, H. Chen, D. Feng, Y. Lv, J. Wang, A. M. Asiri and D. Zhao, *Energy Environ. Sci.*, 2013, **6**, 2765–2776.
261 W. Teng, Z. Wu, J. Fan, W. X. Zhang and D. Zhao, *J. Mater. Chem. A*, 2015, **3**, 19168–19176.
262 J. Wei, Y. Ren, W. Luo, Z. Sun, X. Cheng, Y. Li, Y. Deng, A. A. Elzatahry, D. Al-Dahyan and D. Zhao, *Chem. Mater.*, 2017, **29**, 2211–2217.
263 K. Qian, W. Gu, P. Yuan, F. Liu, Y. Wang, M. Monteiro and C. Yu, *Small*, 2012, **8**, 231–236.
264 J. Wan, K. Qian, L. Qiao, Y. Wang, J. Kong, P. Yang, B. Liu and C. Yu, *Chem. – Eur. J.*, 2009, **15**, 2504–2508.
265 N. Sun, C. Deng, Y. Li and X. Zhang, *ACS Appl. Mater. Interfaces*, 2014, **6**, 11799–11804.
266 X. Yue, A. Schunter and A. B. Hummon, *Anal. Chem.*, 2015, **87**, 8837–8844.

267 C. T. Chen and Y. C. Chen, *Anal. Chem.*, 2005, **77**, 5912–5919.
268 W. F. Ma, Y. Zhang, L. L. Li, L. J. You, P. Zhang, Y. T. Zhang, J. M. Li, M. Yu, J. Guo, H. J. Lu and C. C. Wang, *ACS Nano*, 2012, **6**, 3179–3188.
269 J. Andersson, J. Rosenholm, S. Areva and M. Lindén, *Chem. Mater.*, 2004, **16**, 4160–4167.
270 Y. Li, W. Luo, N. Qin, J. Dong, J. Wei, W. Li, S. Feng, J. Chen, J. Xu and A. A. Elzatahry, *Angew. Chem., Int. Ed.*, 2014, **53**, 9035–9040.
271 M. Etienne, A. Quach, D. Grosso, L. Nicole, C. Sanchez and A. Walcarius, *Chem. Mater.*, 2007, **19**, 844–856.
272 T. Balaji, S. A. El-Safty, H. Matsunaga, T. Hanaoka and F. Mizukami, *Angew. Chem., Int. Ed.*, 2006, **45**, 7202–7208.
273 E. Rossinyol, A. Prim, E. Pellicer, J. Arbiol, F. Hernández-Ramírez, F. Peiró, A. Cornet, J. R. Morante, L. A. Solovyov and B. Tian, *Adv. Funct. Mater.*, 2007, **17**, 1801–1806.
274 G. Sakai, N. Matsunaga, K. Shimanoe and N. Yamazoe, *Sens. Actuators, B*, 2001, **80**, 125–131.
275 P. Horcajada, A. Ramila, J. Perez-Pariente and M. Vallet-Regí, *Microporous Mesoporous Mater.*, 2004, **68**, 105–109.
276 I. Izquierdo-Barba, E. Sousa, J. C. Doadrio, A. L. Doadrio, J. P. Pariente, A. Martínez, F. Babonneau and M. Vallet-Regí, *J. Sol-Gel Sci. Technol.*, 2009, **50**, 421–429.
277 F. Qu, G. Zhu, S. Huang, S. Li, J. Sun, D. Zhang and S. Qiu, *Microporous Mesoporous Mater.*, 2006, **92**, 1–9.
278 H. Y. Lian, Y. H. Liang, Y. Yamauchi and K. C. W. Wu, *J. Phys. Chem. C*, 2011, **115**, 6581–6590.
279 Y. Hu, A. Bouamrani, E. Tasciotti, L. Li, X. Liu and M. Ferrari, *ACS Nano*, 2009, **4**, 439–451.
280 E. Rossinyol, A. Prim, E. Pellicer, J. Rodríguez, F. Peiro, A. Cornet, J. R. Morante, B. Tian, T. Bo and D. Zhao, *Sens. Actuators, B*, 2007, **126**, 18–23.
281 S. A. El-Safty, D. Prabhakaran, A. A. Ismail, H. Matsunaga and F. Mizukami, *Adv. Funct. Mater.*, 2007, **17**, 3731–3745.
282 R. C. Rodrigues, C. Ortiz, Á. Berenguer-Murcia, R. Torres and R. Fernández-Lafuente, *Chem. Soc. Rev.*, 2013, **42**, 6290–6307.
283 Y. Wang and F. Caruso, *Chem. Mater.*, 2005, **17**, 953–961.
284 E. Palomares, R. Vilar, A. Green and J. R. Durrant, *Adv. Funct. Mater.*, 2004, **14**, 111–115.
285 N. T. P. Nhung, P. Van Tong, C. M. Hung, N. Van Duy, N. V. Chien, N. Van Vinh, N. T. Tuyen and N. D. Hoa, *RSC Adv.*, 2016, **6**, 64215–64218.